Simplifying Prototyping of Friction-Based Haptics and Miniature Input Devices for VR

A Dissertation
Presented to
The Academic Faculty

By

Abhijeet Mishra
Roll No. PhD19502

In partial fulfilment
of the requirements for the
Degree of Doctor of Philosophy

Under the Supervision of

Dr. Jainendra Shukla & Dr. Aman Parnami

INDRAPRASTHA INSTITUTE *of*
INFORMATION TECHNOLOGY **DELHI**

Department of Human Centered Design
Indraprastha Institute of Information Technology Delhi

July 2024

Simplifying Prototyping of Friction-Based Haptics and Miniature Input Devices for VR

A Dissertation
Presented to
The Academic Faculty

By

Abhijeet Mishra
Roll No. PhD19502

In partial fulfilment
of the requirements for the
Degree of Doctor of Philosophy

Under the Supervision of

Dr. Jainendra Shukla & Dr. Aman Parnami

INDRAPRASTHA INSTITUTE *of*
INFORMATION TECHNOLOGY **DELHI**

Department of Human Centered Design
Indraprastha Institute of Information Technology Delhi

July 2024

CERTIFICATE

This is to certify that the thesis titled, "Simplifying Prototyping of Friction-Based Haptics and Miniature Input Devices for VR", being submitted by Abhijeet Mishra to the Department of Human Centered Design, Indraprastha Institute of Information Technology Delhi, in partial fulfilment of the requirements for the degree of Doctor of Philosophy in Human Centered Design is an authentic proof of work carried out by him under our supervision. In our opinion, the thesis has reached the standards of fulfilling the requirements of the regulations relating to the degree.

The work in this thesis has not been submitted in any form for another degree or diploma at any university or another institute.

04 - 12 - 2024

Dr. Jainendra Shukla

Assistant Professor, Department of CSE & HCD

IIIT-Delhi

Date of Signature

04 - 12 - 2024

Dr. Aman Parnami

Ex-Assistant Professor, Department of HCD

IIIT-Delhi

Date of Signature

DECLARATION

I hereby declare that the work presented in this thesis titled "Simplifying Prototyping of Friction-Based Haptics and Miniature Input Devices for VR", submitted to the Department of Human Centered Design, Indraprastha Institute of Information Technology Delhi, in partial fulfilment of the requirements for the degree of Doctor of Philosophy in Human Centered Desgn, is an authentic proof of my own work carried out from August 2019 to the present date under the supervision of Dr. Jainendra Shukla and Dr. Aman Parnami.

The work in this thesis has not been submitted in any form for another degree or diploma at any university or another institute. Information derived from the published and unpublished work of others has been acknowledged in the text and a list of references is given.

30 - 11 - 2024

Abhijeet Mishra

Date of Signature

ACKNOWLEDGEMENT

I thank the almighty (Maa Vindhyavasini, Kashi, & Hanuman Ji) for blessing me with an incredible group of people who believed in me and supported me throughout this journey. I want to express my heartfelt gratitude to everyone who helped me reach this significant milestone in my life. This achievement would not have been possible without their unwavering support. As the famous song goes, I truly got by "with support from my friends and family."

First, I extend my deepest thanks to my academic advisors, Jainendra Shukla and Aman Parnami, for guiding me when I was at a crossroads in my PhD journey. Your belief in my abilities and encouragement to pursue my interests gave me the strength to continue. You not only showed me the right path but also set high standards for my research and career aspirations. Your generous support, time, and mentorship created the ideal learning environment for me. I consider myself extremely fortunate to have worked under your guidance.

To my parents, Devinder Kumar Mishra and Gayatri Mishra, and my wife, Priya Mishra, I owe everything. Papa and Mummy, your unconditional love, prayers, and sacrifices made this journey possible. I hope you can now feel at ease and proud of this accomplishment. Priya, your constant support and encouragement have been the cornerstone of all my achievements. Thank you for standing by me every step of the way. I look forward to spending the rest of my life with you. To my daughter, Rashi (Naisha Mishra), you are my greatest source of joy and inspiration. Your smile takes away all my stress and fills my heart with happiness.

I am also grateful to my extended family for their love and encouragement. A special thank you to my sister, Bhawna Mishra, and my best friend, Kushagra Saxena, for always prioritizing my needs, even during your own challenges. I am truly blessed to have you in my life, and I hope our bond only grows stronger with time.

I would like to acknowledge the guidance and support of my committee members, Push-

pendra Singh and Sumit Darak, who provided invaluable feedback on my work. Pushpendra helped me appreciate the importance of research methodology and opened my mind to the field of qualitative HCI research, while Sumit bridged gaps in my understanding of electronics, which was crucial for my research.

My journey would not have been complete without the support of my academic family at the Weave and HMI Labs, as well as my friends at IIIT-Delhi. I am grateful to Piyush Kumar and Harshvardhan Singh for their collaboration and to Ashwini B and Manshul Belani for their constant support. Your camaraderie made this journey much more enjoyable.

I also want to thank the administrative staff at IIIT-Delhi, including the CDNM, PhD administration, and Finance department, for their consistent support. A special mention to Umesh, Anurag Tyagi, Sheetu Ahuja, Priti Patel, Sudhanshu, Raju Biswas, and Anshu Dureja, whose prompt actions and assistance are invaluable.

Lastly, I am grateful to PVM Rao (IIT Delhi), Pradipta Biswas (IISc Bangalore), and Shana Smith (NTU) for taking the time to provide valuable feedback on my thesis. Your insightful suggestions significantly enhanced the quality of my work.

Thank you all for being an integral part of my journey. This accomplishment is as much yours as it is mine.

ABSTRACT

The HCI community widely recognizes the significant benefits of integrating haptic feedback and input devices into digital environments. These integrations are crucial to creating authentic user experiences, enabling users to perceive digital environments naturally, manipulate virtual objects with ease, and engage deeply with digital content and activities. However, despite the potential of integrating these methods into the digital realm, such solutions are often explored or come with significant limitations that are frequently overlooked or not taken into account while designing. These limitations include issues with scalability, complexity (demanding substantial object/user/environment instrumentation or modification), and cost-effectiveness. Consequently, such issues create significant barriers to accessing current proposed solutions, particularly for users in resource-constrained settings, thereby preventing widespread adoption (useful from the perspective of prototyping) and their straightforward use of these methods. Motivated by these challenges, my thesis aims to pioneer the design and development of novel haptic feedback and input device methods that are scalable, simple, and cost-effective. The primary goal is to address the lag in the development of accessible type haptic feedback and input device design methods amidst rapid advancements in other technologies. By emphasizing this disparity, the objective is to catalyze future development and focus on the global democratization of access to these technologies. Because it will allow users all around the world to benefit from simplified prototyping procedures while leveraging the potential of haptic effects and physical interaction approaches.

In the first project, I introduce HaptiDrag, a device that harnesses the electroadhesion phenomenon to produce variable drag effects on physical interfaces. This paper-thin and lightweight solution overcomes the limitations of traditional mechanical and ultrasonic based haptic feedback systems, offering scalability, low-complexities, and adaptability across

various surfaces. Extensive user studies have shown that HaptiDrag effectively enhances VR interactions by enabling users to feel varying intensities of friction, thereby enriching the sensory experience in digital environments. In the second project, I enable in a simplified way the realistic simulation of precise manipulation experiences in VR akin to those experienced with precision hand-held tools in the real world. This work offers an accessible and cost-effective approach, overcoming the challenges of traditional and proposed physical methods, such as complex setups, no realistic experiences, active components, high costs, and sophisticated programming. In the third project, I explore another method for developing miniature input devices for VR while also enabling interaction with everyday physical objects that addresses past challenges with innovative solutions. I have demonstrated that non-smart objects also, e.g., like stylus-type ballpoint pens and fashionable rings, which users typically use for a single purpose, can now also serve as input devices without any additional instrumentation of the objects, the user, or the environment. My approach contrasts sharply with traditional methods that demand explicit instrumentation, showcasing a significant advancement in the usability of non-smart objects and the simplicity of the explored approach.

Collectively, my thesis makes substantial contributions to the field of human-computer interaction. It not only showcases realistic user interactions in a straightforward and lightweight manner within digital environments but also strongly emphasizes and enhances the design accessibility and usability of the proposed haptic feedback and input device methods compared to previous approaches. This facilitates wider user adoption while maintaining enriched digital experiences. Ultimately, my thesis takes a step forward by emphasizing that the true potential of any invented methods can only be realized if they are made accessible to all users, to envision a future of accessible methods (rather than only methods) available to everyone anywhere and everywhere.

TABLE OF CONTENTS

LIST OF TABLES

LIST OF FIGURES

CHAPTER 1
INTRODUCTION

As humans, we rely heavily on the integration of visual, physical, and haptic sensory information to fully comprehend our environment [1]. In virtual environments, haptic feedback and input device technologies are crucial for creating convincing and immersive experiences, as they enable multisensory integration that enhances the plausibility of the illusion [2]. Consequently, both industry and research increasingly emphasize the development of these technologies to meet high user expectations and improve interactions in VR. Moreover, haptic feedback and input devices add tangibility to visual representations, enhancing task performance, realism, and a user's sense of presence [3–5]. The significance of these technologies is most evident when they are absent: without haptic feedback or input devices, we lose the ability to gauge surface texture, sense object manipulation and shapes, or feel the firmness of a handshake. Even tasks like threading a needle would become significantly harder without these senses [6].

Based on these foundational insights, it becomes evident that the integration of haptic effects and input devices into virtual environments offers significant benefits in enhancing user experiences by enabling more natural and immersive interactions. These technologies allow users to perceive virtual environments intuitively, manipulate virtual objects effortlessly, and engage deeply with digital content and activities. However, despite their potential, many prototyping methods for haptic feedback and/or input devices, aimed at integrating them into virtual systems, face significant limitations, including scalability, complexity, and cost. Consequently, these challenges create major barriers to accessibility, especially for users in resource-constrained environments, hindering the ability to prototype such systems effectively and preventing the widespread adoption and practical use of these technologies. The primary challenge associated with implementing/prototyping these technologies lies in the

demand for substantial instrumentation and modification of objects, users, or environments to implement haptic and physical feedback systems. This results in solutions that are often complex, expensive, and not easily scalable. Consequently, while advancements in areas like visual and auditory components of virtual environments have progressed rapidly, the development of accessible and lightweight (basically less resource demanding) haptic feedback and input device mechanisms has lagged behind. This lag leads to a significant gap that hinders the ease of utilizing these methods for prototyping fully immersive and inclusive experiences, particularly for individuals in resource-constrained environments.

Motivated by these challenges, this dissertation presents lightweight, scalable, low-cost, and simple prototyping solutions—one focused on haptic feedback, particularly friction-based haptics, and another on input device development. Through these works, my thesis aims to inspire future researchers and designers to prioritize accessibility and simplicity when exploring any mechanism, whether in the development of haptic feedback or input devices for VR. It's because by embedding this principle into their work, it will enable them to ensure that their innovative solutions are not only cutting-edge but also easily prototyped and accessible, which will empower users to fully engage with and benefit from these technologies. Moreover, emphasizing this approach will also ultimately improve access to rich virtual experiences for users globally, particularly those in resource-constrained settings, while also stimulating new innovations.

Collectively, this thesis, through its projects, highlights the gap in the slower evolution of accessible prototyping methods for haptic feedback and input devices, in contrast to the rapid advancements in other technologies. By focusing on attributes like scalability, simplicity, cost-effectiveness, and user-validated innovations, each project—whether belonging to the haptic feedback or input device domain—underscores the importance of developing methods for VR in a more accessible and lightweight manner. Ultimately, this thesis aims to take a step forward by emphasizing that the true potential of any invented methods can only be realized if they are made accessible to all users, envisioning a future where accessible

methods (rather than only methods) are available to everyone, anywhere and everywhere.

1.1 Literature Survey

1.1.1 Prototyping of Haptic Feedback for VR

Haptic feedback has become integral to the creation of immersive virtual reality (VR) experiences by simulating physical interactions through tactile sensations. The early work in this domain, such as the design of force feedback devices like the PHANToM [7], established a foundation for delivering realistic touch sensations in VR. Other works like the CyberGrasp [8] explored exoskeleton-based systems to simulate force interactions on the user's hand. In more recent years, explored devices, e.g., like ultrasonic-based surface property haptics [9], and Meta's wearable force-sensing gloves [10] have further expanded the capabilities of haptic feedback, providing a greater range of tactile and kinesthetic responses.

However, while these systems demonstrate the potential of haptics in VR, they are often designed with a focus solely on enabling the haptic effect itself, with little attention paid to making these solutions accessible to a wider user base. The complexity of the hardware, the cost of manufacturing, and the need for precise calibration all present significant barriers. For instance, the Haplinkage system, while effective, is highly complex, requiring specialized hardware and setup that makes it impractical for broader use [11]. Similarly, Meta's haptic gloves utilize sophisticated sensors and actuators, which make them inaccessible due to their cost and intricate prototyping process. Thus, although these haptic feedback methods have contributed significantly to VR's immersion, they have been explored primarily from the perspective of enabling haptic effects. They have not adequately considered how to make these effects easily accessible or simple to prototype for a broader range of users, particularly those in resource-limited environments.

1.1.2 Input Device Prototyping for VR

Input devices are crucial for enabling natural interactions in virtual reality (VR). While handheld controllers like the Oculus Touch [12] and HTC Vive wands [13] offer precise tracking and robust control, recent academic research has explored more innovative approaches to input prototyping in VR. For example, Arora et al. presented a modular prototyping toolkit that allows users to create custom VR controllers by combining simple components such as buttons, joysticks, and sliders [14]. This modular approach enables flexibility, but the complexity of assembling and programming these components makes it difficult for non-expert users to prototype their own input devices. Similarly, the works like [15, 16] focused on soft sensors for input devices, offering a novel approach for input prototyping, but the sensors are difficult to fabricate and expensive to implement.

Additionally, in the industrial sector, the Oculus Touch controllers and HTC Vive wands are designed with a focus on performance and precision but lack the simplicity and affordability required for accessible prototyping. These devices are costly and involve proprietary hardware, making them unsuitable for broader experimental use or by hobbyist developers.

Although these research efforts and industrial products have enabled more natural interaction in VR, the prototyping methods focus primarily on functionality and enabling new interaction techniques rather than making these systems simple and accessible to a broader user community. Most of these approaches involve complex hardware or high-end technologies, creating barriers for widespread experimentation and adoption, especially in resource-constrained environments.

1.2 Gaps in Existing Literature

A common issue across both haptic feedback and input device prototyping methods for VR is the significant challenge of accessibility. While substantial progress has been made in advancing these technologies, most of the current solutions are not designed with accessibility

in mind. The existing methods are often resource-intensive, requiring significant technical expertise, specialized hardware, and high costs to prototype. This creates a barrier for early stage researchers and developers, particularly those in resource-constrained settings, who are unable to experiment with or implement these technologies easily. The lack of simple, scalable, and cost-effective prototyping methods limits the widespread adoption and practical use of haptic feedback and input devices in VR systems.

Addressing and emphasizing this gap is essential for enabling more inclusive and widespread access to these technologies (i.e., any kind of haptic feedback and input device prototyping for VR). By exploring lightweight and simplified prototyping approaches in each of the explored areas, this thesis aims to inspire the community to not only enable diverse haptic feedback and input device-based experiences in VR but also to consider how these experiences can be made accessible by incorporating simplified prototyping methods. This will ensure that the developed approaches can be adopted and utilized by a wider audience, including those in resource-constrained settings. The work presented in this thesis emphasizes this dual objective—facilitating innovative VR experiences while lowering the barriers to accessibility. Specifically, in the case of haptic feedback, I explored friction-based haptics and reduced its complexity by providing a lightweight approach that demonstrates how complex haptic effects can be achieved with minimal instrumentation. Similarly, the development of miniature input devices for VR highlights how input methods can be made more accessible without sacrificing functionality. Ultimately, the goal is to ensure that future innovations are not only cutting-edge but also easily prototyped and widely accessible, empowering users across various settings to fully engage with and benefit from these technologies.

1.3 Research Statement

Based on the identified opportunities my research statement is as follows:

To incite and promote ease of approach accessibility and simple usability aspects in the design and development of haptic feedback and input device methods on a global scale,

ensuring that advancements in haptic feedback and input devices are not only cutting-edge but also inclusive and widely accessible to users in diverse and resource-limited settings.

1.3.1 Research Objectives

I further break down the key aspects of my research statement into specific research questions that form the foundation of my investigations for each of the explored work. These research questions, which I extracted from the central focus of my research statement that must be addressed during the exploration of solutions for simplifying the prototyping experience across any domain—whether it relates to any kind of haptic feedback or input device prototypes for VR—are as follows:

- RQ1: What are the key barriers related to any haptic feedback and input device prototyping methods that hinder their accessibility and ease of use for diverse users?
- RQ2: What approaches/technologies can be developed/leveraged to simplify the prototyping process for (complex) haptic feedback and/or input devices?
- RQ3: How effective are the proposed haptic feedback and/or input device methods in maintaining performance and reliability across diverse contexts/environments?
- RQ4: What additional practical benefits can the proposed methods provide to enhance the accessibility of haptic feedback and input device prototyping approaches, potentially leading to wider adoption in VR applications across various industries?

Specifically, based on the core of my research statement and utilizing the outlined questions, within the haptic feedback category, I investigated friction-based haptics and facilitated its lightweight application in VR (chapter 2). In the input device category, I focused on the lightweight development of miniature input devices, enabling a simple and seamless manipulation experience in VR (chapter 3 and 4).

1.4 Technical Contributions

In this thesis, each explored work—whether within the realm of haptic feedback (Chapter 2) or input devices (Chapters 3 and 4)—builds on these foundational contributions, ensuring a cohesive and integrated approach to advancing the fields of haptic technology and input devices. Together, these efforts reinforce key aspects of my research, driving innovation and furthering the potential of these explored systems.

- Explored and developed innovative haptic feedback and input device methods that prioritize scalability, simplicity, and cost-effectiveness, thus focusing on addressing key challenges in design accessibility and usability of approach for diverse users, particularly those in resource-limited settings.
- Performed rigorous technical evaluations to assess the effectiveness and scalability of the proposed method, ensuring robustness and reliability in various contexts.
- Validated each exploration effectiveness with users through comprehensive user studies or by providing implications.
- Finally, discussed and/or demonstrated the practical benefits and potential for widespread adoption through real-world applications that showcase the usefulness of the explored haptic feedback and input device methods.

1.5 Thesis Organization

The remainder of the thesis is structured as follows: Chapter 2 investigates friction-based haptics in VR, offering a contrast to previous methods and introducing our lightweight approach for enhanced user experiences. Chapter 3 explores the development of miniature input devices for precise manipulation in VR, validating this approach through user studies. Chapter 4 expands chapter 3 by demonstrating another method for developing miniature

input devices for VR while also enabling interaction with everyday physical objects that addresses past challenges with innovative solutions. Finally, Chapter 5 presents the conclusion of this work and outlines future research directions.

CHAPTER 2
HAPTIDRAG

2.1 Introduction

Humans rely on surface-related properties, such as friction, to perform everyday actions like walking, grasping an object, and pulling objects from one location to another. Friction also allows individuals to feel the material's texture (a natural haptic feeling) and make decisions about the roughness or smoothness of the material's surface accordingly. In the real world, we can't even imagine doing anything without friction.

While on the digital interface side, the variable friction functionality helps in enhancing user interactions from a performance and emotional standpoint [17]. Examples include pointing [18] and dragging [19], where it is demonstrated that high friction effect helps in improving the precision with which the user points and drags items in digital space, reducing overshoot and errors, while a low friction effect on the surface increases the ease of sliding movement thus lowering the judder effect. Additionally, if users are trying to control chores, e.g., increasing or decreasing the volume by using sliders, adding friction (as haptic feedback) can efficiently indicate to the user whenever they enter into a non-safe sound level range.

Variable friction effects are currently felt primarily on the surfaces of touch-screen devices (to provide tactile effects [20]) and digital table-tops (where variable friction property is rendered to provide a tangible haptic effect [21]). In contrast to touchscreen/digital tabletop surfaces, there are limited options for experiencing variable friction effects and other friction properties (e.g., detents, barrier effects, etc.) when performing (or designing) interaction with light-weight digital devices, prototypes, tangibles, or props related to real or virtual environments on physical surfaces such as wood, paper, and others. Based on prior works, one method that can be used to provide capability to prototypes (or props) for producing varied

levels of friction effects according to digital actions being performed is to use a mechanical phenomenon involving a motor mechanism attached to the object's base, as depicted in [19, 22]. However, this method lacks, in terms of its implementation, ease of integration with lightweight objects and props used in real and VR environments. In addition to that, their presence can even make the prototypes or props bulky, cumbersome, limit applicability to low sizes prototypes, lack in scalability and also cause deployment issues on designed prototypes and/or real objects.

This research introduces the HaptiDrag, a thin (1 mm) and light-weight (2 gram) device that can reliably produce various intensities of friction effects of both types, static and kinetic, on actual surfaces. Thus, allowing designers to use it for designing digital interactions, testing their light-weight prototype experiences or objects, and also with light-weight props used in VR environments, which are being used to enhance the user experience by combining real-world feelings with virtual world experiences. Using this device, designers would be able to take advantage of various modes of friction-design interaction, such as detents, hill climbing, and barrier effect. This is achieved based on the exploration of the electroadhesion phenomenon. Electroadhesion is a potential technology for grasping materials that operates in a similar way to existing technologies like vacuum suction and magnetic adhesion. This method requires minimal instrumentation without surface property alteration, and the device is simple to fabricate in a variety of sizes and can be easily integrated with real objects or prototypes. I determine the minimum size of HaptiDrag (5 cm x 5 cm) over which the device functions reliably based on a series of in-lab tests. With reference to eight distinct surfaces, I show the technical performance of two sizes of HaptiDrag (one is for the explored minimum size and the other is the larger one). After that, I also conducted two user studies, the first of which discovered absolute detection thresholds (ADT) i.e., friction spots of varying intensities that were immediately recognisable among users and common to all surfaces under test. The resulting detection threshold points (i.e., static friction spots) were then validated in terms of their static and kinetic friction perception with all sizes of HaptiDrag and with

varied sizes of weight (tested up to 100 gram) in the second user study. Finally, I showed various use cases to demonstrate the device's use in diverse settings.

Specifically, my contributions are:

- I present a new method for generating and experiencing varied friction by utilising the electroadhesion principle, as well as a low-cost HaptiDrag device fabrication procedure that does not require expensive machines or prior fabrication experience.
- Through our technical evaluation, I determined the minimum size of the HaptiDrag that demonstrated reliable performance on various physical surfaces.
- I present the findings of two user studies, formative and validation, conducted with a total of 18 participants, the first of which investigated the absolute detection threshold points of HaptiDrag and the second of which performed device validation with respect to different surfaces and weights.
- Finally, I provide a various application scenarios demonstrating the use case of HaptiDrag.

2.2 Related Work

I outline related research from two areas that are relevant to this project. In the first section, I discussed how the variable friction (VF) property has been used to enhance digital interaction and also about previous approaches used to implement it. In the second section, I mentioned electroadhesion-based research work in HCI to provide information on previous work on this technique.

2.2.1 Variable Friction & Previous Approaches about Real Surfaces

Prior HCI research has demonstrated that variable friction (VF) improves user engagement with interfaces or simulations by providing tactile feedback, and from a haptic standpoint, it

improves the execution of activities like pointing and dragging. For example, in Teslatouch [20], changing friction effects using electrovibration technology introduces tactile feedback to touch-sensitive devices. Another example is [18], in which researchers used the VF characteristic to increase the effective communication between user pairs chatting through tablets. Weiss et al. [21] used the electromagnetic actuation method to recreate physical effects like weight and detents through tangibles on digital tabletops. Previous VF research has focused on the implementation and exploitation of the VF property to improve user experience on smart devices like tablets and digital tabletops, whereas this research focuses on the ease of implementation and leveraging of VF effects to improve digital interactions in relation to physical surfaces.

The most common way for creating changeable friction effects on a physical surface is to use mechanical characteristics, which involves three distinct methods: lubricants, materials, and rolling [23]. In a recent work [19], where authors used a material-based method to provide variable friction capabilities in their prototype. Another work which showed VF capability through their prototype on touchscreen surfaces only is [22], where a rolling-method (involving motor and other electronics) was used in their design to create a friction effect whenever dragged over the touch screen surface. These methods may be able to change friction effects without changing surface properties, however because of their mechanical nature, they are difficult to create, complex to integrate with prototypes, as well as they make the device bulkier. Apart from mechanical approaches, there are also non-mechanical approaches. For example, Watanabe et al. [24] developed ultrasonic technology that allows users to detect surface friction. However, to develop the friction effect over the surface, this method requires fixed surface instrumentation (i.e., integration of the actuators with the surface) and has never been tested in a scenario where these actuators are integrated into the base of any movable object. Most importantly, this method has primarily been tested on glass as a testing surface, and with user fingers rather than objects, and it does not provide a static friction experience. My device, on the other hand, is simple to construct, portable, and

can be easily integrated with light-weight prototypes and objects without adding additional weight like motors, as well as providing the experience of both static and kinetic friction effects in varying intensities on a variety of surfaces.

2.2.2 Electroadhesion in HCI

Electroadhesion is a potential technique that works similar to popular technologies like vacuum suction and magnetic adhesion in grabbing items [25, 26]. Verma et al. proposed a flying [27] and stick [28] user interface in HCI that uses the gripping properties of electroadhesion to attach a mobile user interface to the wall, consisting of a pico-projector with sensor and controlling unit. Similarly, Hinchet et al. [29] used the gripping concept to develop a wearable glove that uses electrostatic brakes to offer kinesthetic feedback for precise manipulation of virtual objects in AR and VR. In this research, I leveraged electroadhesion technology to create a device that can generate varying levels of friction on a real-world surface without causing any surface modification.

Despite the enormous advantage of controlling friction effects from a haptic or emotional point of view [30], limited work or study in the field of HCI exist that has looked at the electroadhesion notion for creating and experiencing variable friction effects on physical surfaces, both technically and from the user's standpoint. REVEL [31] demonstrates the perception of friction on a real-world object surface using the principle of electrovibration, however requires real-world object surface modification because this process operates only on a conductive surface. There are other works also [32–34] that demonstrate the use of electroadhesive technology for creating friction effects related to interactive tabletop surface containing additional conductive layer on top as a modification on a table top surface, but not with regard to physical surfaces.

2.3 HaptiDrag Mechanism

I first discuss the working principle on which HaptiDrag functionality work, then fabrication, and finally its safety.

2.3.1 Operating Principle

HaptiDrag is a small (1 mm) and lightweight (2 gram) device with two types of metal electrodes: "High Voltage" and "Ground." Both electrodes are of comparable size and are separated from one another on the substrate by a dielectric layer (kapton tape). The electrode location and design in the Haptidrag device is based on parallel plate capacitor design, which I discovered to be simple and easy to create. Any insulating substance, such as paper, plastic, or rubber, can be used as the substrate. Fig 2.1(a) depicts the structure of a HaptiDrag device. Both electrodes are attached to regulating board output terminals (shown later), whose role is to augment (boost) the supplied input supply (i.e. any value between 0 to 3.5 V DC) to 0 to 1.5 KV DC. The maximum current consumption by the HaptiDrag device is found to be only 0.28 mA at 1.5kV DC (more details shown in section 5).

When the (controllable) boosted voltage (V) applied to the HaptiDrag device (in contact with the insulating surface) is zero, no attractive force develops and as a result the device offers no additional hindrance (except normal friction) while sliding it over the surface. When a non-zero voltage is applied to the HaptiDrag device in contact with the insulator surface, an attractive (compressive) force develops due to surface polarization, as described by equations 2.1, 2.2 & 2.3.

$$F_{compressive} = P \cdot \phi + M \cdot G \tag{2.1}$$

$$\phi = E \cdot A \tag{2.2}$$

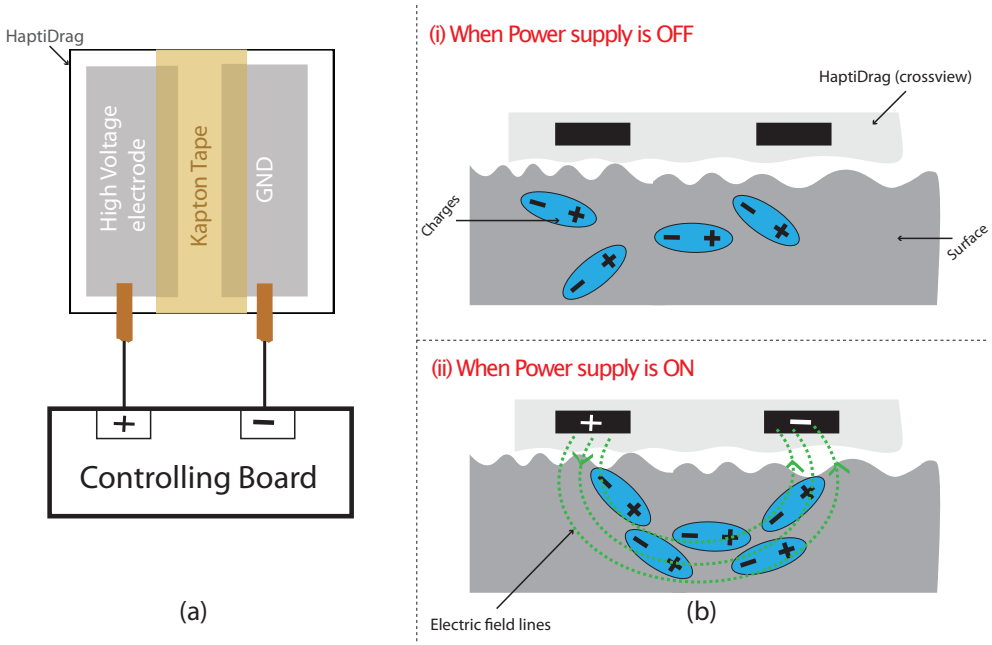

Figure 2.1: a) Left: Structure of HaptiDrag; b) Right: HaptiDrag working is shown in two scenarios, i) when power is OFF, & ii) when power is ON

$$E = V/d \tag{2.3}$$

In above equations, $F_{compressive}$ is the compressive force, (P $\cdot\phi$) is the electro-attractive/adhesive force, P is induced surface polarization, E is the electric field produced between electrodes, which is also directly related to the applied voltage (V) according to equation 2.3, d is the distance between two electrodes that will remain constant once the pad is fabricated, ϕ is electric field flux produced due to the presence of an electric field, A is the area of the electrode, M is the mass of the object below which the HaptiDrag device can be attached, G is the gravitational effect, and product of M and G is the normal reaction force.

Surface polarisation refers to the displacement of electron clouds of the insulator's surface molecules, when exposed to an electric field as shown in Fig 2.1(b) and characterised according to equation 2.4 where ϵ_r is the dielectric constant of the insulator surface.

$$P = (\epsilon_r - 1)E \tag{2.4}$$

This electrically-controlled compressive force then leads to frictional forces between the device and surface according to the equation 2.5 (μ is friction coefficient), which play a role of creating a hindrance while sliding the HaptiDrag.

$$F_{friction} <= \mu \cdot F_{compressive} \tag{2.5}$$

Since, compressive force varies also with the input supply (V), so does the frictional force, allowing the HaptiDrag device to provide a range of hindrance (resistance) from low to high intensity as haptic feedback while sliding over the insulator surface. One of the most appealing aspects of the explored method is that it does not require any surface alteration or instrumentation, making it ideal for surface based haptic feedback applications.

2.3.2 Fabrication of HaptiDrag

The fabrication of HaptiDrag entails following steps:

- creating electrodes on any design software (e.g., Adobe Illustrator, Inkscape) or on rough paper to the desired dimensions
- transferring the planned file to a vinyl cutter for cutting aluminium foil into electrodes; alternatively, the user can cut the aluminum foil by hand
- placement of electrodes on an insulating paper (e.g., paper) with a maximum gapping of 10 mm.
- applying a Kapton tape as a dielectric layer to cover the gap between two electrodes
- finally, attaching a copper tape to make device connection with small size lightweight hardware and adequately sealing all two electrodes from the corners areas using masking tape.

The method requires no industrial-grade equipment and uses significantly less expensive materials. In Fig 2.2, I depict the visual production process of a HaptiDrag device in both

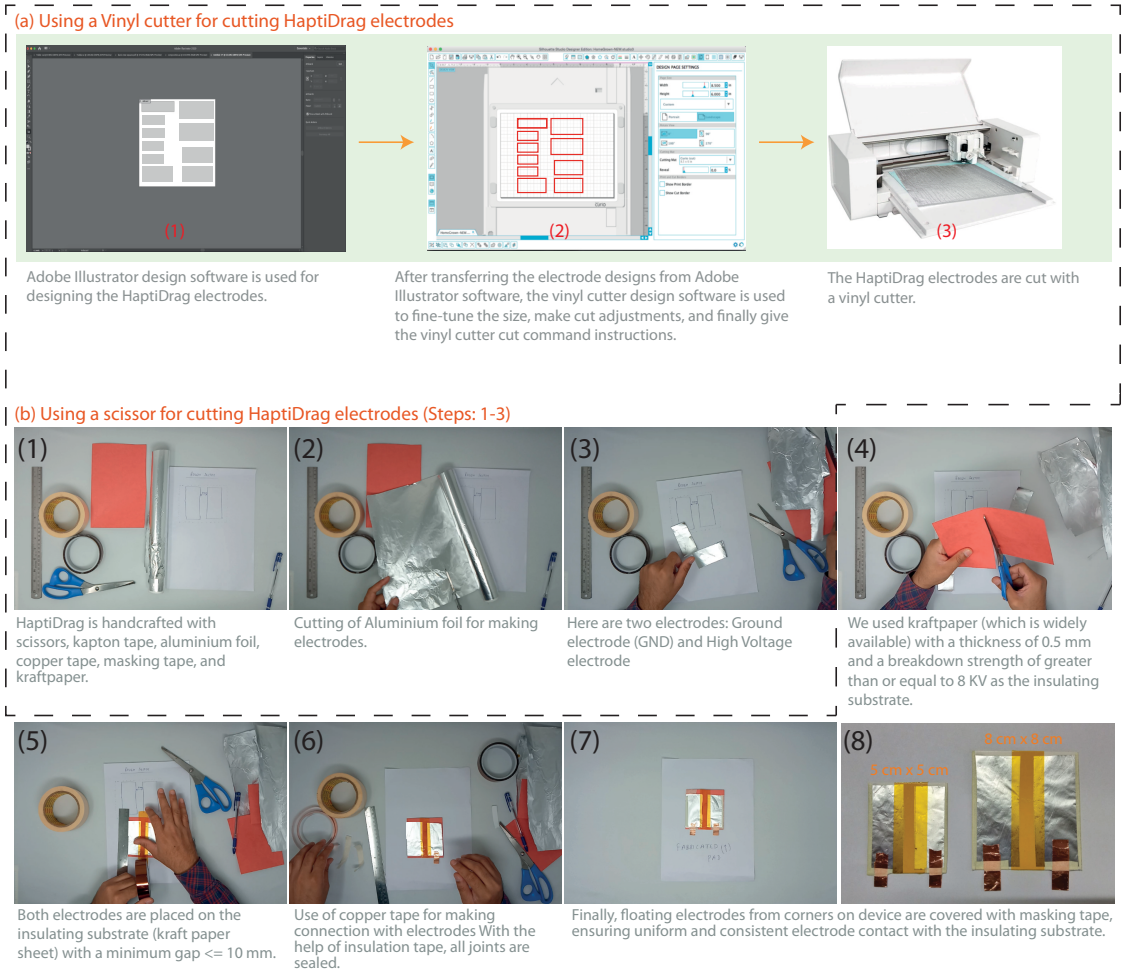

Figure 2.2: Visuals of the fabrication procedure of the device: in Part (a), making use of the vinyl cutter, from left, pad designs are made on vector software, which is then transferred to vinyl cutter software, and finally to a vinyl cutter machine, which is used for cutting the pad electrodes; and in Part (b), the manual cutting of pad electrodes with a scissor is shown in Steps 1-3. Furthermore, the complete manual fabrication process of the HaptiDrag pad is shown in steps from 1 to 8.

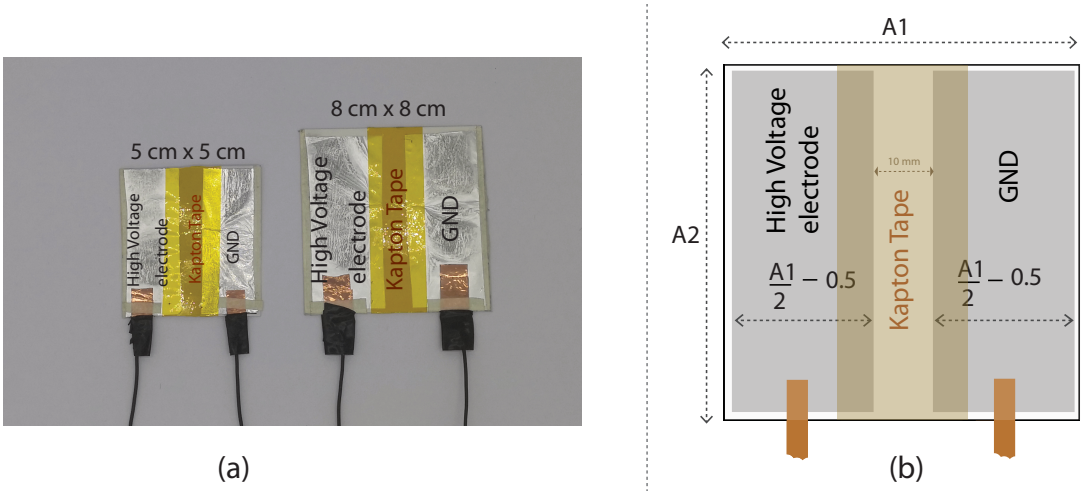

Figure 2.3: a) Left: Actual images of HaptiDrag (manually fabricated) are shown, which is also the pad bottom view that will be in contact with the surface ; b) Right: HaptiDrag pad dimensions

manual and vinyl cutter modes. To cut electrodes, only a normal low-cost machine, such as a vinyl cutter (in Fig 2.2a3), will suffice. If this equipment is also unavailable, we can cut electrodes from the material with scissors (in Fig 2.2b2). After the electrodes (aluminum foil with a thickness of 0.2 mm) are cut using any of the ways, they must be assembled using Kapton tape (dielectric constant: 3.4, 0.03 mm thick, & breakdown strength is 303 kV/mm), copper tape, and insulating substrate. I used kraft paper (which is widely available) with a thickness of 0.5 mm and a breakdown strength of greater than or equal to 8 KV [35] as the insulating substrate.

The manual procedure is as follows: We first cut the major section with a scissor, noting the same dimensions on the metal foil, as per the design on illustrator or on paper. Once the electrodes are cut, we will have two electrodes: high voltage and ground. After that, both electrodes are placed on the insulating substrate (such as a kraft paper sheet) with a minimum gap of 10 mm. Guo et al. [36] showed that as the distance between the electrodes exceeds 10 mm, the electroadhesive force weakens to practically nothing. As a result, we always kept the gap in our design below 10 mm. Kapton tape is then used to fill the space between the electrodes. Copper tape terminals are then created on each electrode, with half

of each copper terminal residing on the electrodes and the other half floating in the air for soldering the wire onto to connect to the controlling board. The terminals outside the pad area are effectively sealed with insulation tape after the wire is soldered to these floating copper terminals. Finally, masking tape is applied to the electrode corners on the pad (i.e., the constructed device) to ensure proper insulation and uniform and consistent electrode contact with the insulating substrate. The electrodes on the pads were not covered by any other film. The entire fabrication process takes less than 30 minutes.

In this way, I fabricated many pads in various dimensions (A_1 cm x A_2 cm) to test and evaluate the drag effects functioning based on the electroadhesion principle, such as 3 cm x 3 cm, 4 cm x 4 cm, and so on till 8 cm x 8 cm. The relationship between the dimensions of the pad and the electrode contained in it is shown in Fig 2.3b, and in Fig 2.3a, I display an actual image of the pads.

2.3.3 HaptiDrag Safety

Current, not voltage, is the most important aspect in ensuring safe operation [37]. The safe range current limit for devices that will be regularly touched by user skin (direct contact), such as capacitive touch screens, is within 0.5mA, according to the International Organization for Standardization (ISO) and the International Electro-technical Commission (IEC) [1]. HaptiDrag's current consumption is already much less than 0.5 milliamperes as per the human electrical safety design guidelines given in [38], putting it within a safe operating range. However, to maintain additional safety for its use in public settings, a current limiter circuit that ensures current consumption is always less than 0.5 mA can be easily added to the design. Furthermore, because the Haptidrag is not a wearable device, no actual charge will pass through the skin because no direct contact is required. I followed standard industry practices [37] such as adequate grounding of the control electronics and proper insulation of electrodes with high breakdown strength insulating tape to further safeguard the user and

[1] https://www.flukebiomedical.com/blog/electrical-safety-standards-basic-testing

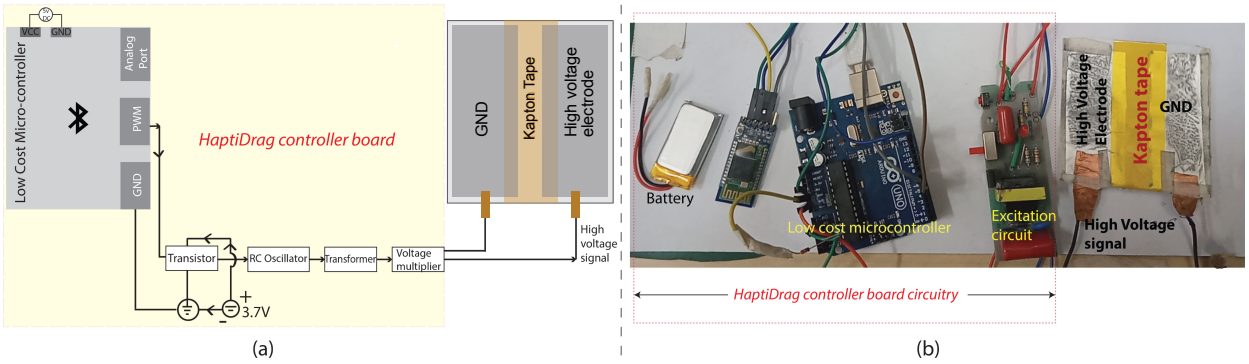

Figure 2.4: a) Left: Hardware schematic diagram is shown; b) Right: real electronics

assure safety. I also looked at other HCI papers [20, 29] to see how they assured safety in their prototype. Despite the fact that these prototypes need human skin contact or fall into the wearable category, I observed that they all used the same insulation approach to avoid skin contact with the functioning prototype and related electronics. For example, Dextres, a wearable haptic device [29] that supplies 1.5KV and 0.5mA current to its prototype, uses insulation gloves and human grounding to protect users. Another instance is Sparkle [39], a touch based haptic feedback that uses high voltage (3 KV) and current (0.5mA) for generating electric arc as a haptic feedback, where user safety is ensured by proper grounding of their prototype.

2.4 Implementation

HaptiDrag's hardware and software architectures are described in this section. Fig 2.4 shows schematic block diagrams and key components of the board that help HaptiDrag function as an actuator.

2.4.1 Control Electronics

As seen in Fig 2.4a wire soldered onto the copper electrodes coming out of the pad is connected to the HaptiDrag controller board. To digitally control the operation of the HaptiDrag device, I used a low-cost microcontroller, the Arduino UNO, which features an

AT-mega328 running at 16 MHz clock speed [2]. This demonstrated that the hardware design isn't bound by the necessity for a specific microcontroller to function. Instead, it give designers the freedom to choose any microcontroller they wanted, allowing them to further miniaturise the total circuit in terms of size, weight, and functionality (e.g controller having inbuilt Bluetooth features, high processing power and memory). I used an external power supply (Keysight [3], model no. E36300 Series) to provide 5V to the Arduino UNO, and a 3.7 V battery connection provision was provided to a custom designed excitation circuit so that the required input supply (digitally controlled from Arduino UNO PWM pin) could be given as an input to the excitation circuit as shown in Fig 2.4a. We've also added a Bluetooth module to the Arduino to take commands (related to drag effect intensity) wirelessly from any digital device, such as a laptop, workstation, or phone, depending on the type of digital interaction being conducted.

The operation of control electronics is described as follows:

- the microcontroller pin provides a PWM signal (with a frequency of 980Hz) between 0 and 5 volts as a signal to the transistor (working in the active region) to only transmit that much voltage (between 0 to 3.7 V) to the excitation circuit. The output DC voltage of the excitation circuit is linearly mapped to the voltage of the excitation circuit input, for example, 1.5 kV (DC) output corresponds to 3.5-volt input.

- Upon receiving the input voltage signal by the excitation circuit it boosts to high voltage (DC) which is then given as an input to HaptiDrag device to create the appropriate strength of friction sensation across the surface.

- When this boosted voltages (DC) delivered to the HaptiDrag change due to a change in the input supply (controlled by the PWM pin), the intensity of the electric fields varies, and hence the surface polarisation, as shown in equations 2.4 & 2.5.

[2]https://store-usa.arduino.cc/products/arduino-uno-rev3/

[3]https://www.keysight.com/in/en/products/dc-power-supplies/bench-power-supplies/e36300-series-triple-output-power-supply-80-160w.html

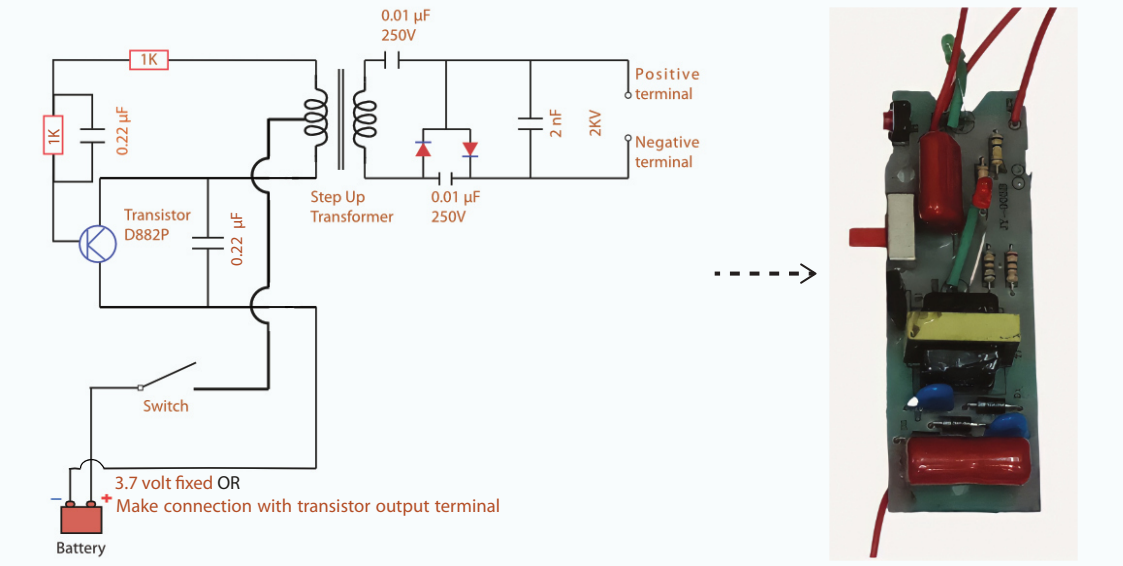

Figure 2.5: Excitation circuit schematic design and real image of board (right)

- As a result, the electrostatic attractive force effect on the surface changes, allowing for different amounts of resistance to be experienced.

2.4.2 Excitation Circuit

The RC oscillator circuit, transformer circuit, and lastly voltage multiplier circuit make up the excitation circuit, which is primarily used to boost the input voltage (which ranges from 0 to 3.7 V). The maximum input voltage that an excitation circuit can accept is 5 volts. The RC oscillator circuit generates a 6 kHz high-frequency alternating current that passes through the 35-turn primary side of the transformer, due to which an approximate 22 V drop occurs on the primary side (EE-type ferrite core) before being boosted nearly to 1.1 kV (maximum AC) on the secondary side (having 1800 turns). This voltage is then boosted using a voltage doubler circuit made up of two 1N4007 diodes and two capacitors (0.0022 uF) to approximately two times its original value, i.e. 2.2 KV (1.5kV value is w.r.t 3.5 volt). A polypropylene capacitor is then used to store the final stepped-up voltage. The board's maximum current usage is 0.581A. (max w.r.t 3.7 volt). The HaptiDrag electrodes are powered by the stored energy in the polypropylene capacitor. Fig 2.5 shows the complete

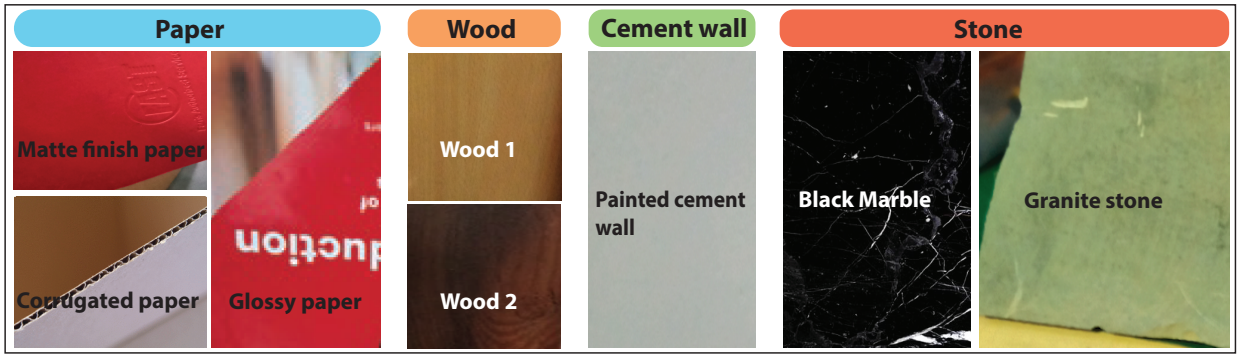

Figure 2.6: a) All eight surface information, where Wood-1 (W.L-2) and Wood-2 (W.L-1) represents wooden laminate having suede and brushwood texture

schematic of the excitation circuit with a real board. The entire dimensions and weight of the excitation circuit board are 60 mm by 25 mm and 40 gram, respectively. For a fully portable application, this custom-designed board can be readily substituted with a voltage boosting IC [4] (AGH Series) to reduce the overall system size, weight, and form-factor.

2.5 Technical Evaluation

In this section, I present the study on force distribution to drag the HaptiDrag over surfaces at different operating voltages in order to better understand its structure and performance as an actuator. All of the required experiments were carried out in the following conditions: humidity ranged from 45 to 58 percent, and temperature ranged from 18 to 21 degrees Celsius. The chosen experimental and user studies (described later) testing condition lies within the optimal indoor-work environment, i.e. 17-21 degree celsious [40] & 30-60 % humidity [41]. The eight insulator surfaces on which I conducted experiments belong to one of the following classes, i.e., wood, cement, stone, and paper as shown in Fig 2.6. These types of surfaces are ubiquitous and can be found in almost any setting (indoor or outdoor). The texture or material composition of these surfaces differs. Two surfaces are from the wooden laminate category, one is from cement (white paint on top of a black cement and pop mixture), two are from stone (one is black marble and the other is granite), and three

[4]https://www.xppower.com/product/AGH?m=AGH30N-5

Table 2.1: Power consumption (P.C) (in Watt) of the control circuit (C) with HaptiDrag (H) and just HaptiDrag (H)

Pad Size	**P.C at 3.5 V**		**P.C at 5 V**	
	C + H	**H only**	**C + H**	**H only**
5 x 5 cm	1.4 W	0.24 W	2.2 W	0.47 W
8 x 8 cm	1.8 W	0.42 W	2.8 W	0.61 W

are from paper (corrugated, matte, and glossy finish). I chose most commonly occurring forms of the chosen categories.

2.5.1 **Procedure**

I physically manufactured several pads (with good insulation on (and around) the entire electrode area) in various dimensions (A_1 cm x A_2 cm), such as 3 cm x 3 cm, 4 cm x 4 cm, 5 cm x 5 cm, and 8 cm x 8 cm, to evaluate the HaptiDrag functionality and identify the optimal (minimum) size of pad. The fabrication process is mentioned in section 3.2. Each pad weighs no more than 2 gram.

During testing, I used a Keysight power supply (Model No. E36300 Series) to power the excitation circuit separately. It's because of the flexibility it provides, as it allow to change the input supply value to the excitation circuit whenever required, rather than changing the PWM value in software and uploading it to the Arduino each time, which would take too many steps. Our method for measuring high voltages was based on the voltage divider rule (VDR), and the resistance I used in parallel to the HaptiDrag was a 10 M Ohm resistor (made up of a series combination of available quarter-watt 1 M Ohm resistors (total of 10)). The work of Li et al. [42] demonstrates that the VDR technique can be easily used to measure high DC voltages (in kV). Moreover, Küchler et al. [43] confirmed that the resistance divider is one of the most appropriate methods among the many divider designs presented in their work, particularly for measuring DC voltages. The high-value resistor was chosen empirically because I wanted to keep our board's overall power consumption minimum. VDR rule states

that if R identical resistors are connected in series and the voltage across one resistor is known, such as Y volt, the total voltage applied across the series combination of resistors can be calculated by simply multiplying the voltage (Y) by a factor of R. I used a voltage divider ratio of 1:10 to measure the high voltages. I chose this method because it allowed us to use the available measuring instrument (i.e., multimeter [5] in voltmeter mode with a 10 M ohm input impedance) to measure the total voltage (greater than 1 kV) applied to HaptiDrag, as shown in Fig 2.7a. Further, since I used an external load that is a high-value resistor (as previously mentioned) on the excitation circuit to measure the high voltages across HaptiDrag. As a result, I maintained the same loading effect on the excitation circuit in all subsequent evaluations.

To determine the current drawn by the HaptiDrag when in contact with the surface and when in air, a multimeter (in ammeter mode) was used in series with the HaptiDrag (without removing the resistor from the circuit). Fig 2.7b depicts the actual image of the current measurement process.

[5] https://www.keysight.com/in/en/product/U1252B/handheld-digital-multimeter-4-5-digit.html

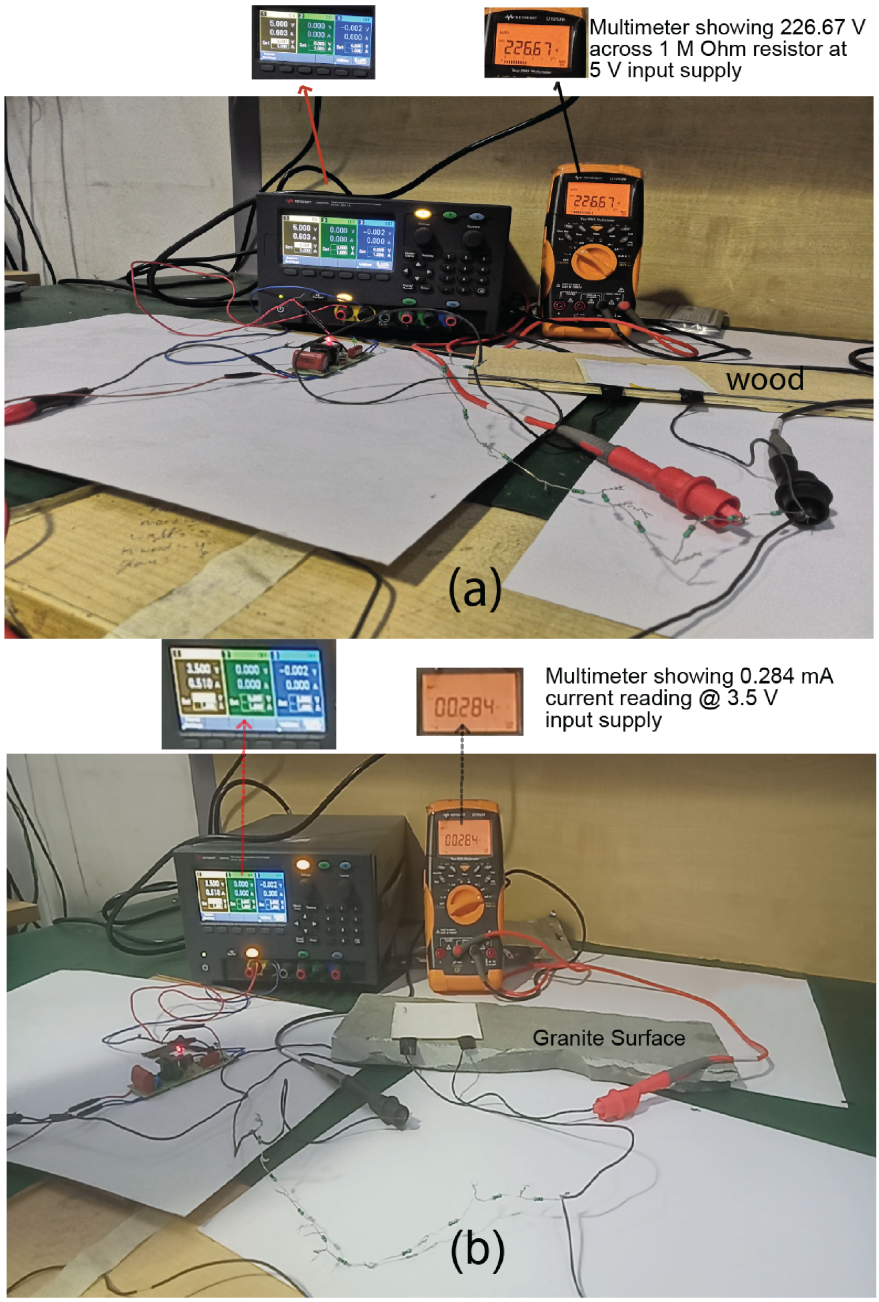

Figure 2.7: Voltage and current measurement setup. Figure a): presents a voltage measurement results across 1 M Ohm resistor which correspond to total voltage of more than 2 kV applied to HaptiDrag when 5 V input is applied to excitation circuit, and b): represents the maximum current reading obtained with respect to granite surface at 3.5 V input supply with respect to pad size of 8 cm x 8 cm.

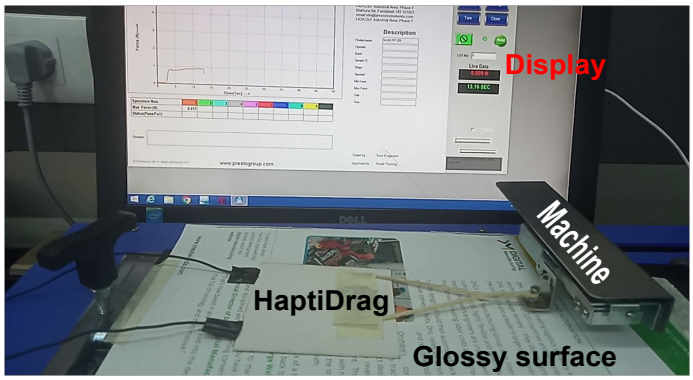

(a)

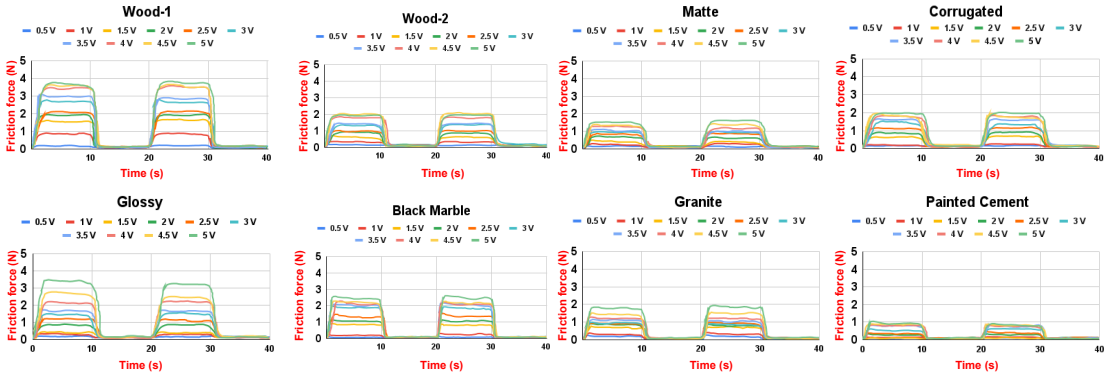

(b)

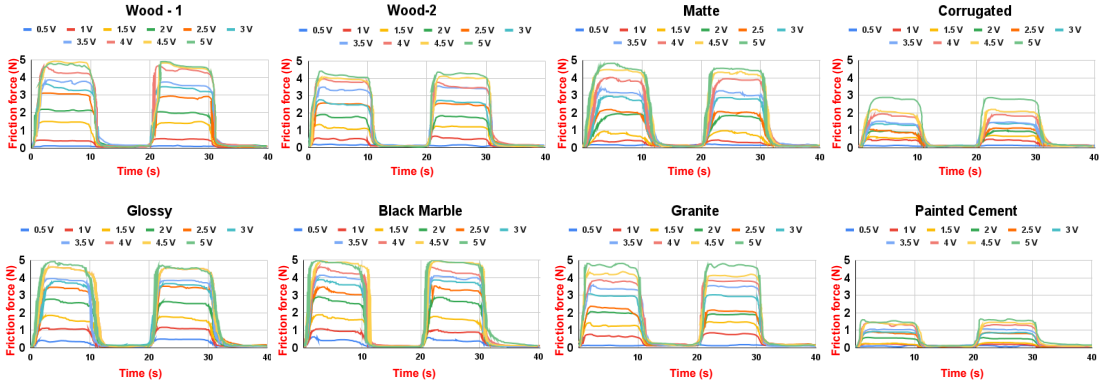

(c)

Figure 2.8: Measurements of friction (resistive) force offered by HaptiDrag at different voltages on all eight surfaces; In figure a): I show a measuring device in connection with HaptiDrag, b): result of friction force (N) vs. time (sec) by Pad1 (5 cm x 5 cm), and c): result of friction force (N) vs. time (sec) by Pad2 (8 cm x 8 cm).

Table 2.2: Input voltage (V) given to excitation circuit and output voltage obtained from excitation circuit

Input (V)	0.5	1.0	1.5	2.0	2.5	3.0	3.5	4.0	4.5	5.0
Output (V)	2	280	590	820	1109	1335	1585	1810	2070	2290

Setup for Conducting a Friction Measurement Test

I start by examining the performance of each size of pad (beginning with 3 cm x 3 cm) on each of the eight surfaces one by one (see Fig 2.6). The input supply to the excitation circuit for powering the HaptiDrag was adjusted in 0.5 volt steps from 0 to 5 volts. I mounted the device on a digital friction measurement tester (Presto, Model No. PCOF – S03 (C) [6]) equipped with a 30 N load cell to measure the static and kinetic friction force. The benefit of using this digital instrument is that it provides both static and dynamic friction data. Second, the results obtained will be less prone to human error (or observation error [7]), which is likely to occur when taking measurements manually. This instrument allowed us to drag the device horizontally along the surface without any manual support, up to 200 mm, while measuring the friction force, as shown in Fig 2.8a. A light-weight thread was attached to the pad (on the insulating side) for making connections with the load cell. I placed the minimum load (i.e., M = 0.010 kg) on the device every time while experimenting due to the light-weight nature of HaptiDrag and to keep the device in contact with the surface (when the supply is off during testing) while the machine is pulling the device (horizontally) along the surface. I chose this load because preliminary testing (without applying any voltage to HaptiDrag) revealed that the effect of load on friction between devices and surfaces was negligible (close to zero). With the power turned on, I began testing HaptiDrag. For each size of HaptiDrag, I ran two cycles (in one go) per surface per voltage at a constant speed of 2.5 mm/sec. Each cycle consists of one ON (for 10 seconds) and one OFF (for 10 seconds) process. Furthermore, 5 cm x 5 cm was the minimum pad size above which pads started to

[6] https://www.prestogroup.com/products-new/calculating-coefficient-of-friction/

[7] https://en.wikipedia.org/wiki/Observational$_error$

work well across the input supply range of 0 to 5 V and on all surfaces. Pads up to 4 cm x 4 cm in size did not show any force perception during testing. As a result, I chose 5 cm x 5 cm as the minimum reliable dimension for the design of HaptiDrag based on the findings obtained after evaluating all pad sizes.

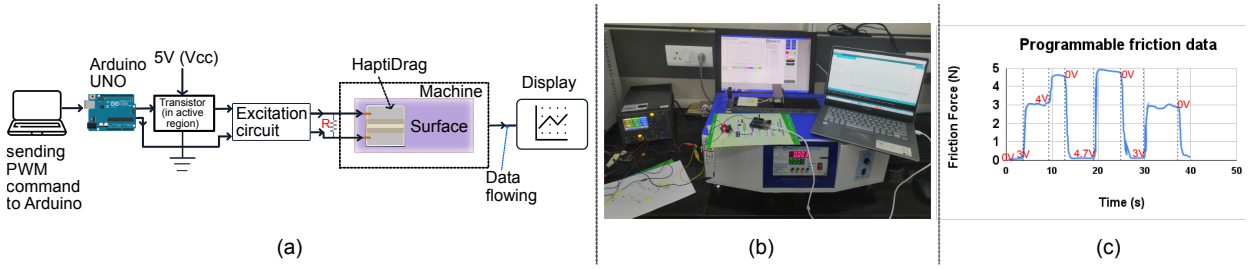

Figure 2.9: a) Left: Hardware schematic diagram is shown; b) Mid: real image of instruments and electronics used, and c) Right: Obtained friction result vs time. Values in red color, denote the programmed voltages given as an input to the excitation circuit.

Setup for Conducting a Programmable Friction Test

Following the technical exploration of HaptiDrag's friction behavior, I performed preliminary testings to see how the friction variation of HaptiDrag will occur while moving over the surface if the excitation circuit's input supply is changed programmatically. To conduct this experiment, I randomly selected the larger size (8 cm x 8 cm) pad. The following items were used in the experiment: surface (stone category), a laptop, an Arduino connected with the laptop, an excitation circuit, a friction measurement setup to drag HaptiDrag across the surface at a speed of 2.5 mm/sec, display (system) connected with friction tester machine to show real data, and a power supply to power the transistor (working in the active region). Fig 2.9 depicts a schematic (a) and a real image (b) of setup. During testing, only the PWM value (between 0 and 255) was changed on the serial monitor. Whenever the signal (PWM) was received, the transistor supplied only that amount of voltage as an input to the excitation circuit. The obtained friction variation result for each change of programmable input voltage is shown in Fig 2.9c (and in the video), confirming that the friction effect can be controlled programmatically.

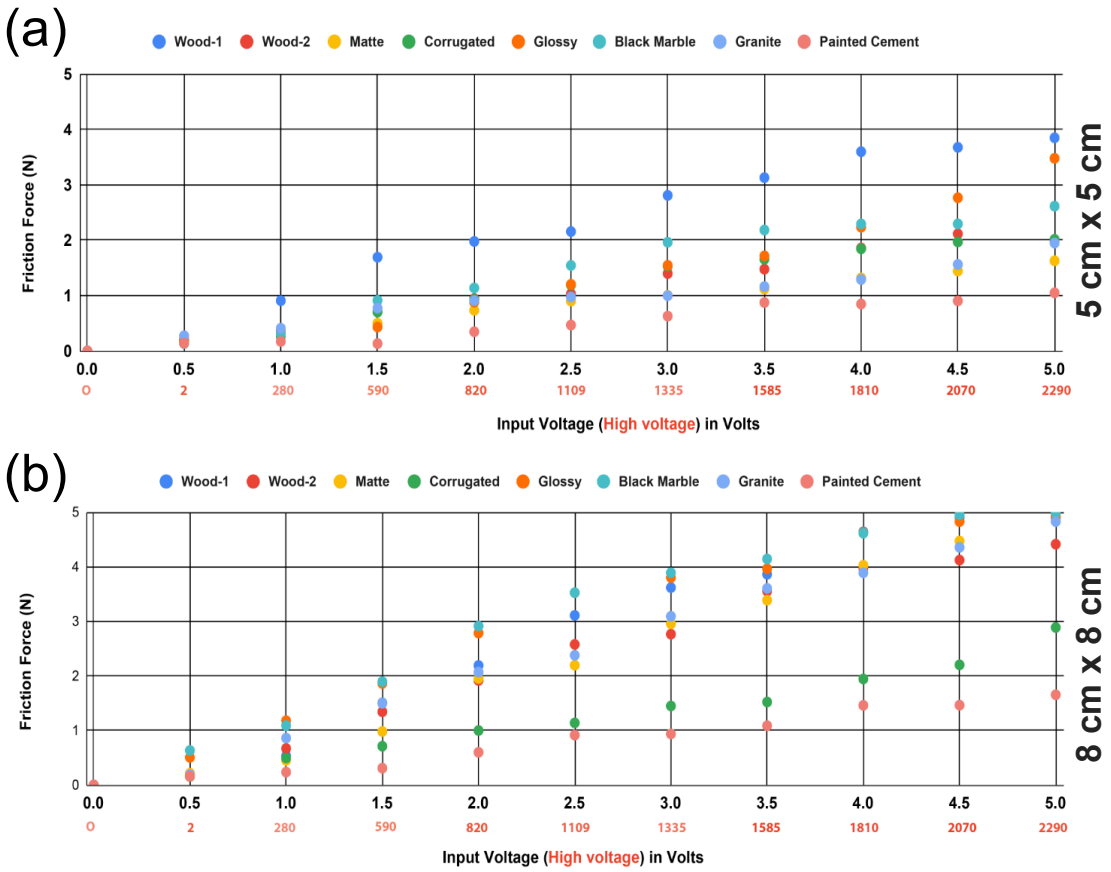

Figure 2.10: Friction (resistive) force vs. voltages with respect to all eight surfaces; In figure a): I show a result of friction force by Pad1 (5 cm x 5 cm), and b): result of friction force by Pad2 (8 cm x 8 cm); The X-axis in both graphs (a and b) provides details of both input and output voltage related to the excitation circuit. The estimated output voltages (i.e., in red) are derived from table 2.2.

2.5.2 Results

For a pull speed of 2.5 mm/s and DC actuation voltages ranging from 0 V to 5 V (i.e., from 0 V to 2.3 kV), Fig 2.8 (b & c) presents the friction force behavior with respect to time on various voltages for two different sizes of pad: 5 cm x 5 cm and 8 cm x 8 cm. I noticed that the force begins at zero and rapidly increases as slack is taken up. After that, the force reaches a plateau that corresponds to the braking force. When we switched the input supply between 0 V and 5 V, I discovered that the charging (activation) and discharging (release) times for the paper category of surfaces differed from the other three categories of surfaces. HaptiDrag demonstrated a discharging time of approximately 1.5 seconds on the paper category type of surface, whereas for the other three categories of surfaces, I discovered that HaptiDrag could only discharge within 1 second. Furthermore, for all eight types of surfaces, the charging time was found to be close to or within 1 second. I found that the HaptiDrag was able to discharge rapidly due to the external load (i.e., resistance) connected in parallel to the output of the excitation circuit (i.e., in parallel with HaptiDrag). External load added in this fashion worked like a bleeding resistor, creating a discharge path for the capacitor's residual charge to be rapidly released whenever the power supply was turned off (0 V). Based on this observation, it is recommended to place the resistor on the board during experimentation and mass production of high voltage circuit boards. Fig 2.10 depicts how the static friction force provided by HaptiDrag (both sizes) increases as the input supply changes for all eight surface materials and two different pad sizes. It indicates that the electroadhesive force rises with it as the input voltage rises. A total of 320 experiments were conducted (4 pad size x 8 surfaces x 10 voltage points). According to the findings, granite was the only surface on which HaptiDrag (both sizes) consumed the most current out of the eight. At a 3.5 V input supply, the maximum current value obtained for the 5 cm x 5 cm pad size was 0.137 mA, and the maximum current value obtained for the 8 cm x 8 cm pad size was 0.28 mA. In contrast, HaptiDrag (both sizes) consumed even less than 0.15 mA on the other seven surfaces (i.e., at 3.5 V). HaptiDrag (both sizes) current consumption in

the air was not more than 0.004 mA. Table 2.1 shows the data for HaptiDrag's maximum power consumption with (and without) control circuitry at two operating voltages, 3.5 and 5 volts (i.e., with respect to the granite only). Table 2.2 shows the input voltage (0 to 5V with a 0.5V step size) to the excitation circuit and the corresponding boosted voltage by the excitation circuit.

2.6 Formative Study

I conducted an exploratory study to look into the following two major concerns: 1) What is the minimum input driving voltage needed to provide a drag (or resistance) sensation across a surface with HaptiDrag above user perception? 2) What other input driving voltage point exists between 0 and 3.5 volts (max is 3.7-volt input supply) at which participants' drag (or resistance) sensation experience would be easily different from previous obtained points? I recruited 8 people with an average age of 25 (five males and three females) for this study, and each participant wore earplugs for the first two studies to eliminate biases from surrounding noises. For each of the eight surface materials, both research questions were assessed. I used the sliding gesture (Fig 2.11c) to experience a varying resistance effect with HaptiDrag on a surface. Instead of sliding the pad directly with the hand, which could introduce weight due to finger pressure, a lightweight fish-like object (randomly chosen to provide ease of holding) was attached to the pad, as illustrated in Fig 2.11a (type: wood, weight: 25 gram, dimension: 60 mm X 30 mm), and participants were requested to conduct the sliding action with it by holding it from the side. Furthermore, all participants were advised to hold this object (fish type) with only two fingers (i.e., thumb and index or middle finger) of their dominant hand during the experiment, as illustrated in Fig 2.11c. I did this to reduce the amount of pressure or additional weight on the device, which could cause biases in the results due to differences in hand weight.

All user studies (section 2.6 and section 2.7) conducted as part of this research were approved by the Institutional Review Board (IRB) of IIIT- Delhi. The study was carried

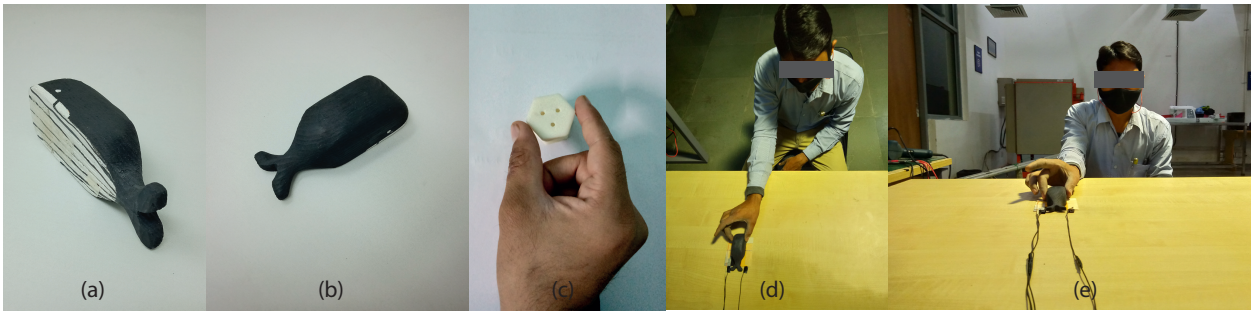

Figure 2.11: (a), (b)Fish object attached with HaptiDrag Pad used to slide pad over a surface; (c) Shows a two finger hand gesture adopted to hold fish object, and (d), (e): Shows real image of participant activity during a study

out in accordance with the ethical guidelines outlined by the board to ensure participant safety and well-being. Specific precautions were taken given the use of voltage step-up to the kilovolt range during the experiments. Comprehensive risk assessments were performed, and all participants provided informed consent prior to the studies. The devices used in both studies were designed to meet safety standards, ensuring no harm or discomfort to the participants."

2.6.1 **Procedure**

I used a minimum-sized prototype with dimensions of 50 mm × 50 mm to conduct the experiment because it was the smallest size prototype that was found to be functional throughout technical testing. Furthermore, the results obtained with this pad could also be used to validate other pad sizes and determine HaptiDrag overall accuracy. All participants were given device-related safety guidelines and requested not to share or discuss the device's performance with other participants after the study. There were two parts to the experiment: first, I gathered answers from participants to determine the first absolute detection threshold (ADT), or the least input supply for each surface at which participants felt resistance while dragging HaptiDrag. The second phase was dedicated to locating a new level of drag (or resistance) effect points that can be distinguished from the previously obtained absolute detection threshold points.

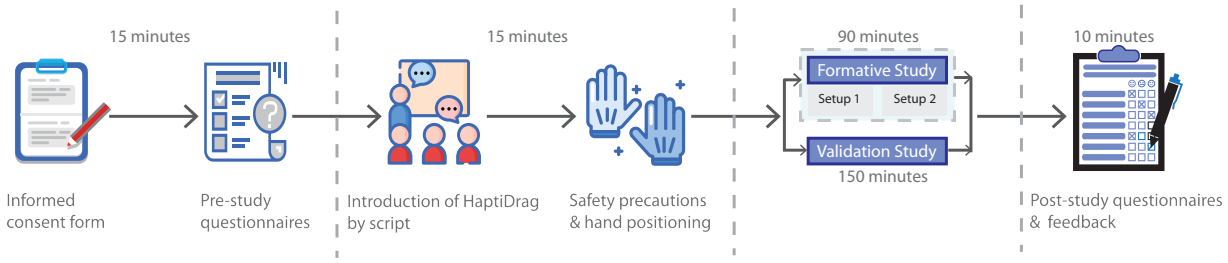

Figure 2.12: The procedure adopted to conduct both user studies: formative as well as validation

The data obtained will provide information on the optimal input driving voltage points to utilise with HaptiDrag as an actuator for interaction purposes. During the study, I employed an external power supply to actuate the HaptiDrag numerous times at varying input driving voltages. Fig 2.12 depicts the overall flow of the formative study.

2.6.2 Setup-1: Find Absolute Threshold Point where Force Can Be Noticed

I used a random (double) staircase approach [44] to discover all detection threshold points within a voltage range of 0 - 3.5 volts to investigate both research questions. This methodology is based on a review of numerous previous HCI research papers in which authors have utilised this method to determine the absolute detection threshold (ADT) point. For example, HapSense [45] used this method to determine the minimum perceptible intensity of vibration levels. Other works, such as PoCoPo [46], used this method to determine the virtual object's minimal size, while Jetto [47], used it to determine the smallest detectable change in force magnitude. To investigate this first research question, I assembled eight different types of surface materials, as described in the technical evaluation section. I used 20 steps per staircase in the random (double) staircase method. The descending staircase's beginning stimulus intensity for HaptiDrag was 3.5 V, with a step size of 0.5 V (a point where drag is maximum, in a voltage range of 0 to 3.5 V). I kept the 0.5-volt step size because the difference in drag effect was found to be modest during pilot testing within the 0.5 range.

HaptiDrag's floating parts, such as its floating copper electrodes, were properly insulated

Table 2.3: Absolute detection threshold value (in Volts) per participant for each of the eight surfaces where resistance (friction) effect is perceived

Surface Name	P1	P2	P3	P4	P5	P6	P7	P8
Wood1	1.32	1.2	1.11	1.37	1.18	1.35	1.4	1.38
Wood2	1.1	1.43	0.9	1.15	1.26	0.98	1.32	1.37
Black Marble	0.765	0.92	1.12	0.87	1.2	0.73	1.03	0.86
Granite	0.87	0.71	0.82	0.9	1.1	0.96	0.77	0.79
Matte Paper	1.22	1.15	1.4	1.33	1.21	1.77	1.15	1.18
Corrugated paper	1.4	0.98	1.36	1.22	1.07	1.3	1.26	1.18
Glossy Paper	0.9	1.2	1.12	1.06	1.17	0.93	1.15	1.3
Painted Cement Wall	1.35	1.47	1.4	1.72	1.65	1.57	1.7	1.2

according to industry standards [37]. In the method demonstrated in Fig 2.11c, participants maintained contact with the pad by the use of a fish object. I advised users to rest their arms on the table during the trial to avoid any interaction effects caused by weariness. Each participant then tested the pads on all eight surface materials.

Participants were permitted to drag HaptiDrag numerous times in order to memorise the perception of the initial drag (or resistance) effect once the voltage is applied. A minimum stimulation duration gap of 5 s was provided between each change in input driving voltage. During this 5-second period, the pad was kept at 0 V to ensure participants that there was no adhesive effect between HaptiDrag and the surface material. Participants were asked to answer "Yes" or "No" to the following question: "Do you experience any drag (or resistance) impact" for each step change/iteration, so that the next input driving voltage level given to HaptiDrag could be adjusted accordingly. Finally, the absolute detection threshold was calculated by averaging each ladder's last ten reversals.

Results

Table 2.3 depicts the absolute detection threshold point (i.e., a minimum input voltage) for all surfaces where each participant felt the applied force to drag HaptiDrag. It can be observed (Table 2.3) that the absolute detection threshold for all surfaces is less than 1.8 V. According to these findings, for delivering noticeable stimulation (i.e., initial resistance effect)

with HaptiDrag actuation to a wide range of users on many types of surfaces, keeping the input driving voltage at least 1.8 volts (absolute detection threshold point) is recommended. The corresponding high voltage value of 1.8 V is 748 V. Because the obtained absolute detection threshold value is significantly lower than the maximum input driving voltage (i.e., 3.7 V) that can be delivered to HaptiDrag, there is room to explore other detection threshold points capable of producing a perception of resistance effect of a different intensity than that experienced at 1.8 V. In the next section, I expand on the experiment that was conducted to investigate another detection threshold.

2.6.3 Setup - 2: Determine New Threshold Value where Drag Easily Discerned

I next looked into the second research question (RQ-2), which was to locate another input driving voltage point between 1.8 and 3.5 volts (max is 3.7 volt input supply) at which participants' drag effect experience would be easily distinguishable from drag (or resistive) effect at 1.8 V. All of the participants were first told about the second study's purpose. Then, one by one, each participant was assigned to a user study area based on their preferred time slot. In this investigation, I employed the same setup and random (double) staircase approach [44] as in the prior study.

Because I needed to locate another drag effect point separate from the drag effect at 1.8 V, the beginning stimulus intensity for ascending staircase in this experiment was 1.8 V (result from the first study). The investigation began with a 1.8-volt driving voltage so that each subject could memorise their perception of drag at this voltage. Participants were also free to request that they be given the 1.8 V experience again after completing any iteration (in any sequence, ascending or descending).

After each step/iteration, each participant had to respond to the following question: "How was the intensity of the drag effect experienced as compared to the effect at 1.8 V?" in terms of "Higher (Yes)" or "Lower/Same (No)" so that the next input driving voltage level applied to HaptiDrag could be adjusted accordingly. Finally, the threshold was calculated

Table 2.4: Another distinct (second) detection threshold point (in Volts) per participant for eight surfaces where resistance (friction) experience differed from the previously obtained ADT value (i.e., 1.8 Volts)

Surface Name	**P1**	**P2**	**P3**	**P4**	**P5**	**P6**	**P7**	**P8**
Wood1	2.81	2.89	2.57	2.71	2.94	2.88	2.72	2.51
Wood2	2.56	2.72	2.7	2.89	2.91	2.97	2.77	2.67
Black Marble	2.3	2.36	2.21	2.41	2.37	2.45	2.15	2.34
Granite	2.42	2.25	2.17	2.38	2.3	2.43	2.31	2.2
Matte Paper	2.7	2.77	2.68	2.91	2.96	2.78	2.88	2.51
Corrugated paper	2.54	2.76	2.81	2.72	2.91	2.86	2.93	2.97
Glossy Paper	2.78	2.83	2.67	2.79	2.66	2.72	2.88	2.91
Painted Cement Wall	3.2	2.91	2.96	3.1	2.96	2.84	2.86	2.96

by averaging each ladder's last 10 reversals. Between each change in HaptiDrag's input driving voltage, a minimum stimulus duration interval of 5 s was provided. During this 5-second period, the pad was kept at 0 V to confirm that there was no adhesive effect between HaptiDrag and the surface material.

Results

Participants' responses are shown in Table 3.1, which shows the detection threshold of sensations at which the higher drag (or resistance) effect was felt. As shown in the table, the threshold point for paper and wooden surface materials ranges between 2.5 and 3; for stone, it varies between 2 and 2.5; and for cement, it varies between 2.5 and 3.2. And if I have to pick one value that will function for all surfaces and produce resistance (or friction) sensations that will be different from those obtained at 1.8 V, then, based on the results, it is recommended to keep the threshold point at least 3.2 V (corresponding high-voltage value is 1410 V) for delivering distinct stimulation (or resistance effect) to a wide variety of users. Because the other detection threshold point obtained is close to 3.5 V, there's no room for another ADT point to be found in the voltage range of 0 to 3.5 V.

2.7 Validation Study

In the formative study, I obtained two detection threshold points, 1.8 V (748 V) and 3.2 V (1410 V), with the smallest size of pad at which the perception of initial resistance (or drag) effect was easily distinguishable due to the difference in their friction intensities (i.e., the resistance effect perceived is greater at 3.2 V than at 1.8 V). In this section, I aimed to answer the following questions in order to validate the distinguishability of both detection threshold points and generalise them to other sizes of HaptiDrag devices:

- 1) On all surfaces, how accurately can a user distinguish between the perception of two intensities of the device's initial resistance effect at both HaptiDrag detection threshold points?
- 2) On all surfaces, how accurately can a user distinguish between the perception of two intensities of the drag effect (i.e., resistance experience while moving) offered by the device at both HaptiDrag detection threshold points when the device is in motion?

The overall flow of the validation study is depicted in Fig. 2.12. Both research questions were also tested with different weights (i.e., up to 100 gram) to see how weights affected user perception. Two different sizes of prototypes were used in this study to validate and generalise the obtained threshold points. One is 50 mm x 50 mm in size, while the other is 80 mm x 80 mm in size.

2.7.1 Participants

I recruited ten people for this study (M = 24; SD = 2.63; 4 females). The tasks were completed by the participants on each type of surface (a total of eight, as shown in Fig. 2.6). Resistance sensations at these two detection threshold points, 1.8 V and 3.2 V, were validated on all 8 types of surfaces and with all subjects. Participants first completed a static friction perception study (when the device was initially at rest), followed by a kinetic (or moving) friction perception study (when the device was initially in motion).

2.7.2 Procedure

Below, I explain three sections, the first of which discusses steps taken to validate the initial resistance force offered by the pad, the second of which discusses steps taken to validate the study conducted on resistance force perception while the device was in motion. Finally, in the third section, I mentioned steps that were common to both studies.

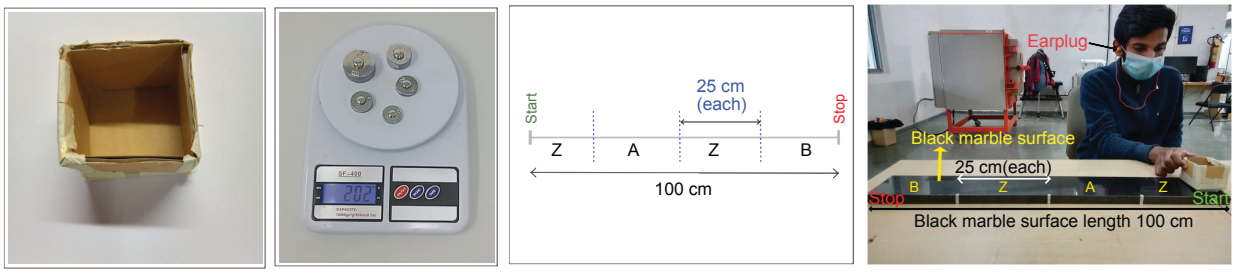

Figure 2.13: (a) Light-weight corrugated cubioid shape object used with pad during the study, (b) Weights using which combination of weight were prepared upto 100 gram, (c) Kinetic study scenario related to the perception of varying resistance effect on surfaces when the device was in motion initially, d) real kinetic study scenario

Static Friction Perception Study Procedure

Participants in this study were told that they would have to distinguish between two intensities of the device's initial resistance effect. There are four possible combinations with two inputs (1.8-Low, 3.2-High): HL, HH, LL, and LH. As a result, each participant had to complete four iterations, one after the other, on all eight surfaces and with varying weights. During the experiment, the effect was first introduced in the device, and then participants were asked to experience and memorise the device's initial resistance effect while slowly dragging it over the surface. In this manner, after experiencing both effects one after the other (referred to as one iteration), participants were required to identify the intensity of both impacts, i.e., which is higher and which is lower, after each iteration. Furthermore, if the strength of both impacts was the same, they had to determine the type of both effects, such as whether they were High or Low in intensity, and then mark them on the sheet accordingly.

Before the start of the first effect, in between the two effects during the study, and after the completion of each iteration, the pad was always kept at 0 V to confirm that there was no adhesive effect between HaptiDrag and the surface material. The minimum duration for which the device was kept at 0 volts during the study was no more than 5 seconds.

Kinetic Friction Perception Study Procedure

Participants in this study were told that they would have to distinguish between the perception of two intensities of the device's drag effect (also called continuous friction effect) while in motion. To begin this experiment, I arranged all eight types of surfaces to have at least 100 cm x 10 cm dimensions. The overall study flow is shown in Fig 2.13c, and the two marked positions with the letters "A" and "B" are where the effect was introduced in the device. Participants were instructed that in each iteration they would be required to slide the device (HaptiDrag) across the surface for atleast 100 cm continuously. They were also told to not slide the device at a speed of not more than 3 cm/sec (on which more details are presented in next paragraph). And while sliding the device, they would then encounter two resistance effects at these two points (labelled as 'A' and 'B' in Fig 2.13c and also in real image of the study in Fig 2.13d), which they needed to experience and remember. Once they had gained experience, they had to mark their response on the sheet, i.e., which drag effect was higher and which one was lower, after each iteration. Furthermore, if the strength of both impacts was the same, they had to determine the type of both effects by mentioning in the same sheet, such as whether the drag effects were High or Low in intensity. There are four possible combinations with two inputs (1.8-Low, 3.2-High): HL, HH, LL, and LH. As a result, each participant had to complete four motion iterations, one after the other, on all eight surfaces and with varying weights. To confirm that there was no adhesive effect between HaptiDrag and the surface material, the pad was always kept at 0 V in the following cases: before the start of the study, at these positions labelled with Z shown in Fig 2.13c i.e., during the study, and after the completion of each iteration.

To ensure that participants slide the device over the surface at a minimum speed (not more than 3 cm/sec) during experiments, I ran a practice session based on a method of repetition [48] prior to the start of the experiments in which each participant slid the device over the surfaces 5 times per weight. During the practice sessions, no drag effect was introduced in the device. It is because I wanted each participant to become used to of this kind of slow motion so that they could easily use this understanding in real experiment. Each participant was explicitly told that they had to complete their sliding distance (100 cm) not before 35 seconds. In practice sessions, I used the following items: a measuring tape to mark the 100 cm distance across the surface and a timer to provide visual feedback to participants on their training results. All participants were trained on all eight surfaces.

Common Steps Taken in Both Previous Two Studies

To hold and drag the device on the surface in both studies as well as in training sessions, I attached a light-weight cuboid shaped corrugated sheet box (dimensions: 4 cm x 4 cm x 4 cm) which was opened from the top as shown in Fig 2.13a. It was kept open from the top so that I could easily change the weight with another one in a combination of 25, 50, 75, 100 gram. I tested both sizes of the HaptiDrag device up to 100 gram and started the study with 25 gram of weights. All participants were instructed to use their dominant hand during the study and wear earplugs to eliminate biases from surrounding noises. I used an external power supply in both studies to actuate the HaptiDrag at different thresholds. To eliminate the learning effect, I randomised the order of the test parameter combinations (a total of four combinations) for all participants. Prior to the commencement of the actual study on each surface and with each type of weight, each participant went through two training iterations to familiarise themselves with both thresholds. Individuals were also given a 10-second break in between iterations to refresh their minds. During the iteration, participants were also free to ask the facilitator to repeat any effect. A total of ten people participated in each of the two studies (static and kinetic). Of a total of ten participants, half of the ten participants

performed experiments with lower-sized prototypes (5 cm x 5 cm) and the other half with higher-sized ones (8 cm x 8 cm).

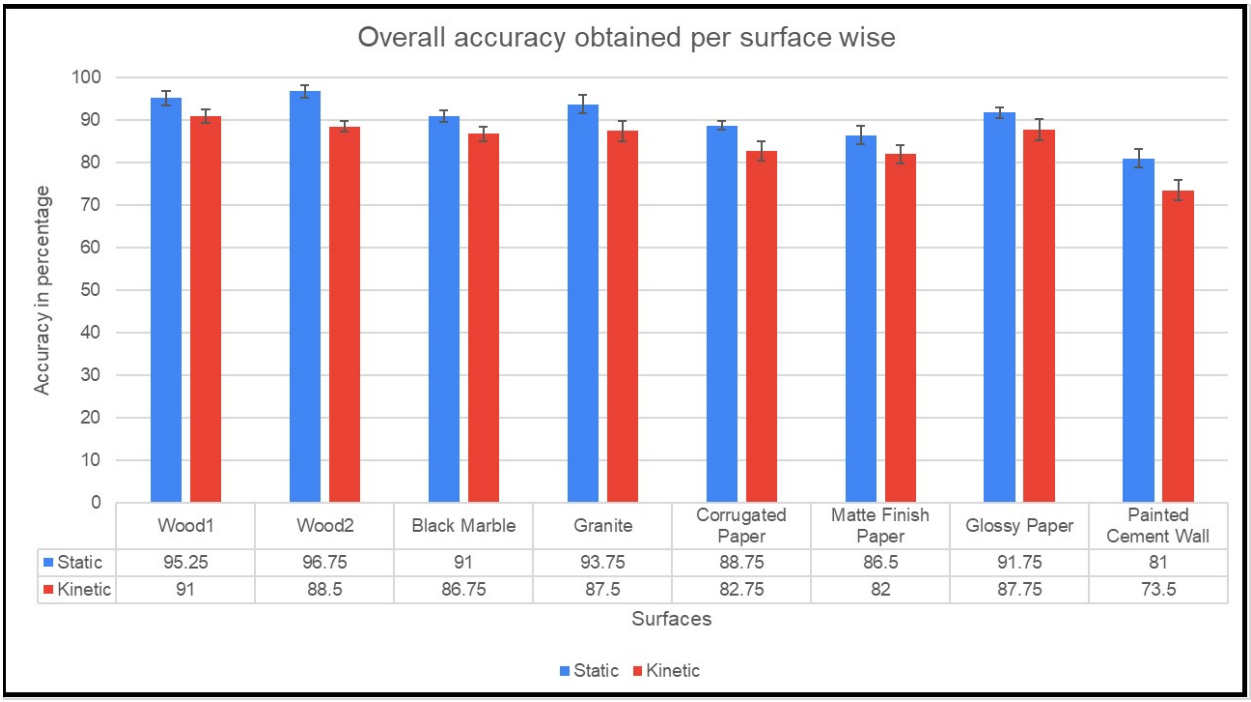

Figure 2.14: Participants average accuracy obtained surface wise

Following the completion of each experiment per surface and weight, participants were asked to rate their effort on a 7-point Likert scale, which they exerted in distinguishing and accurately identifying both effects and thresholds. On a 7-point Likert scale, 7 means no effort at all and 1 indicates too much effort. A total of 5120 data points were collected using the prototype (10 participants $\times$ 8 surface material $\times$ 8 iteration (4 in static case + 4 in kinetic case) x 2 threshold points x 4 weights). The duration of the validation study was about 2.5 hours per participant.

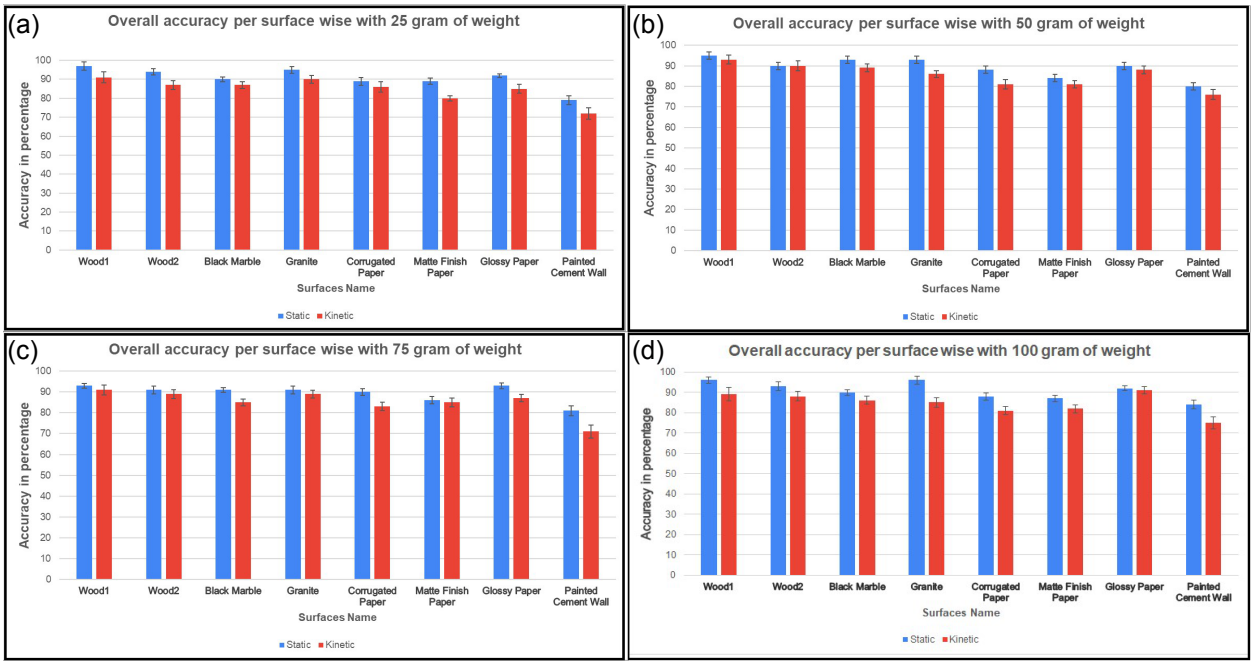

Figure 2.15: Participants overall average accuracy obtained per surface and weight wise starting from a)top left: 25 gram, b) top right: 50 gram, c) bottom left: 75 gram, and d) bottom right: 100 gram

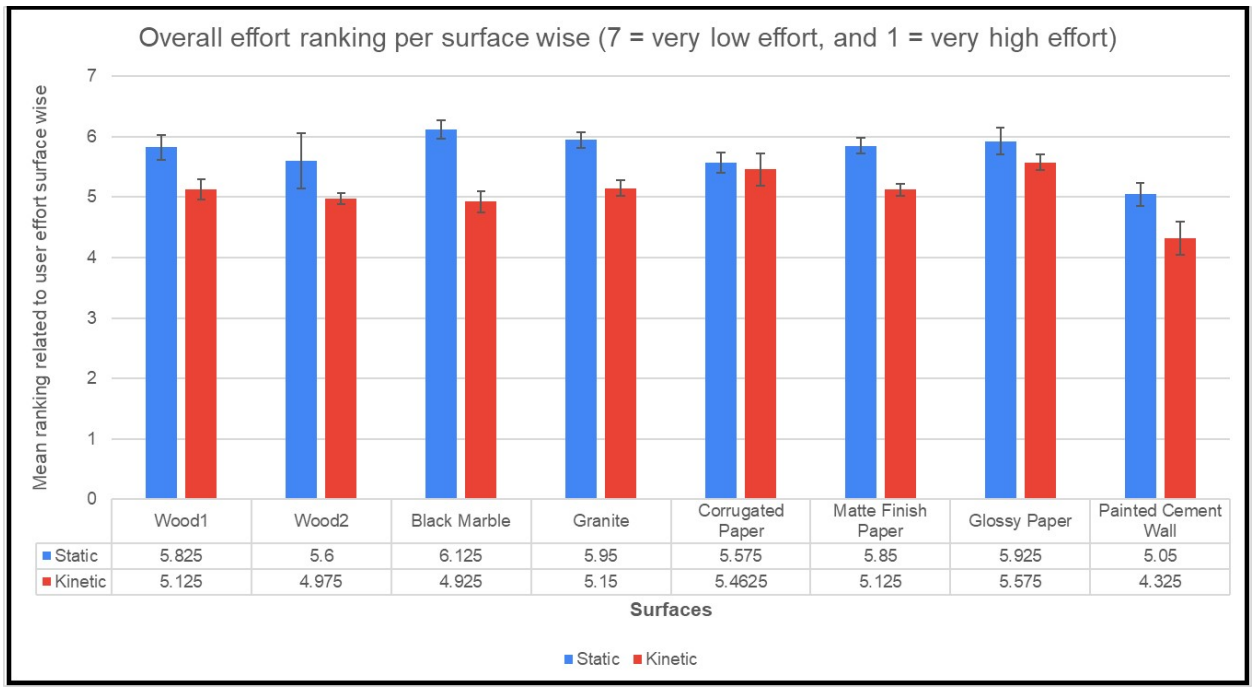

Figure 2.16: Mean ranking orders with Standard Deviation surface wise

2.7.3 Results

The data from the training blocks was not used in the outcome analysis. Fig. 2.14 depicts the participant's average accuracy per surface in each case, static and kinetic, in correctly identifying both HaptiDrag absolute detection threshold points. The overall average accuracy for static cases was determined to be 90%, and for kinetic cases, it was determined to be 85%. For the wood, stone, and paper categories, the average accuracy in each static and kinetic part remains close to or greater than 90% and 85%, respectively. While the accuracy for cement categories was found to be close to 80% in the static case and 73% in the kinetic scenario. It is worth mentioning that the accuracy of the cement surface was less than that of the other three categories, but not by much, so that the cement surface can be overlooked while designing digital interactions. Fig 2.15 represent the weight wise results in both scenario static and kinetic. As can be seen in Fig 2.15, except for the cement surface, and even testing with different weights in discerning between both thresholds in both static and kinetic scenarios, I found no significant change in overall user perception accuracy for other surfaces when each scenario (static and kinetic) was examined separately. However, I discovered a slight difference in user perception accuracy between the kinetic and static scenarios, as confirmed by the Friedman test ($\chi^2(1) = 8$, $p < 0.05$) and post-hoc Wilcoxon signed-rank test ($p < 0.05$), indicating a statistically significant variation between the two conditions. This difference was driven by the fact (i.e., post-study feedback analysis) that the initial resistance felt by participants with respect to any weight and surfaces from HaptiDrag in the static scenario at both thresholds was higher and differentiable than the resistance felt when the HaptiDrag was in motion at both thresholds (a kinetic scenario). For this reason, participants were able to perceive and more accurately differentiate between resistance effects at two thresholds in the static case than in the kinetic case. I also found as per participants post-study feedback analysis that, despite that, the resistance perceived at two thresholds while dragging HaptiDrag over the surfaces (in the kinetic case) was less intense, but they were still able to differentiate with good accuracy. Moreover, for some surfaces, it was close

to 90%. It was due to the fact that the intensity of friction force increased significantly in the presence of electroadhesive force compared to when there was no electroadhesive effect [49]. The user study results also confirm that it was the effect of the electroadhesive force (explored in technical evaluation section 5) that, whenever introduced in addition to the normal reaction force (due to weights), caused the participants to experience different intensities of friction force from the same surface in both scenarios, namely when there was no electroadhesive effect between the HaptiDrag and the surface and when there was an electroadhesive effect. And, as shown in Fig 2.16, the effort put in by participants to recognise both thresholds (ADT) was found to be moderate (not at all very high) in both static and kinetic cases, according to 7-point Likert scale responses. However, according to the responses obtained, participants put slightly more effort into recognising the threshold when the device was initially in motion (i.e., a kinetic scenario) as opposed to the static case, i.e., when the device was initially at rest.

2.8 Example Scenarios

The examples provided show how HaptiDrag can be utilised in a variety of scenarios.

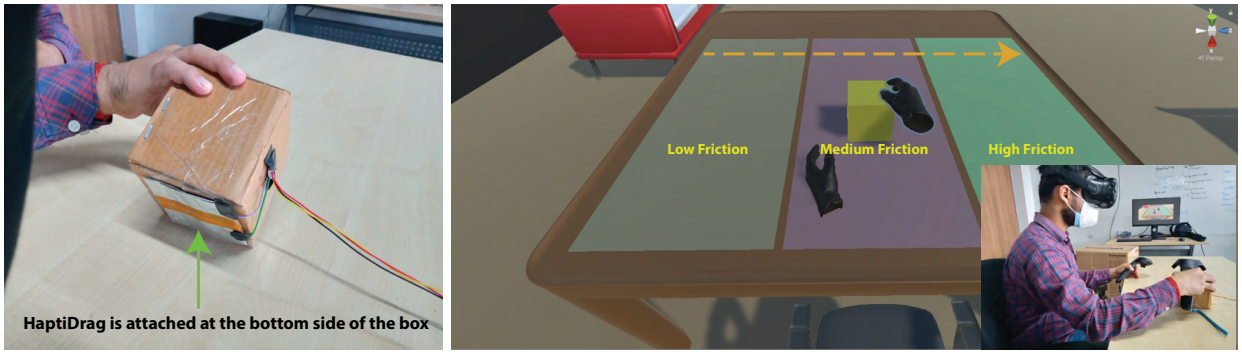

Figure 2.17: Supporting the learning experience of variable intensity of friction effects in VR

2.8.1 VR Scenarios

Perception of Friction:

Simulators are now being used to illustrate and teach users about abstract concepts that are generally difficult to grasp [50–52]. Simulators have an advantage over traditional laboratory experiments in that they can be configured in a variety of ways and used for a variety of purposes. Because of the benefits of simulation-based learning, I show that the HaptiDrag device while dragging in the real world can simulate a variable-intensity friction effect of different surfaces in a virtual reality environment, allowing users to learn friction concepts or experience different surfaces' roughness in virtual reality. For example, in Fig 2.17, I showed three surfaces in a VR world. And when the user drags the light-weight corrugated sheet prop as a counterpart to the VR box three times across all three surfaces, the user will experience a different intensity of resistance effect on all three surfaces. This experience will not only increase their understanding of the concept but also enhance their engagement with it.

2.8.2 For Visually Impaired People

Visualisation of Graph on Desktop

HaptiDrag's integration with devices like the mouse can make graph patterns easier to visualise for visually impaired. When dragging the mouse (weight of mouse was 60 gram and model [8]) over the graph area on the screen, for example, the mouse will offer a minimal (or zero) drag effect, which makes the user's motion perfect; however, once the mouse moves away from the graph line, the user will encounter a high resistance effect through the mouse. This experience demonstrates the potential for visually impaired people to gain confidence by visualising the graph for better understanding Fig 2.18a.

[8] https://www.lenovo.com/in/en/accessories-and-monitors/keyboards-and-mice/mice/KB-MICE-BO-300-Wireless-Mouse-WW/p/GX30K79401

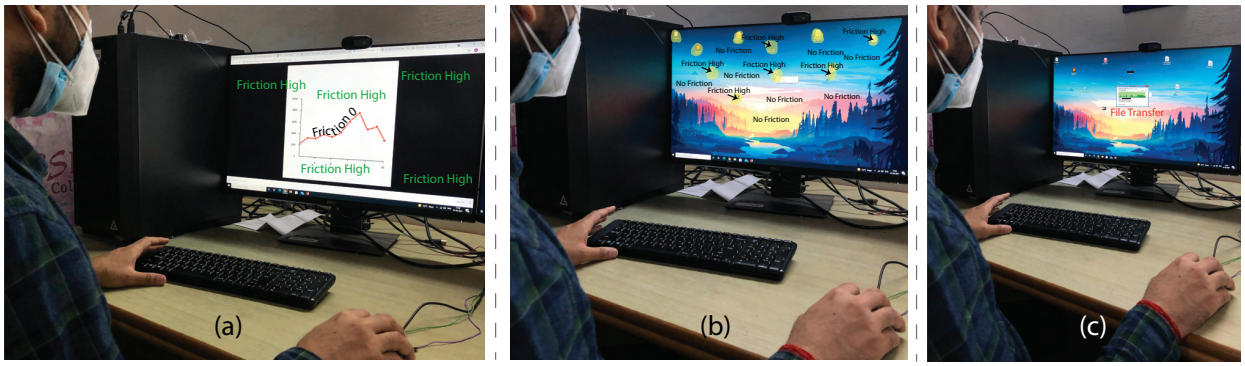

Figure 2.18: (a) Supporting graph visualisation, (b) and perception of icon while hovering HaptiDrag over it, (c) Dragging a file

Feedback of Icon Perception While Hovering the Mouse

Another scenario is when the mouse is hovered over the icons. The mouse will give them a lot of resistance as a signal that they're on an icon, but no resistance in other areas (when the cursor isn't on icons) Fig 2.18b.

Dragging a File

When dragging a file from its place towards another folder. In this case, varying the drag effect's intensity could give visually impaired people a sense of the size of the file they're dragging to. When dragging, for example, a KB file will provide zero resistance, an MB file will provide low resistance, and a GB file will provide high resistance as depicted in Fig 2.18c.

2.9 Limitations

In this research, I presented a device that can provide variable friction effects with respect to real physical surfaces. Perception of friction effects has been investigated on flat surfaces but not on curved surfaces. Apart from this, I excluded the following category of surfaces from our investigation: one is metal and the other is plastic. They were not included because, in the metallic surface case, due to the electrical nature of the device, the whole body of

the metal surface becomes too conductive, creating discomfort, and for plastic category surfaces like acrylic, the voltage requirement to polarise the surface was more than 3 KV. I intend to include these types of surfaces in future work by developing a method in which users can experience variable intensities of friction effects through devices without modifying the surface texture and/or generating very high voltage to polarise these surfaces. Other than this, the control circuit, especially the excitation circuit, which looks a little larger in size, can be easily replaced by smaller size and lightweight IC's [9], thus opening the option to use HaptiDrag even for portable applications. Additionally, in future work, I also plan to conduct studies in other environmental conditions to make the explored device robust with respect to all environmental conditions. Another limitation of HaptiDrag is its discharging time (as found during technical evaluation), which was approximately 1.5 seconds on paper-like surfaces, compared to under 1 second on other surfaces. While user perception studies indicated that this delay did not significantly impact the overall experience in standard interaction scenarios, it may become more noticeable in fast-paced applications where immediate feedback is essential. However, this is not a major concern, as it can be addressed by integrating an optimized RC circuit (comes in many sizes, e.g., CMOS RC timers[10]) with HaptiDrag. These minor enhancements would reduce latency perception while preserving the system's simplicity and accessibility.

2.10 Conclusion and Future Work

Prior methods to create variable friction effects have primarily relied upon mechanical approaches and hence, they are difficult to create, integrate, and programmatically regulate or control. To this end, I proposed HaptiDrag which is a thin device that can produce different levels of drag effects on multiple surfaces. I hope that this will enable designers to use such (drag) effects as haptic feedback to improve users' digital interaction. The HaptiDrag functionality was tested and validated in a technical and user-based study. I showed examples of

[9] https://www.xppower.com/product/Q?m=Q20N-5
[10] https://shorturl.at/BTmhq

HaptiDrag in action, demonstrating how it can be used to create meaningful and practical interactions. HaptiDrag will inspire designers and researchers to further explore this technology and develop novel interactions based on the feedback capabilities it provides. HaptiDrag will pave the way for futuristic interactions in a variety of application areas, including the design of haptic VR controllers and tangible haptic interfaces.

We demonstrated HaptiDrag's capability on eight different types of surfaces. However, its utility can be extended to other surfaces following the similar design methodology as proposed in the current work. Future work can extend this utility and can further evaluate variety of other HaptiDrag shapes and sizes, including higher weights and higher speeds. Further, the size of the controlling board can be minimized to make it even more portable and lightweight.

CHAPTER 3
MOBITANGIBLES

3.1 Introduction

Numerous precision hand-held tools embedded with a miniature control exist, e.g., as shown in Fig. 3.1, which are used in tasks like crafting, detailed engraving, precise cutting of materials (e.g., sheets, fabrics), precise measurements, precise airbrushing. The operational efficiency of such hand-held tools depends on the effective and accurate manipulation of their embedded miniature control. Hence, significant proficiency and extensive hands-on experience with the miniature control of hand-held tools are necessities in order to maximize precision and control during intricate tasks [53]. Additionally, this expertise with hand-held tools' miniature control empowers users to finely manipulate the tool's functions, ensuring accuracy and efficiency in tasks that demand meticulous control and attention to detail [54, 55]. For instance, when precisely carving surface [56], polishing/finishing intricate jewelry designs [57], precisely dispensing droplets in chemical reactions [58, 59], or delicately desoldering SMD components from PCBs/motherboards [60, 61]. Virtual reality (VR) technology serves as an excellent training tool in various fields, from operating surgical instruments to space mission training [62, 63]. However, using a VR device controllers for realistic training on the intricate nuances of precise miniaturized interactions intrinsic to precision hand-held tools, as shown in Fig. 3.1, poses a challenge as it typically offers only a button-pressing experience ([64–67]).

Furthermore, existing methods, e.g., [11, 68], to enable hand-held tools' miniature control interaction experiences in VR also suffer from significant drawbacks in terms of prototyping complexities. To design and prototype each precise and constrained type of miniature control manipulation in functional form, the complexity associated with such approaches includes

significant electronics parts and motor integration, design software-based prototyping and extensive assembly processes, and the need for technical expertise. As a result, this presents a significant barrier for early-stage learners who have not been exposed to such knowledge and also for those who have limited resource availability or accessibility, particularly in low-resource settings. As per the UNICEF report [69, 70], the population of individuals in this category is considerably larger, especially in resource-constrained settings, compared to those who have access to essential technical knowledge and resources.

Furthermore, numerous other studies (e.g., [14, 71–76]) have demonstrated diverse applications of their proposed hardware prototypes for simulating VR experiences across various domains, including entertainment and gaming. However, they notably lack in simulating hand-held tools' miniaturized control interaction experiences in VR, which are critical for remote working (and handling) and skill training related to such hand-held instruments beyond entertaining experiences [77–81]. Therefore, a solution is required that is a low-cost, user-friendly, simple-to-use VR platform that can offer realistic hand-held tool's miniature control interaction experiences and does not include such complexity in its technique.

Accordingly, in this work, I introduce MobiTangibles, a novel concept that enables hand-held tool's miniaturized control interaction experiences in VR. MobiTangibles, developed after a detailed analysis of over 30 commonly used precision hand-held tools, can simulate two fundamental types of hand-held tools' miniature control manipulation motion—specifically, single-axis linear translation and single-axis rotation motions. At the core of MobiTangibles lies the foundational principle of magnetic field sensing, harnessing the inherent capabilities of modern smartphones to enable the execution of these intricate physical manipulations, i.e., miniature controls, within the immersive VR environment. Operating in a passive manner without requiring external power sources, these physical manipulation proxies, namely MobiTangibles, are capable of delivering authentic miniature control interactions of hand-held tools in the VR environment. Their functionality is effortlessly activated by connecting them to a smartphone, a device ubiquitous today, thus eliminating the logistical challenge of ac-

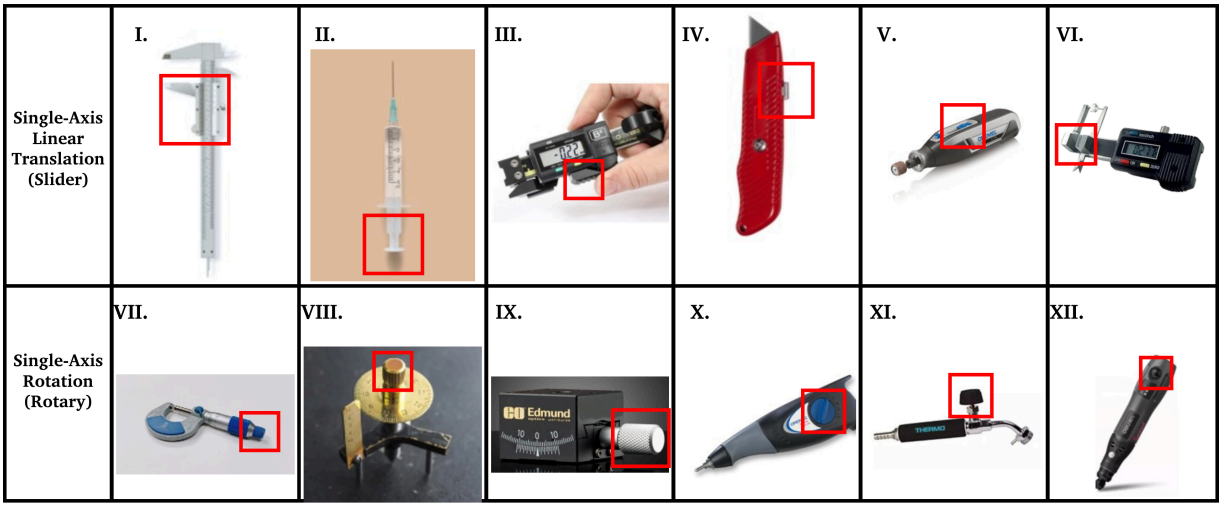

Figure 3.1: A design space of virtual miniature controls found in precision hand-held tools derived from 37 types of existing tools, instruments, and devices (few of them are shown in the image). It includes two motions types as miniature control kinetic characteristics.

quiring and assembling electronic resources. This approach not only streamlines the process of using MobiTangibles but also removes the burden or barrier associated with traditional electronic setups, paving the way for seamless and efficient hand-held tool's miniaturized interaction experiences in VR.

In summary, the contributions of this work are as follows. I introduce MobiTangibles, portable and passive proxies for handheld tools' miniature control that can be easily attached and detached for use in VR environments. I demonstrated the robust functionality of MobiTangibles in various conditions, highlighting the reliability of sensor signals against interference. Results from a user study with 15 participants showed that MobiTangibles enhance VR interaction by providing a realistic & low-fatigue manipulation experience of miniature control of virtual tools.

3.2 Related Work

3.2.1 Physical Manipulation in VR

Previous studies in human-computer interaction (HCI) have demonstrated that tangible interaction has a number of advantages over purely virtual interaction [82–84], such as better

task performance [72, 85–87], better spatial memory [88], and faster and more intuitive interactions [62, 89–91]. As a result, many VR-related efforts have concentrated on mimicking various virtual objects' functionalities by physical proxies, providing users with a realistic and tangible experience in a virtual environment (VE). For example, Arora et al. [14] and Feick et al. [72] introduced modular toolkits incorporating attachable/detachable blocks pieces for making proxy related to entertainment and game domains. As by replicating various features and qualities of the virtual object, physical proxies enable users to engage in tactile exploration and interaction, resulting in enhanced realism, presence, and fluidity in virtual interactions [62, 72, 92–94]. Capitalizing on the advantages of tangible engagement in VR, this work enables realistic interaction with miniature controls in VR.

Furthermore, since this design appears to be a tangible case for a smartphone combining distinct miniaturized physical manipulations, I discovered that there are other works that have also suggested the smartphone tangible case. After carefully reviewing each of them, I discovered that several of the approaches (e.g., [95, 96]) are active in nature. This implies the requirement for extra electronics around the smartphone and an additional battery (i.e., demand of external power) to facilitate tangible interactions. Consequently, making such approaches less cost-effective, complex to develop, and adds weight to the overall case. While passive techniques (e.g., like these [97–99]) have the following issues: first, they use complex ML algorithms in order to recognize events connected with tangible control manipulation, making it unsuitable for early stage prototypers or students to use directly or to build upon (who are generally not aware of such advanced programming). Second, none of the works have demonstrated what design space their method can accommodate. Because enabling realistic sensations of the miniature control interactions inherent in hand-held tools in VR was not their main goal. Moreover, none of these passive approaches—even the active kind—have assessed their work with users on any aspects of VR (e.g., realism)—an essential step in understanding the advantages of any approach prior to its application in VR. Apart from that, these works, i.e., [14] and [11], have also not assessed the applicability of their technique

on any aspects from users, resulting in no information and details on user experiences about how they have found these approaches while utilizing it in VR.

In order to fill this gap, I have started by demonstrating the design space from which miniature tangible controls, or MobiTangibles, originate. Then, I have developed a functional tangible case, or MobiTangibles case (containing MobiTangibles), based on the findings of the design space, which enables MobiTangibles use as a miniaturized tangible control proxy for the miniature control of precision hand-held tools in VR. Furthermore, our design feature—using only one magnet—is novel in that it enables a variety of miniature control manipulation experiences exhibited in this research with respect to precision hand-held tools in VR with the least amount of resources, unlike previous research [97, 100], which requires a magnet for every tangible input design if their method is used. As a result, our technique also lowers the barrier from the programming side by eliminating the requirement to utilize the sophisticated algorithm provided by [101], which must be used if more than one magnet is included in the tangible case design in order to separate the magnetic fields between the two magnets. Finally, I also conducted technical and user evaluations, demonstrating the viability of our proposed MobiTangibles interface for use in VR. Table 3.1 offers additional comparison between our work and other custom built physical input devices.

3.2.2 Smartphone use in VR

In the VR environments, researchers have also investigated the use of smartphones and their sensors in recent years. For example, the Phonetroller [102] allows users to utilize their smartphones to give precise touch input within the virtual environment. Similarly, Lipari et al. [103] suggested a system that enables users to choose, navigate, and modify the parameters of VR objects using their smartphone's touchscreen. Another work is [104], where the TMMD system projects the pose of an externally tracked phone into virtual space and lets users choose things either through ray casting or by walking up to the objects and using touch input to attach to them. Translating and rotating the object is then possible

using touch gestures on the phone. While touch gestures on the phone can make it easier to translate and rotate things, users may find it difficult to move objects precisely due to the absence of tactile feedback and accuracy, which can frustrate them and result in a poor user experience. Handycast [105], another recent research work that poses such issues, utilizes the smartphone's touch input and other sensors to interact with and manipulate virtual items. As the aforementioned studies enabled a variety of interactions in VR through the use of smartphones because of its easy accessibility and ubiquitous presence. Utilizing the same benefits, through this work I demonstrated its (i.e., smartphone) utilization towards enabling nuanced and realistic precision hand-held tools miniature control manipulation experiences in VR, thus extending its span of use.

3.2.3 Magnetic Field Sensing

In the field of HCI, researchers have explored various innovative techniques to input data into the computer interface using magnetic field sensing. These methods aim to address several issues related to user interaction. For instance, in Abracadabra [106], researchers devised a novel input mechanism by attaching a magnet to the user's finger, thus expanding the input area to several times the size of the device's screen. In another example, Nenya [107], researchers shifted the magnet's placement from the finger to the ring to provide analog inputs to the interface through the same magnetic field sensing approach. Similarly, other works, such as [108–110], utilized this sensing strategy to develop new input methods. Similarly, I leveraged this state-of-the-art sensing technology via smartphone applications to develop passive, lightweight miniature controls called MobiTangibles. While it is possible to make functional MobiTangible by the use of external sensors, cables, and microcontrollers. But the benefit that a smartphone brought to my strategy was that it transformed the approach into an accessory, devoid of any electronics or batteries and, consequently, any sort of assembling procedure. This made the method easy to use, adaptable to even the most novice VR users, and ultimately inexpensive overall.

Devices/Attributes	C	Cost	S	UA
VirtualBricks [14]	M	>$35	L	L
Tangi [72]	M	>$25	L	M
Haplinkage [11]	M	>$30	M	L
Vidgets [98]	H	<$10	L	L
ShiftIO [95]	H	>$50	L	L
Phidgets [96]	M	>$20	L	L
Voxelhap [68]	M	>$60	L	M
MobiTangibles (Presented Work)	L	<$10	H	M

Table 3.1: Comparison with respect to custom-built physical input devices. For **Complexity (C)** - Low (L): No electronics and advanced programming needed; Medium (M): Include basic electronics and/or simple programming; High (H): Requires advanced electronics and/or advanced programming (e.g., ML). For **Scalability (S)** - Low (L): Approach having limited or no capacity for designing different types of miniature physical manipulations; Medium (M): somewhat scalable and can handle a moderate variety of miniature physical manipulations development; High (H): can easily be adapted to design a wide range of different miniature types of physical manipulations. For **User Adaptability in VR (UA)** - Low (L): No user evaluation on any parameters, lacks evaluations from user perspectives; Medium (M): Conducted some evaluations in VR to assess feasibility from user perspectives; High (H): Comprehensive (longitudinal) user evaluations conducted in VR to assess feasibility from user perspectives.

3.3 MobiTangibles Mechanism

3.3.1 Working Principle

Magnetic field sensing in HCI has been extensively explored for mobile and wearable interactions [111–113]. Explored approach is based on the concept that when a magnetic field source (e.g., a magnet) is constrained to travelling solely along a straight path (e.g., L1 in Fig. 3.2) parallel to the line L2 on which fixed point P (a magnetic field intensity measurement location) is placed. Then, in such a case, the total magnitude of the magnetic field (B_T) effect of magnet tracked at the same specific fixed point (P) parallel to the magnetic field source line (L1) is thus generally given by 3.1

$$B_T = B_m + B_e = \frac{\mu \cdot m}{4 \cdot \pi \cdot r^3} + B_e \tag{3.1}$$

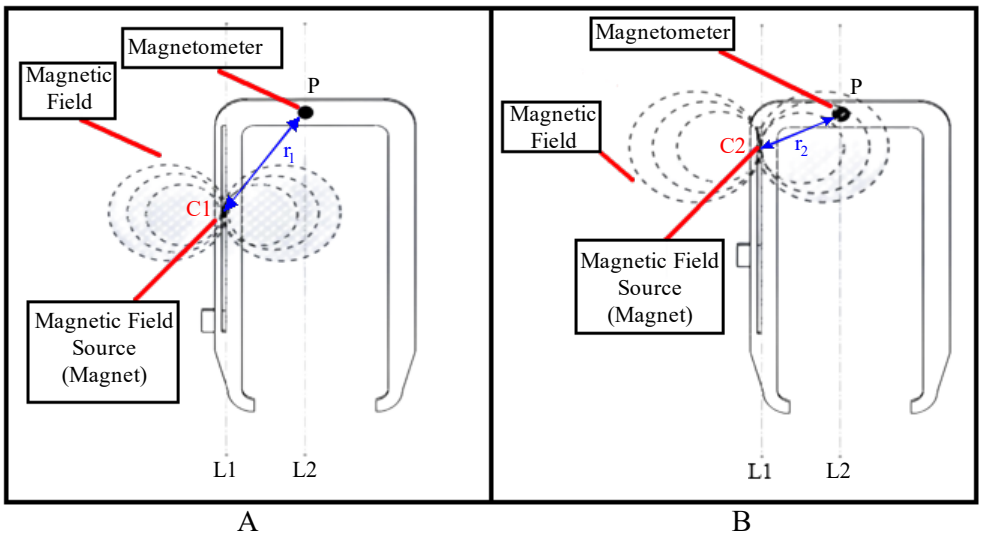

Figure 3.2: MobiTangibles working principle is depicted in two scenarios, A) when magnet was at a distance 'r1' from point P, & B) when magnet distance from point P is changed by bringing it to other position along the line L1 only, i.e., 'r2'. C1 and C2 denote positions of magnet when moved along the straight path L1, which is parallel to L2.

where, μ is magnetic permeability (constant value), m magnetic moment of magnet (which is also constant for a magnet), π is constant, r is the variable distance between magnet and fixed point 'P' (which is magnetometer sensor location), and B_e is environment (earth) magnetic field. Notably, the magnet's magnetic field (B_m) dominates the effect of the Earth's magnetic field [111]. Since the Earth's magnetic field (B_e) varies only between 22 μT and 67 μT depending on location [114], the influence of B_e on point P appears to be negligible compared to the magnet's effect. This is because the magnet effect, on the other hand, can exert a substantial impact of several hundred or even thousands of microteslas (μT) as it approaches point P (as confirmed by the Section 4 findings as well).

$$B_T \approx \frac{\mu * m}{4 * \pi * r^3} \approx B_m \tag{3.2}$$

Therefore, 3.1 can be effectively modified as 3.2, thus demonstrating that variations in the magnetic field at point 'P' are mostly caused by changes in the distance between the magnet and the fixed point of measurement (which, in a smartphone, would be the location

of the magnetometer).

This is due to the fact that, in 3.2, every parameter has a constant value except distance "r". This fine-grained understanding of magnetic field interactions at a specific location 'P' allowed us to design a variety of manipulation controls for smartphones (without any explicit modification to the smartphone), which are discussed in more detail in the following section. Incredibly because it provide two benefits from smartphones: first, the magnetometer sensor's location (or point), at which the magnetic field is measured remains constant, and second, 1-D movement can be easily achieved by moving a magnetic field source (e.g., a magnet) on the sides of the smartphone. With this knowledge, it can be seen that the configuration shown in Fig. 3.2, which was used to describe the general working principle, can be easily implemented on any smartphones. Moreover, it is also essential to note that the magnetic field strength (B_T), as given by the above formula, is independent of any speed term, which indicates that the obtained magnetic field strength with respect to any position of the magnet (when moving it along a straight path, e.g., "L1" shown above) will not be dependent on the speed with which user has moved (or shift) the magnet (e.g., through a tangible control to which magnet is linked) to that position.

3.3.2 Design Space of Virtual Tools Miniature Controls of and Fabrication

Comprehending the kinetic dynamics of hand-held tools' miniature control (i.e., a motion associated with them) that exist by necessity (or are found inherently) in numerous precision hand-held tools was crucial to bringing accurate hand-held tools' miniature control interaction realism to VR. I looked at various types of precision hand-held tools—manually operated and powered, using following sources, which includes previous literature [115–117], ecommerce platforms (like Amazon), and inspirational image sources (like Pinterest and hand-held tools websites). This was done in order to understand the kinetic dynamics associated with the embedded miniature control that a user in reality experiences when interacting with it in order to control or manipulate the hand-held instrument's working

mechanism/behaviors. After studying 37 distinct frequently used precision hand-held tools, both manual and powered, equipped with a miniature control operated by hand that needs to be handled carefully while operating the hand-held instrument, I discovered that the movement of embedded hand-held tools' miniature control follows a specific axis. I organized the collected items based on the kinetic characteristics of the embedded miniature control in hand-held tools. From this categorization, I identified two significant and frequently found to be utilized kinetic motions, which are mainly associated with a miniature control of precision hand-held tools manipulation aspects and play a major role overall in ensuring and providing precise control over the operation of precision hand-held tools/objects.

These miniature type kinetic motions include one is single-axis linear translation and another is single-axis rotation, as also depicted in Fig. 3.1. These motions are the main factor (apart from holding a tool in hand) that enable users to precisely manipulate the precision hand-held tool parameter with their fingers while using a tool (which could be anything like speed, air flow, temperature, vibration, focus adjustments, light intensity, part of a tool movement). After analyzing, I also found that the single-axis rotational type mechanism involves motion in a fixed direction and the single-axis linear type mechanism involves to and fro straight type motion, both typically within a small range (i.e., distance).

Fabrication

In this section, I present detail on the fabrication process of these two physical miniature manipulations within a single unit called the "MobiTangibles case", following the principles explored in the section 3.1. I have also included real handheld tool images alongside each proposed motion (translation and rotation) as an example (Fig. 3.3), which feature similar miniature controls to those proposed, to enhance the understanding and visualization of the physical interface.

- **Single-axis Linear Translation Manipulation:** Single-axis linear translation manipulation involves movement of miniaturized control along a straight path in any

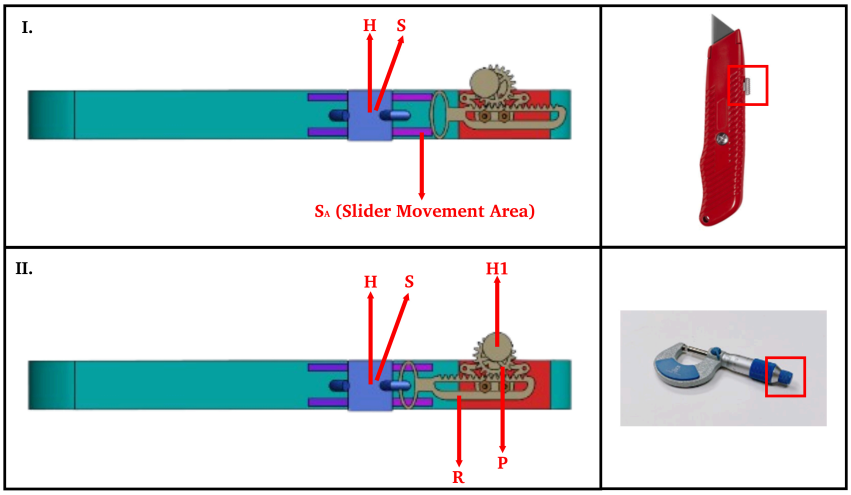

Figure 3.3: "H" is a holder that is also referred to as a Slider (S) control. When H is not connected to another tangible (for example, as shown on the right side image), "H" behaves as a slider type miniature control. I) Above, a slider-style MobiTangible movement is shown; II) Below, a rotary MobiTangible and its connection to "H" is shown. Both figures depict a side view of the case. Included real tool images (as an example) with each motion to enhance interface visualization.

direction, i.e., in forward and then backward, similar to motion as depicted in Fig. 3.1. The slider (marked with S) manipulator operates with a small holder (marked with H) connected to a strip (marked with S1 3.4I) along the edge of the mobile phone through a 3D-printed groove. When the holder is pushed forward, the strip (S1, which has a fixed magnet (M, Fig. 3.4) at its tip) shifts in the same direction, and when brought back, it returns to its original position as shown in Fig. 3.3I.

- **Single-axis Rotation Manipulation:** Single-axis rotation manipulation involves motion of a miniaturized control along a certain specific axis and only in one direction, as depicted as an example in Fig. 3.1. It uses a rack and pinion mechanism that allows for single-axis rotation. The circular part protruding from the rack (R) connects to one of the holder's joints. When the handle (H1) on the pinion (P) is rotated clockwise or anticlockwise, the rack, connected to the holder, moves the strip (S1) with the attached magnet forward or backward accordingly (as shown in Fig. 3.3 II).

I utilized a smaller size neodymium magnet with dimensions 10 mm x 3 mm (thickness 1

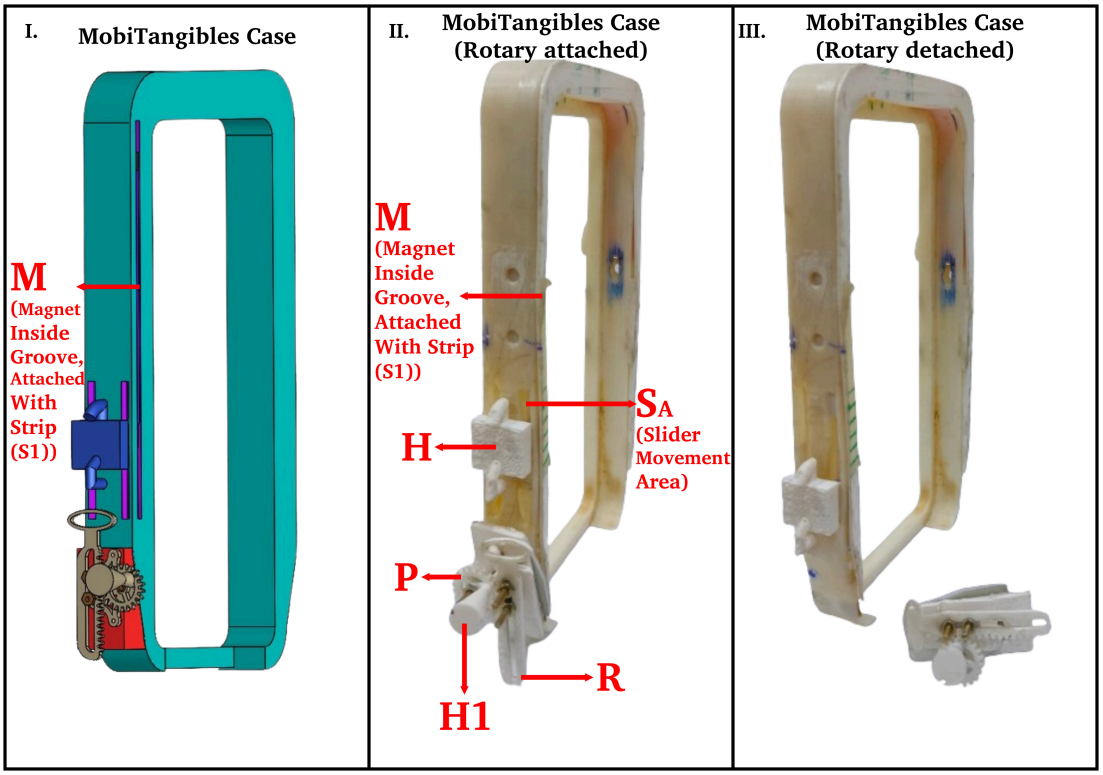

Figure 3.4: I.) Left side: side tilted view of a 3D model is displayed; II.) Middle: side titled view of real MobiTangibles case (with rotary) is displayed; and III.) Right: side titled view of MobiTangibles case without rotary.

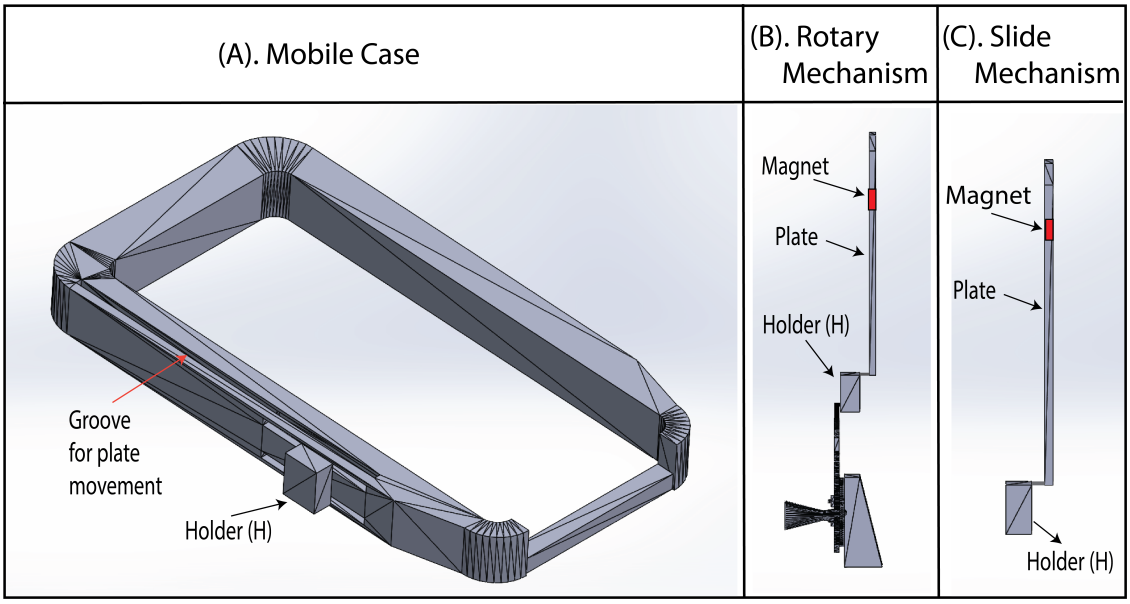

Figure 3.5: More details about each manipulation

mm), which was attached at a distance of 4.5 cm from the top of Android [118] smartphone (156 mm x 75 mm x 8.2 mm,), i.e., just at the tip of the strip placed in the groove. As during pilot testing, I discovered that beyond this distance (i.e., when the magnet moved towards the smartphone's top corner), the magnet magnetic field effect began to develop at the magnetometer sensor position (located in the smartphone almost at the middle of the top side). In Fig. 3.4, I depict the real (attached with a smartphone) and 3D image of the MobiTangibles case. Utilizing an Ultimaker S5 [119] and PLA material, all components of the two manipulations (previously stated) were 3D printed. The overall dimension of the designed MobiTangibles case (including all two proxies, i.e., "MobiTangibles") is 165 mm (length) x 90 mm (breadth) x 12 mm (thickness), and the weight is 42 grams. Moreover, the total cost of designing the MobiTangibles case is only $9. Other than this, the explored working principle (section 3.1) gave the design of the MobiTangibles case another benefit. It allowed the MobiTangibles (such as the rotary type and even other kinds as well, which this approach can enable (section 6)) to be used in VR in a plug-and-play manner based on the type of miniature control embedded within precision hand-held tools, which typically feature only one type of miniature control within them (e.g., as shown in Fig. 3.1). I used the 3M double sided thin tape for easy attaching and detaching of MobiTangibles.

3.4 Technical Evaluation

The main goal of this evaluation is to ascertain whether the MobiTangibles case supports and functions in accordance with the previously established working principle, which states that as the distance decreases, the magnetic field increases, and vice versa while interacting with MobiTangibles. Furthermore, the second step is to observe the effect of metallic objects on the investigated pattern, as obtained in the previous scenario. It is because MobiTangibles operational efficiency may experience a decline when situated in close proximity to metallic objects, especially those with ferromagnetic properties. To assess the impact of substantial metallic entities on MobiTangibles performance, I conducted a systematic analysis involving

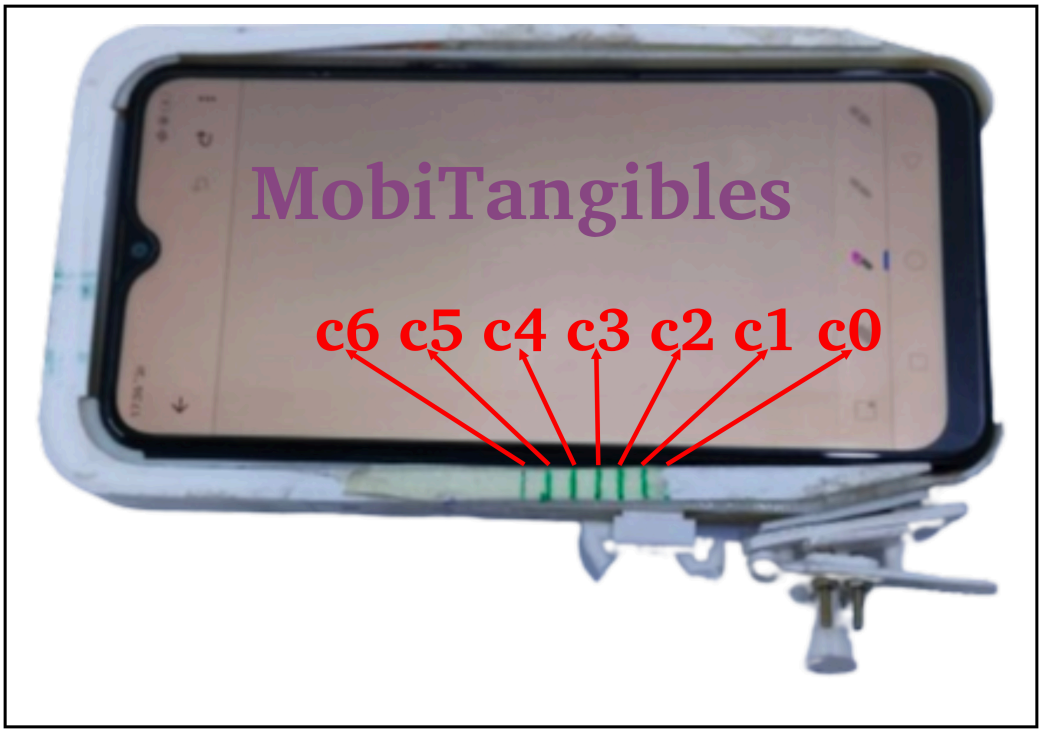

Figure 3.6: MobiTangibles testing setup.

such frequently utilized devices – a smartphone, a workstation, an air purifier, and a laptop (akin to the reference [110]). These devices were selected due to their likelihood of coexisting in the immediate vicinity of MobiTangibles' case during its indoor operational scenarios.

3.4.1 **Apparatus**

To carry out the experiment, I used the same MobiTangibles case shown in Fig. 3.4 and an Oppo A5s smartphone [118] to conduct all our experiments. I utilized the phyphox Android app [120], which is freely available in both the iOS and Android App stores, to see and record the variations in the magnetometer signal during testing. This application captures magnetometer signals at 50 Hz, and the evaluation was conducted in a room of size 25 ft x 35 ft.

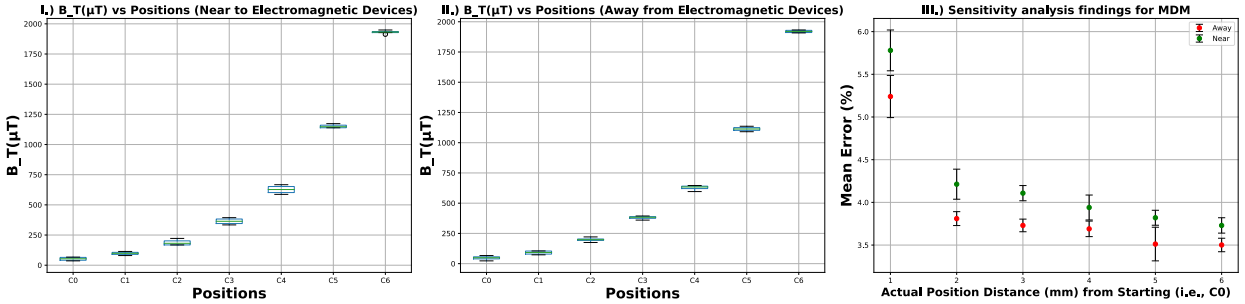

Figure 3.7: The image above depicts the obtained magnetometer sensor reading (B_T) for each position (C0 to C6) in the two scenarios. The readings obtained near electromagnetic devices are on the left (I), and readings far from them are on the right (II). μT is micro Tesla. The image III shows MDM findings for each position.

3.4.2 Exp. - 1: Magnetometer Signal Variations due to Holder Position Shifts

Procedure

In order to determine how the magnetometer signal responds to each shift in the holder's (H) position, I first carried out a controlled experiment. Specifically, the goal was to examine the signal range and any emerging patterns between the magnetometer signal data (B_T) and the positions (C0 to C6). The testing setup is depicted in Fig. 3.6, with the highlighted spots placed equidistantly between C0 and C6 (the maximum shift in position). These equidistantly positioned dots will also help us confirm the precise manipulation aspects of a MobiTangible (one of the evaluation aims), which is to determine whether MobiTangibles can be manipulated precisely. To carry out this experiment, I simply employed the linear translation manipulator (one of the MobiTangible containing holder on top of it) and performed the experiment under two scenarios. In one scenario, I carried out the experiment near the electromagnetic devices (<5 cm), involving a workstation, and a laptop on the table. In the second scenario, I conducted the experiment far from the electromagnetic devices (>250 cm). In each scenario, I placed a smartphone (connected to the MobiTangibles case) on the table surface and gathered magnetometer sensor data four times (each of 60-seconds duration) at each point indicated on the MobiTangibles case (C0 to C6, Fig. 3.6). C0 represents the magnet's initial location where its distance from the magnetometer sensor is

maximum (i.e., no effect on the sensor), whereas C6 indicates the magnet's distance from the magnetometer sensor is closer. Within four data collection events related to each position in each scenario, data was gathered two times in the vertical (portrait mode) orientation of the smartphone and two times in the horizontal (landscape mode) position of the smartphone. I also performed the smoothing (sample size 20) on the collected data in order to remove any minor fluctuations (if any). The start and stop times of the data collection were also noted when collecting data for each position and each time. It was done in order to quickly segregate the data related to each position for further analysis. When data was collected at a particular position (i.e., by bringing a linear MobiTangible to that position), I first relocated the linear MobiTangible back to the C0 position before moving it on to the same or next position. I simply recorded the magnitude variation of the magnetometer sensor signal (B_T), as it contains the overall influence on magnetometer signal variations along all three axes (x, y, and z). While conducting this experiment and later experiments, I used the traditional gesture of holding miniature controls (basically MobiTangibles) involving the index and thumb fingers because it provided stability in easily bringing the holder to the desired position during the data collection process. I also utilized a timer because I had to collect data for 60 seconds at each spot each time. In total, I ran 56 tests, i.e., 4 times x 7 positions (C0 to C6) x 2 situations. The total distance from C0 to C6 is 36 mm.

Additionally, I conducted a sensitivity analysis to determine minimum detectable movement (MDM) for reliable miniature control interactions in VR. Using the same procedure as used in the above experiment, data was collected at 1 mm intervals over a total distance of 6 mm between C0 and C1.

Results

After analyzing the collected smoothed sensor signal response (i.e., sensor mean value of all data (B_T) collected) in relation to each position and scenario (as shown in Fig. 3.7), I observed varying sensor values (B_T) corresponding to changes in position. Additionally, I

noticed a consistent trend for both scenarios, indicating that the magnetometer sensor values (B_T) increase with position values (i.e., from C0 to C6). Comparison of the data (as depicted in Fig. 3.7 (I and II)) using the Wilcoxon signed rank test revealed no significant effect of electromagnetic devices on the measured magnetic field intensity values for each position (z = -0.3381, $p > 0.05$). Both graphs also demonstrate a similar pattern of signal change with respect to each position. Obtained results also suggests that the sensor data (after basic smoothing) could be used with best fit equation directly in VR to control virtual hand-held tools' miniature control movements through MobiTangibles without the need for complex algorithms.

For the MDM analysis per scenario, I input each recorded magnetic field (MF) value per position between C0 and C1 into an equation - 3.3 relating MF strength to position, yielding predicted position values. I compared these to actual positions to calculate the error. The analysis showed that increasing the MDM reduced the mean error across all scenarios. A 2 mm shift (for away scenario) resulted in a minimum mean error of 3.812% (S.D. 0.081), while a 1 mm shift produced an error of 5.242% (S.D. 0.24). Fig. 3.7III shows the overall results for both scenarios: near and away from electromagnetic devices.

3.4.3 Exp. 2: Magnetometer Signal Variability in various Scenarios

Procedure

The purpose of this evaluation is to see and validate that sensor signals (B_T) also continuously vary throughout the position (i.e., from C0 to C6) according to the working principle when MobiTangibles are manipulated throughout their full movement. Additionally, to observe and verify that the range of magnetic field variation is the same throughout the testing situations and iterations. To assess these aspects, I systematically interacted with both types of manipulators, moving them entirely up and down twice (i.e., two iterations). While moving, I also took intermittent stops at random points between zero (C0) and full movement (C6) to observe signal stability. I conducted this experiment in three scenarios. In the first

scenario, the MobiTangibles case was in the middle of the room and held in hand, far (> 250 cm) from electromagnetic devices like the workstation, laptop, and refrigerator. Second, when the MobiTangibles case was held quite close (< 5 cm) to these devices, i.e., on a table containing all such electrical devices (a workstation and laptop). Finally, in the third scenario, MobiTangibles case was moved in a circular path (radius = 1 meter, within the room) by holding it in hand, where the holding position was also getting changed after completing one full circle (i.e., one iteration). The advantage it will provide by moving on a circular path is that it will help us to see and evaluate the overall effect of change in direction (user and device) on the magnetometer signals. As by moving in a circular path direction by default keeps on changing. Thus, in turn, it will help us to assess the robustness of the continuous variation in signal. And the findings from the first two scenarios will enable us to assess any potential impact of nearby electromagnetic or metallic objects on signal variations, contrasting with the baseline scenario where no electromagnetic devices were in proximity to the MobiTangibles case.

I interacted with the linear translation type manipulator entirely (up and down) twice (i.e., two iterations) with random stoppage in all three conditions by bringing (i.e., passing) the holder from all these respective marked places. Furthermore, in each setting and iteration, I changed the orientation of the phone (i.e., how it was held) during the experiment. Because it will allow us to demonstrate that users can grip or grab the MobiTangibles case in any way they want while engaging with the VR controls via the MobiTangibles. I simply recorded the magnitude variation of the magnetometer sensor signal (B_T). Because there was no control over the manipulation speed and no constraints, the speed altered automatically each time the slider manipulator was interacted with (i.e., passed through the highlighted spots) during the experiment. I did not want to limit it either because varying speeds will further help illustrate the robustness and independence of the signal change. I also did not set a speed limit while walking in a circular motion, for the same reason. Instead, normal walking was performed (which is below, i.e., 3.52 km/h (0.98 m/sec) [121]). Following that,

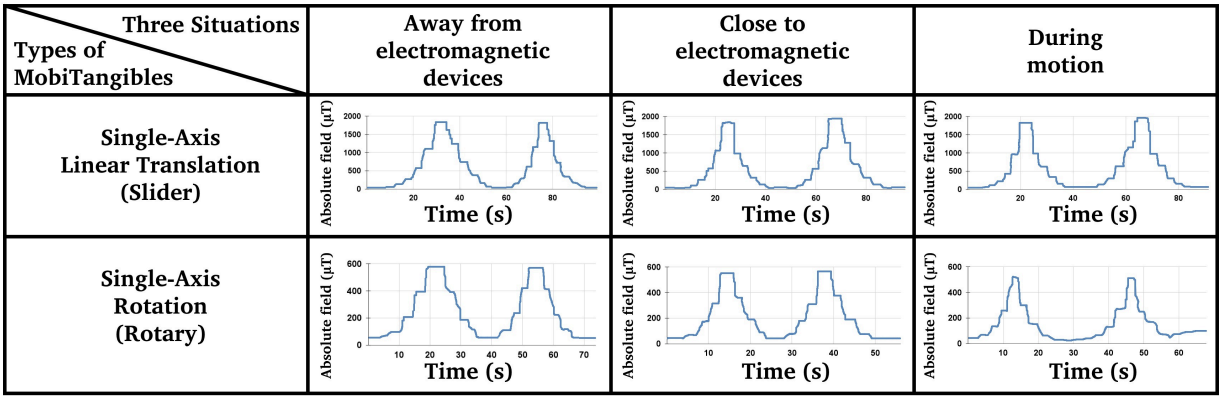

Figure 3.8: Results (raw data) for both manipulations across three scenarios.

I repeated the same process with one remaining MobiTangibles (rotary) to ensure that variations in the magnitude of the magnetometer signal are within the range discovered in the previous study. It is because rotary MobiTangible motion is also bound to C0 and C6. I tested rotary type MobiTangble in each of the three previously described scenarios twice to further verify that variance with regard to this physical control is the same and consistent throughout. With rotary control, the motion begins at C0 and progresses to C4 (which means the pinion fully rotated in one direction) only. In total, I ran 12 tests, i.e., 2 iterations x 2 physical controls x 3 situations.

Results

The findings from the comprehensive testing scenarios, encompassing various physical manipulations of the MobiTangibles case, offer insightful revelations into its magnetic field sensing capabilities. Fig. 3.8 provides an overview of the magnetometer signal magnitude observed across different physical manipulations, highlighting their consistency and distinct ranges. As depicted in Fig. 3.8, the investigations reveal a consistent and intriguing trend: the magnetometer signal magnitude remains invariant for each type of physical manipulation, regardless of the presence or absence of metallic objects, and even during dynamic movements. This underscores the robustness of the MobiTangibles design, affirming its ability to deliver consistent realistic physical experience within virtual environments. A notewor-

thy outcome of the investigation is the compelling contrast between the impact of magnet movement within the MobiTangibles case and that of Earth's magnetic field. Specifically, the magnetic field's change caused by MobiTangibles magnet motion from C0 to C6 registers at a substantial magnitude of approximately 1800 µT, dwarfing the comparatively modest impact of Earth's magnetic field (Be) at the same point P, which ranges merely between 22 µT and 67 µT [111, 114]. This substantial disparity, amounting to approximately 38 times, underscores the device's potency in generating controlled magnetic field variations.

Furthermore, the efficacy of MobiTangibles mechanism becomes even more apparent when considering the signal fluctuations observed at intermediate positions. These findings demonstrate that despite the relatively confined range of 22 µT to 67 µT characterizing Earth's magnetic field variations, the signal strength at intermediate positions showcases markedly larger magnitudes, ranging from approximately 3 times (at C1) to an impressive 38 times (at C6) the intensity of Earth's magnetic field. This pronounced deviation accentuates the device's capacity to generate substantial magnetic field changes, transcending the influence of inherent environmental factors. The observed correlation between the distance-dependent magnetic field variations and the physical manipulations performed on MobiTangibles aligns precisely with the premises encapsulated in 3.2. This alignment reinforces the theoretical foundations of the device's functionality and substantiates the exclusion of Earth's magnetic field. Importantly, a clear pattern emerges wherein advancing the holder's position, such as from C1 to C2 (or other combinations), consistently augments the signal strength. Conversely, backward movement, as from C6 to C5 or other combinations, consistently yields diminished signals relative to prior positions. Furthermore, the findings unveil distinct signal ranges for different MobiTangible interactions. The slider manipulation manifests within the constrained variance range of 50 µT to 1900 µT, while the rotary control manifests signal variance ranging from 50 µT to 600 µT.

The implications of these results are far-reaching, suggesting avenues for both software development and device design. The consistency of signal trends implies that developers can

implement straightforward, lightweight methodologies (i.e., without involving any advanced ML algorithm similar to previous approaches [97–99]) when integrating MobiTangibles cases into virtual interactions. From a design perspective and regarding magnetometer position and calibration, the adaptability of the MobiTangibles approach remains intact, regardless of potential variations in magnetometer sensor placement across different smartphone models. This issue can be resolved by adjusting the magnet intensity in the code to match the phone's magnetometer range, calibrated during the app's initial setup based on the phone model, and/or by strategically relocating physical manipulations.

3.5 User Evaluation

In the VR domain, previous works have underscored the importance of physical manipulation of the virtual object feature for enhancing realism, presence, and interaction fluidity [72, 93, 94, 122]. Building upon this foundation, the IRB-approved study aims to explore initial perceptions of users towards the realism factor (akin to [64, 71]), explicitly focusing on the realism of the manipulation process of virtual hand-held tools' miniature control using MobiTangibles. To achieve this, I compare the MobiTangibles interactions with two commonly employed conditions in the VR world: Bare hands and VR controllers.

3.5.1 Participants

I ran this study with 15 participants (5 Females, Mean age 24, SD 4.94). Seven of our participants reported that they had never used VR before, five had used it a few times (one to three times a year), and three other subjects use it on a regular basis (more than 12 times a year). The duration of the study was approximately 50 minutes per participant. The participants were all right-handed users.

3.5.2 Apparatus & Conditions

There was a chair and a table in a 15 ft x 9 ft space, and I asked participants to sit on the chair. On the table was a Lenovo laptop -Legion 5 (running a VR program in Unity3D [123], a MobiTangibles case, and Android smartphone [118]. I used the MATLAB app [124] (available freely on the Android Play Store) for transferring data from the mobile magnetometer sensor (at 50 Hz) to the MATLAB program (running in the background on the laptop) connected with the Unity3D software running on the same laptop [125]. I have employed a smoothing filter with a window size of 20 samples in the MATLAB code to effectively eliminate any potential noise on the receiving magnetometer signal from the MATLAB app running in a smartphone (attached with a MobiTangibles case), ensuring seamless user interaction with a virtual miniaturized control of hand-held tools.

I used the findings from Section 4.2 on magnetic field fluctuation with respect to each position (C0-C6) to map the motion of MobiTangibles with a virtual hand-held tool's miniature control. I initially calculated the final mean value for each position (by averaging values acquired in two scenarios per position), as there were no significant variations between the data for each position under the two conditions. It was done to establish a one-to-one relationship between MobiTangible positions and their corresponding sensor values, as well as to obtain the best-fit equation so that it can then be used directly in MATLAB code to link MobiTangible movement with virtual hand-held tool's miniature control motion.

$$Position = 1.65 \cdot \ln B_T - 6.60 \tag{3.3}$$

After analysis, I discovered the logarithmic equation - 3.3 to be the best fit between the MobiTangibles' positions and the associated sensor values. In Fig. 3.9, I depict a graph for the same and obtained model coefficient of determination value (R^2) was 0.997.

Interactions working in each of the three conditions were as follows:

- With Oculus Quest controllers: The "virtual precision hand-held tool" was coupled to

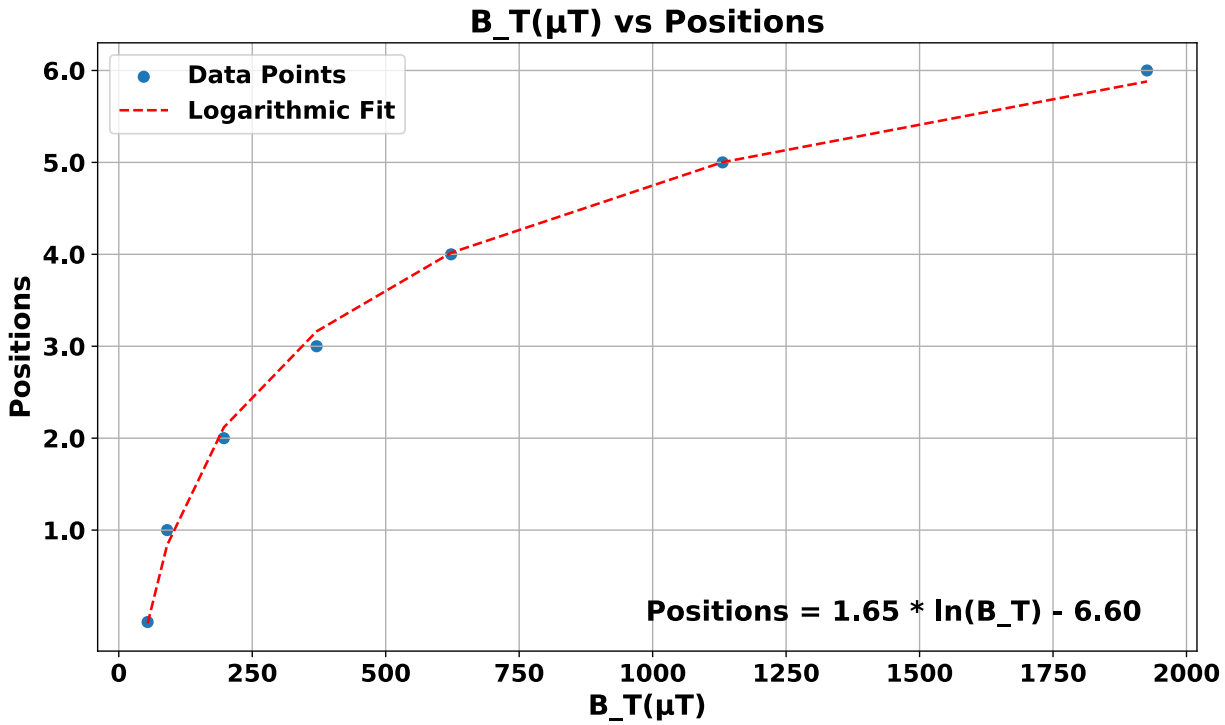

Figure 3.9: The plot above depicts significant fit between sensor values (B_T) and positions (0 to 6) along with best fit natural logarithmic equation.

one of the VR controllers in VE and moved in VE in response to the same VR controller movement, which is tracked. The second VR controller was utilized to manipulate the "miniature control of virtual precision hand-held tool" (for example, to move the jaw of the vernier caliper or to adjust air flow using the knob of hot air flow holder). To execute the necessary hand movement gesture, the user must press and hold the trigger button on the second Oculus controller near the miniature control.

- With Oculus Quest hand tracking: I used the Oculus Quest hand tracking capability to track users' hands in VR. The "virtual precision hand-held tool" was attached to one of the hands and moved in tandem with the tracked hand. The other tracked hand was used to manipulate the "miniature control of a virtual precision hand-held tool." The user needs to pinch their index finger and thumb to manipulate the "miniature control of the tool."

- With tracked MobiTangibles case: To enable tracking of the MobiTangibles case, the VR controller was attached to it (taking reference from following kind of works, e.g., [102, 126, 127]). Then, by using an appropriate MobiTangible for the application in VE, users were required to operate the "miniature control of virtual precision hand-held tool".

I also made use of the controller's vibration to distinguish between powered and manual types of precision tools. I derived this knowledge from the fact that, just as in real life, when a powered type precision tool's miniature control alters, the vibration that the tool provides to the user's hand likewise changes correspondingly (i.e., faster vibration corresponds to tool operating at higher speed, slower vibration corresponds to tool operating at lower speed). Therefore, in a similar manner, I also mapped the vibration intensity of the controller with which the virtual tool was linked to the variation of miniature control of the powered-type precision hand-held tool. This allows the user to experience distinct vibration while manipulating the powered-type tools functioning as per requirements in a virtual scene through a miniature control in both conditions (apart from the bare hands condition, in which a user does not hold anything in hand). While for manual type precision instruments in VR, which typically do not include any vibration in their real-world operation as well, I only employed visual feedback in VE. I compared our three conditions' experiences with respect to executing two separate types of miniaturized interactions (involved in precision hand-held objects), one of which is rotation and the other is translation. Participants wore noise-canceling headsets in every condition to mitigate the impact of aural cues as a confounding factor.

3.5.3 Procedure

Participants interacted with six basic virtual world applications, each including one sort of virtual precision hand-held tool, and a simple associated task involving interaction with the virtual hand-held tools' miniature control (as explained in the next paragraph). In this manner, each participant interacted with six virtual applications, basically six distinct virtual hand-held tools (Fig. 3.10) in each condition (total is three). Three of the hand-held

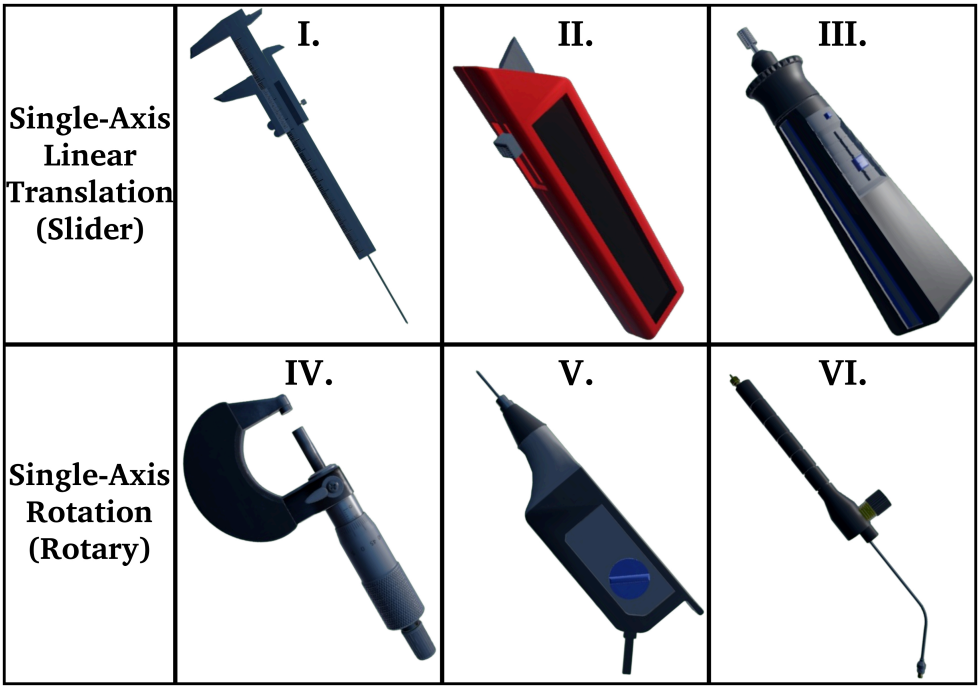

Figure 3.10: Six virtual precision hand-held tools are shown, each for a different VR application. They include a vernier caliper, retractable knife, powered grinder, micrometer, powered engraver, and hot air flow.

tools (out of six) involved precise miniaturized interaction of the single-axis linear translation type, while the other three involved single-axis rotary manipulation.

Each of the six of these virtual environment-related tools is shown in Fig. 3.10 and their associated virtual scene in Fig. 3.11. The following are more details regarding the basic tasks connected to each of the six virtual applications (basically with six precision virtual tools) that were designed: The first application (Fig. 3.10I and Fig. 3.11I) requires the vernier caliper jaws to be adjusted (through linear miniature control) one by one according to the thickness (indicated as small, medium, and large) of three different virtual metallic plates placed on the table surface using a caliper miniature control; the second (Fig. 3.10II and Fig. 3.11II) in which the retractable knife blade protrusion must be adjusted one by one in accordance with the three soft type material sheets of varying thickness (indicated as very thin, thin, and thick) placed on the surface; a third (Fig. 3.10III and Fig. 3.11III), where a final stage crafted ceramic sheet placed on a table surface with three different size impurities

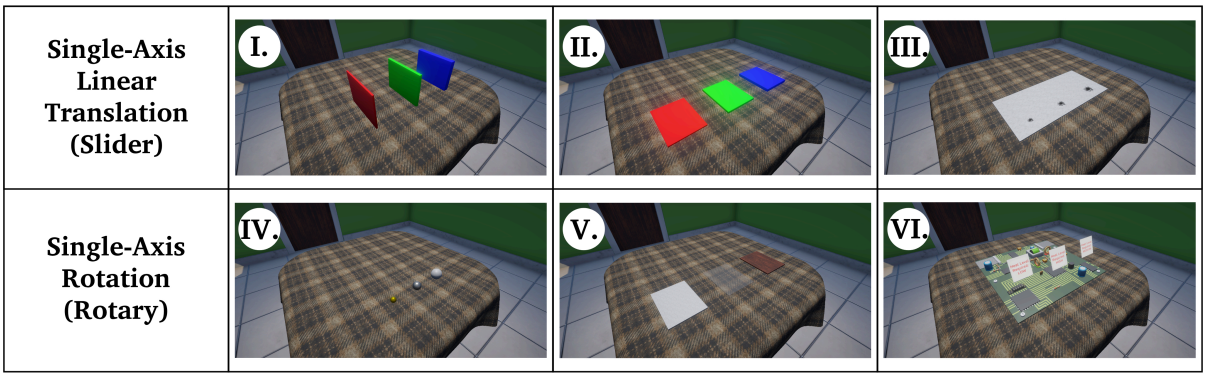

Figure 3.11: Six VR applications corresponding to each tool are displayed. The order matches virtual tools in Fig. 9, depicting that tool in Fig. 9(I) is only related to virtual application shown in Fig. 10(I), and so on.

(small, medium, and large) needs to be removed as indicated in the virtual scene using a virtual hand-held grinding machine in order to provide accurate finishing to the ceramic sheet, wherein tool grinding speed associated with each impurity size is in terms of low, medium, and high; a fourth (Fig. 3.10IV and Fig. 3.11IV), where the virtual micrometer motion to be adjusted one by one according to the diameter (indicated as small, medium, and large) of three different metallic spheres placed on the table surface using a rotary type miniature control of virtual micrometer; in the fifth part (Fig. 3.10V & Fig. 3.11V), the virtual hand-held engraving tool speed must be adjusted in terms of low, medium, and high as indicated against each material slab (i.e., marble (high), acrylic (medium), and mdf (low)) so that a clear thick visible straight engraved line can be marked upon each distinct material; in the sixth (Fig. 3.10VI and Fig. 3.11VI), the flow from the virtual hot air holder must be adjusted (through rotary knob) one by one according to the indication of heat requirement (in terms of low, medium, and high) against each of the three distinct smd type IC components soldered on pcb. In order to let participants know that they have moved or adjusted the miniature control of a virtual tool to the appropriate position (according to the task requirement in VE), I used a color indicator in all of the virtual settings (where green indicates correctly manipulated and orange indicates not).

I also told all participants in this study that they had to interact with all applications

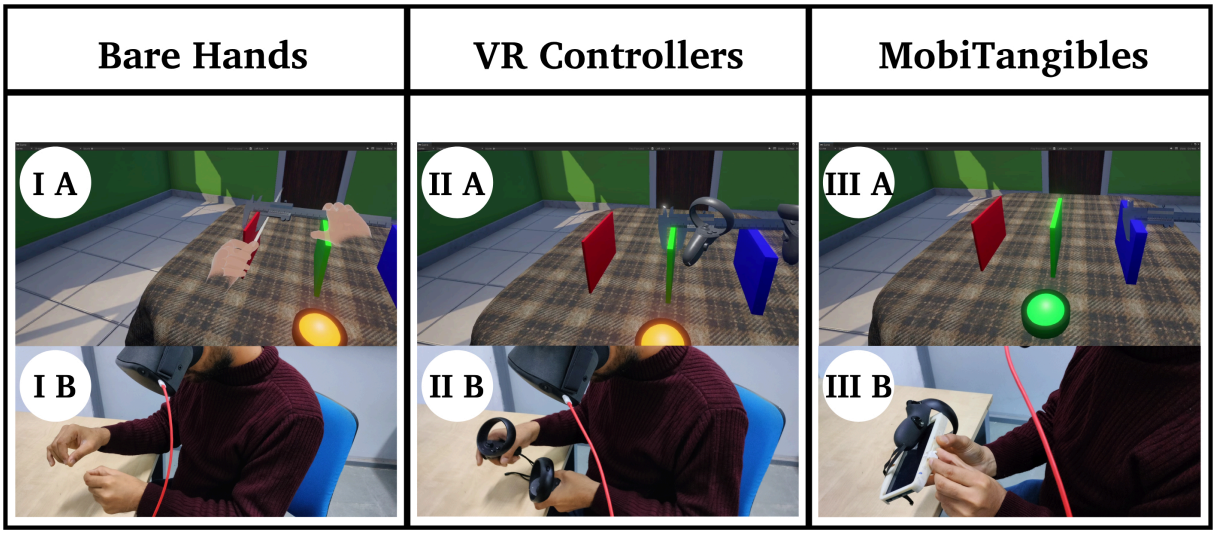

Figure 3.12: Regarding translation type miniature control: the images depicts a user interaction for one of the scenarios under all three settings, namely handling a virtual vernier caliper tool and controlling its miniature control.

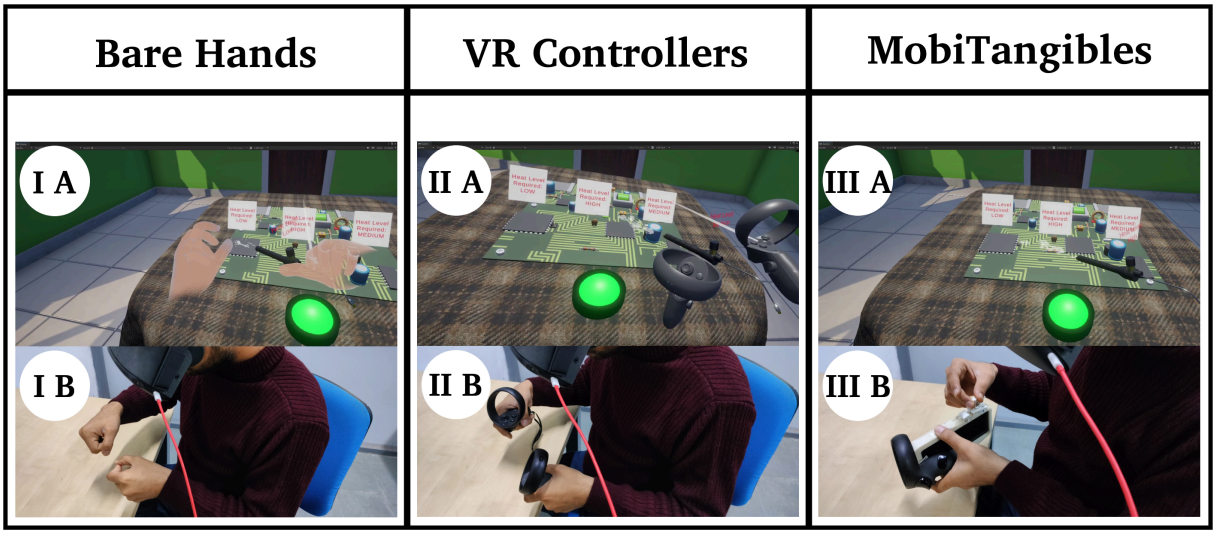

Figure 3.13: Regarding rotary type miniature control: the images depicts a user interaction for one of the scenarios under all three settings, namely handling a virtual hot air flow tool and controlling its miniature control.

by holding the MobiTangibles case in their hand (the same instruction was followed for VR controllers as well), similar to real-world scenarios, as in reality also users have to hold the hand-held type tools in their hand to operate them. However, they were free to adjust the MobiTangibles case's and VR controllers' holding position in their hands as they do in the real world. I employed a randomization method (akin to, e.g., [64, 72]) to counterbalance the order of conditions. This approach ensures that any potential order effects are minimized and that the results are not biased by the sequence in which the conditions or applications were experienced. Specifically, the sequence of the three conditions (Bare hands, VR controllers, and with a MobiTangibles case) was randomized for each participant. Additionally, the presentation order of the virtual applications was also randomized for each user. Each participant was explicitly introduced to and given experience with each sort of manipulation in relation to all three conditions during the trials (i.e., before the commencement of the actual tests). During the trial and experiment periods, participants were free to interact with applications in all three settings (or conditions) for as long as they wanted. While using a linear translation type MobiTangible, a rotary MobiTangible was not connected with the MobiTangibles case. The trial period gave them the opportunity to familiarize themselves with VR, the study task, and the condition. They were also asked to think aloud while the experiments were taking place, and the experimenters recorded their observations. Fig. 3.12 and Fig. 3.13 depict user interaction for each kind of manipulation (i.e., translation and rotary).

In addition, after completing all six virtual applications in each condition, participants completed a questionnaire form that included two questions on a seven-point Likert scale. Specifically, the questions were: How realistic was the feeling of manipulating and interacting with a miniature control of virtual precision hand-held tools? (Scoring: "1 - extremely unrealistic" to "7 - extremely realistic"). This question assessed the degree of realism perceived by participants while interacting with a miniature control of virtual precision hand-held tools with respect to each condition. How much fatigue have you experienced while manipulating a

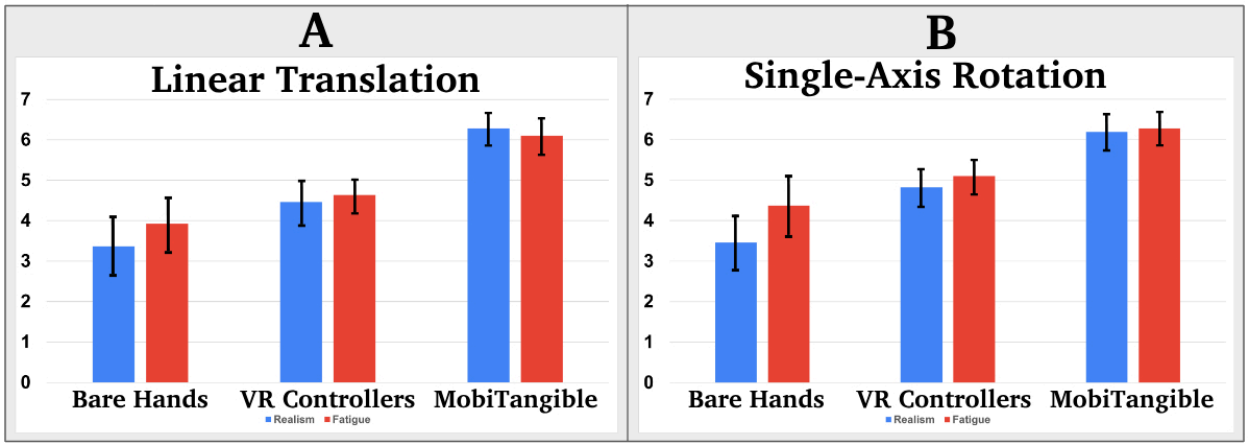

Figure 3.14: Questionnaire responses. Red bar is related to fatigue and Blue bar is related to realism.

miniature control of virtual precision hand-held tools? (Scoring: "1 - extremely high fatigue" to "7 - extremely low fatigue"). In total, I conducted 270 tests, involving 15 participants who completed 6 manipulations each across 3 different experimental conditions (Bare-hand, VR controllers, and MobiTangibles).

3.5.4 Results

Fig. 3.14 shows the obtained results. I ran a non-parametric Friedman test on our two Likert scales. There was a statistically significant difference in the realistic rating for slider ($\tilde{\chi}^2$ (2) = 21.375, p < .00002), and rotary ($\tilde{\chi}^2$ (2) = 20.125, p < .00003), and so I performed a post-hoc Wilcoxon signed rank test. I found that the MobiTangibles case performed significantly better than bare-hands condition (p < .05) in terms of realism with respect to both manipulations. I also found that the MobiTangibles case performed better than the VR controllers (p < .05) in terms of realism aspects with respect to both manipulations. There was a significant difference in terms of realism between the bare-hands and VR controllers for the slider ($\tilde{\chi}^2$ (2) = 6.75, p < .00937) and rotary ($\tilde{\chi}^2$ (2) = 8.3333, p < 0.00389), so I performed a post-hoc Wilcoxon signed rank test. I found that VR controllers performed better than bare-hands condition (p < .05) in terms of realism with respect to both miniaturized manipulations. For fatigue, I found no significant difference between bare-hands and VR

controllers for slider ($\tilde{\chi}^2$ (2) = 2.0833, p < .14891) and rotary ($\tilde{\chi}^2$ (2) = 3, p < .08326). I also found that in terms of fatigue aspects, MobiTangibles case performed significantly better (i.e., low fatigue) than bare-hands with respect to all two miniaturized manipulations: slider ($\tilde{\chi}^2$ (2) = 15.5417, p < .00042), and rotary ($\tilde{\chi}^2$ (2) = 16.625, p < .00025), which was later also confirmed by the post-hoc Wilcoxon signed rank test (p < .05).

3.5.5 User Feedback

Bare Hands

Participants navigating the bare-hands condition offered varied perspectives on the interaction with miniature controls of precision hand-held tools, regardless of their familiarity with VR. Some found the freedom of such manipulations engaging, yet a common theme emerged regarding the challenge of maintaining focused and precise hand movements. As one participant remarked, *"It was tricky to get the exact adjustments. My hand movements didn't always move as intended."* Moreover, many participants also reported that they did not feel like they were actually manipulating constraint kind manipulation because of no constraints kind feeling experienced on fingers while manipulating controls in air. These sentiments echo the findings from the results section, where realism was identified as challenges in the bare-hands condition. Additionally, users also reported experiencing fatigue in their arms, despite the absence of any physical object to grasp which further added another layer of complexity. Many participants' feedback underscored this, with one expressing, *"I didn't expect my hand to tire out. It felt like every time I was reaching for something that wasn't there."*

VR Controllers

In contrast to the bare-hands condition, participants using VR controllers noted a sense of holding an object. However, they encountered difficulties in achieving a high level of realism due to the dual demands of handling the controllers and interacting with virtual content.

A participant noted, *"The VR controller added a sense of weight, but there was not much feeling that I am interacting with constrained type manipulations as appear in the virtual environment"*. Another participant stated that *" It felt like there is a clear gap between what I was doing with the controller and what I expected in my thought to do with such miniature controls of tools"*. Participants also noted that using instruments like a knife and a grinder, which they expected to handle naturally with one hand, felt highly unrealistic with VR controllers.

MobiTangibles

The introduction of the MobiTangibles case brought about a notable transformation in the user experience. Participants universally reported a direct and realistic interaction with virtual miniature controls of hand-held tools, replicating the sensation of adjusting parameters of real-world precision hand-held tools. As one participant articulated, *"With MobiTangibles, it felt like I was actually holding the tool and manipulating its parameters as I expected. The tactile feedback from the slider and rotary controls made it easier to achieve precise adjustments."* Furthermore, an additional participant stated, *"I could easily control the knife blade motion just with a single hand similar to how I interact in real life."* Additionally, many participants expressed positive feedback, by reporting that *"MobiTangibles provided better understanding of handling and manipulating hand-held tools' miniature controls"*. These participants' feedback aligns with the results showcasing the significant improvement in realism with MobiTangibles. Unlike the previous bare-hands condition, the absence of reported fatigue by participants further strengthens the case for tangible controls, as another participant mentioned, *"I could manipulate the controls comfortably. There was no strain, and interacting with the miniature controls felt much more natural."* – attributing it to the device's design and support for various manipulations, which allowed for satisfied and comfortable manipulation of miniature controls in VR. These insights emphasize the superiority of MobiTangibles in providing realistic and comfortable interaction experiences with miniature

controls of hand-held tools in VR, addressing the challenges identified in the bare hand and VR controller conditions. In essence, the participants' comments shed light on the nuances of each condition where MobiTangibles emerged as a preferred solution for miniaturized tangible control interaction experiences in VR. This demonstrates that MobiTangibles can bridge the gap between virtual and real-world hand-tool's miniature control manipulation experiences. Furthermore, this research aligns with the work of Bossavit et al. [128], who emphasized the significance of employing appropriate metaphors. According to their findings, individuals tend to grasp (and learn) a technique more swiftly if it shares similarities with familiar actions or operations. This finding also underscores the value of selecting relatable metaphors in the learning and interaction process. Overall, these findings confirm MobiTangibles' potential and its uses in revolutionizing VR training and operations for high-precision tasks (e.g., crafting, engraving, measurements, etc.) where traditional controllers fall short in providing necessary realistic fine motor control.

3.6 Limitations and Future Work

While MobiTangibles presents a robust solution for hand-held tools' miniature control interaction, it is essential to acknowledge certain limitations. Firstly, magnets pose a potential risk to certain objects like credit cards and magnetic hard disks, as noted in previous studies [97, 113]. However, modern mobile devices' flash memories and IC chips on credit cards are unaffected by magnets. Second, it is not possible to use all MobiTangibles simultaneously. Future development may enable multi-dimensional and multi-modal input capabilities. One possible way to achieve this is by optimizing the design, utilizing the mobile phone case's surface area for specific motions, and employing pattern recognition techniques like Independent Component Analysis to differentiate between tangible signals. Third, although the experiments showed no significant effect of electromagnetic devices, strong magnetic fields or objects in environment could still interfere with device's functionality. Future work could involve testing device in various strong magnetic field zones to better understand the impact

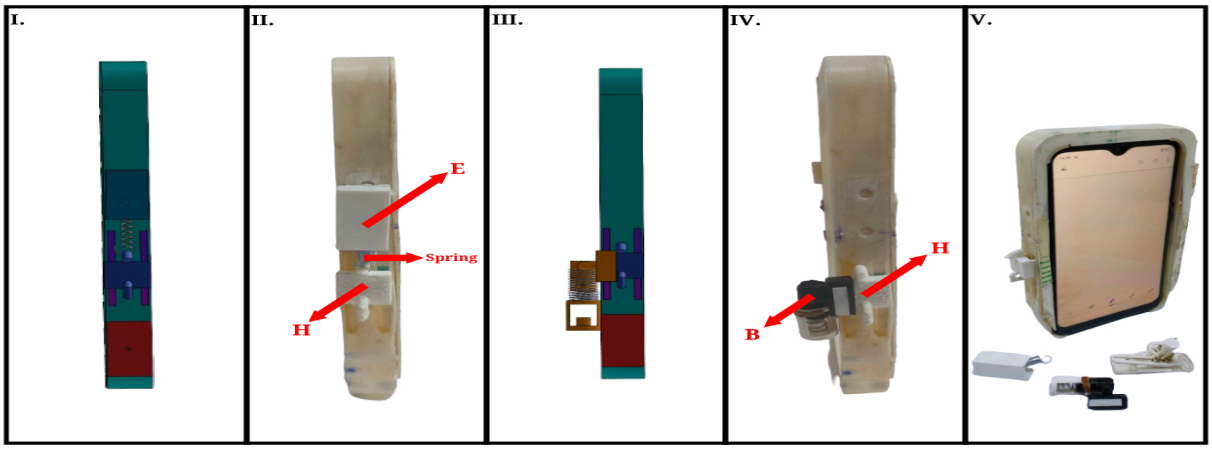

Figure 3.15: Fig. I shows MobiTangibles case with linear stretchable controls; Fig. II displays Fig. I real image. Figs. III & IV show 3D and actual images of push-button controls. Fig. V displays all connectable MobiTangibles.

of such interferences on system performance. Fourth, we did not use validated questionnaires like NASA-TLX and SUS, opting instead for streamlined evaluation methods based on recent works (e.g., [64, 71, 80]). This choice was made because administering and analyzing data from NASA-TLX and SUS assessments can be time-consuming and resource-intensive. The method I opted for has been common and acceptable for such analysis as highlighted by recent literature. In future endeavors, these assessment tools could be utilized to comprehensively evaluate user cognitive load, performance, and usability. Fifth, I did not compare our approach with other constrained input methods. While the evaluation aligned with common practices in the field, e.g., [64, 72, 80], it may limit the comprehensiveness of the findings. Future work can conduct a comprehensive evaluation by comparing with constrained input methods. Sixth, the presented low-fidelity approach does not fully replicate shapes of precision hand-held tools in VE. Future work could enhance fidelity of tool representation for a more accurate virtual experience.

Looking ahead, future endeavors in such miniaturized interaction experience domain may encompass refining the design of MobiTangibles and broadening its support for other kinds of hand-held tools' miniature manipulation experiences as well. While there could be many types of MobiTangibles designs, as an example of possible future paths for developing the

idea, I provided two further designs of miniaturized controls based on the explored design approach. This not only demonstrates the technique's versatility in offering an authentic experience of a variety of miniature controls in VR, but it also lays the groundwork for future research into different types of MobiTangibles design. The below-presented designs are related to the following types of miniature control: one is push-button, and another is linear variable stretching.

- **Stretching Type MobiTangible:** This type of MobiTangible uses a compressed spring within an enclosure (E), whose exposed end connects to the holder. As the holder (H) is stretched backward, the attached strip (S1) with a magnet moves in the same direction. Upon release, it swiftly returns to its original position, allowing for a realistic experience of a miniature control manipulation involving stretching & releasing actions (Fig. 3.15 I & II).

- **Push Button Type MobiTangible:** A part of a button (B) connects to the holder (H), as shown in Fig. 3.15 (III & IV). When the button is pressed, the holder (H) moves downward, causing the strip (S1) with the magnet to move backward. Upon release, the combination returns to its original position, simulating the button's press and release action.

Moreover, in future work, additional research could be conducted on longitudinal user studies to gain greater insight into the impact of MobiTangibles on users' learning experiences in VR connected to the efficient manipulation aspects of the hand-held tools miniature control. This study could assess the impact of the practical application of knowledge acquired in VR environments towards efficiently utilizing such precision hand-held tools on a given task. In addition, further research could include comparison studies examining the differences between learning in virtual environments and traditional, in-person settings.

3.7 Conclusion

In conclusion, in this work I introduces MobiTangibles from the perspective of enabling simplified miniature input device prototyping in VR, a novel concept that enables precision hand-held tools' miniaturized control interaction experiences in VR, beneficial for skill training and hand-held tools' understanding. Users using MobiTangibles can physically experience and interact with various kinds of miniature controls of precision hand-held tools (or similar objects) involving motions, e.g., translation, rotation. The explored approach offers users a passive, lightweight, easy-to-use, easy-to-setup, and portable means to experience and engage in various physical miniaturized interactions with precision hand-held tools within the VR environment. This research includes a rigorous technical evaluation that not only demonstrates the strong correlation between magnetic field variations and the performance of MobiTangibles but also affirms the device's robustness against potential electromagnetic interference. This validation underscores its technical reliability, particularly in indoor settings. Additionally, this work user-centric evaluation findings highlight MobiTangibles' capacity to deliver enhanced realism while interacting with miniaturized controls of precision hand-held tools in VR, making it the preferred choice among the participants.

CHAPTER 4
EXPLORING MAGNETIC FIELD SHIELDING AS AN INPUT-SENSING TECHNIQUE

4.1 Introduction

In the ever-evolving field of human–computer interaction (HCI), the pursuit of innovative input-sensing methods plays a prominent role in research endeavors. Just like the fabrication toolkit empowers users with various options, such as 3D printing [129–131], laser cutting [132], circuit printing [133, 134], and vacuum forming [135, 136], to create prototypes based on their skills and available resources, the diversification of input sensing methods becomes essential. This diversification allows users to adapt to alternative approaches when faced with challenges, such as during early-stage prototyping, or when a particular input-sensing method becomes less reliable due to constraints in resources or complexity. Moreover, a wide range of input-sensing methods fosters the development of intuitive and efficient user interactions with digital devices and applications, serving as critical conduits between users and digital environments. For example, ultrasonic sensing, originally explored in the early 1930s for object detection and distance measurement, has now gained widespread adoption in HCI, facilitating functions like hand [137, 138] and face [139] gesture-based control. Another notable example is electrical impedance tomography, which was first developed as a medical imaging technique in the late 1970s but has now been found to used for HCI applications. These applications include detecting human touch on surfaces [140] (or paper [141]) as well as various hand gestures [142]. Similarly, techniques such as frustrated total internal reflection (FTIR; which provides a unique way of detecting touch [143]) and spectroscopy [144], originally developed for specific purposes 50–60 years ago, have found new uses in diverse HCI applications. These technologies enhance human interaction with digital information

(or objects) in captivating ways. The field of HCI, which is constantly evolving, requires continuous innovation in input-sensing techniques. These techniques are crucial for providing users with flexible and efficient ways to interact with digital environments, ensuring an intuitive, responsive, and immersive experience. Existing methods, including ultrasonic and spectroscopy-based sensing as well as established capacitive sensing [145], continually push the boundaries of interactive technology.

This study introduces a new approach to input sensing by utilizing magnetic field shielding (MFS) principles. In previous instances, MFS has mainly been used to protect sensitive materials from magnetic interference and reduce the impact of magnetic fields on existing sensors, such as electronic devices and human health [146, 147]. For instance, in the case of earphones, a magnetic shield is strategically included in the design to contain the magnetic field within the casing, thus avoiding prolonged exposure of human ears to magnetic field strengths that may pose potential health risks [148]. A similar protective measure is observed in smartphone styluses, where a magnetic shield is incorporated within or on the surface of the stylus. This shield effectively protects external objects, such as IC cards and flash storage devices, from magnetic interference that may originate from the magnet within the stylus [112]. Notably, Liang et al. showcased the application of MFS in their GaussStones project [149]. In this project, MFS was utilized to safeguard electronic components and prevent any potential interference caused by magnetic fields. Traditionally, MFS has primarily been investigated in the fields of electronics and materials science for protective purposes. **However, despite these advancements, the potential of MFS as an input-sensing method remains largely unexplored.**

To address this gap, this study investigates the potential of MFS to facilitate input sensing, utilizing the inherent characteristics of magnetic fields. I explore the theoretical foundations of MFS and provide a detailed explanation of its technical implementation methodology. Additionally, I present empirical evidence that demonstrates the effectiveness of MFS as an input-sensing technique through controlled experiments. By capturing vari-

ations in the signal of the sensor (i.e., magnetometer) using both basic programming logic and advanced machine learning techniques, the experiments highlight the practical value of the MFS approach for input sensing. The findings demonstrated that the MFS method can be utilized to create input in any form, i.e., binary/analog and also indicate that variable-type metal shields can also be easily classified with more than 94% accuracy. As a result, it not only demonstrates MFS's effectiveness for researchers, designers, and innovators, which they can leverage to investigate new innovative interaction paradigms and potential interactive interfaces (e.g., in gaming, entertainment, and novel artifacts), but it also provides an economical means for early-stage prototyping of passive yet functional input controls.

4.2 Related Work

In the field of input sensing, numerous approaches have emerged over the years, each significantly impacting user interactions and interface technologies. This diversity allows researchers and designers to explore innovative ways of interacting with devices and environments, potentially leading to the development of groundbreaking applications, as noted by Hinckley et al. [150]. Moreover, it enables user customization by empowering them to choose input methods that align with their preferences and requirements [151, 152]. For instance, capacitive sensing [153], which originated in the early 1960s, initially focused on proximity detection and touchscreens. However, with the advent of smartphones and tablets, it became crucial in HCI, introducing touch-based gestures and multi-touch capabilities, thereby revolutionizing modern touchscreen technology. Modern magnetic field sensing technology [154], rooted in principles of magnetism dating back centuries, emerged in the mid-20th century. It has gained importance in HCI, particularly as an input method for specialized applications such as stylus devices [112] and smart rings [107]. By detecting changes in magnetic fields caused by the movement of magnets, this technology enables precise and controlled user interactions. This capability is especially beneficial in scenarios like digital drawing (e.g., in AR or VR environments) using hand gestures [155] and ensuring unhindered user interaction

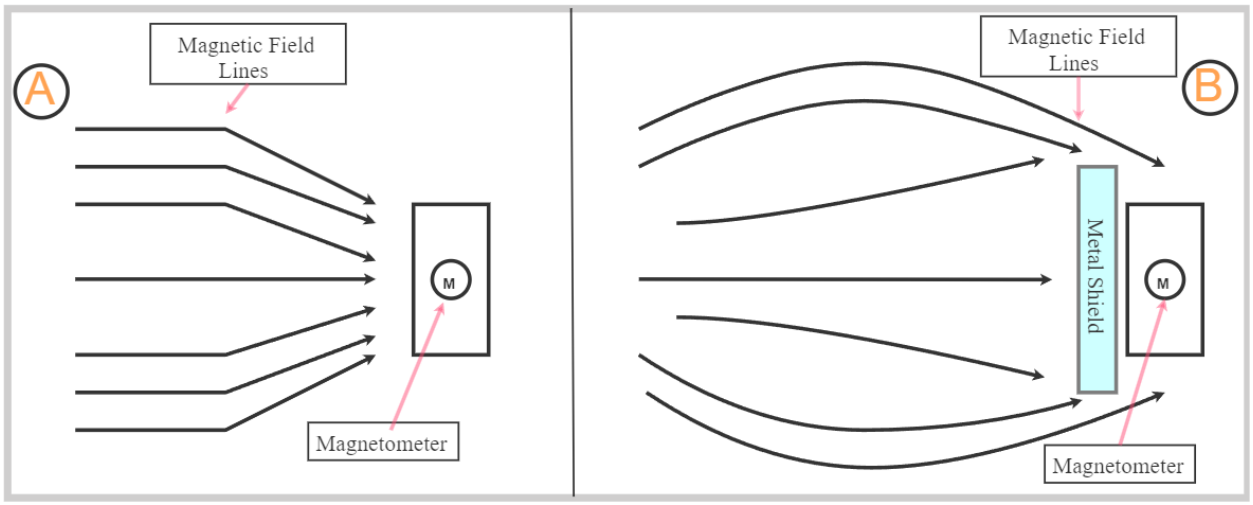

Figure 4.1: Illustration of magnetic field shielding mechanism: (A) without a metal shield and (B) with metal shield.

with digital devices [106] such as smartwatches and smartphones.

In this study, I investigated MFS as a new method for input sensing, which represents an innovative frontier in HCI. Similar to previous approaches that initially focused on specific functions but ultimately revolutionized HCI with groundbreaking human–technology interactions, MFS holds potential for an exciting new phase in this ever-evolving field. This emerging method of input sensing will allow researchers and designers to push the boundaries of technological interaction in various contexts, encouraging the development of novel interaction patterns and potentially transformative interfaces.

4.3 Magnetic Field Shielding Mechanism

MFS is a common method used to protect electronic components from electromagnetic (EM) interference. This process involves encasing the object, which could be anything from electronic components to other sensitive items, with a metallic shield. By positioning the metal casing or a portion of it between the object and the magnetic field lines, the magnetic field is redirected; it passes over the surface but does not permeate the shield, thus reducing the object's exposure to the magnetic field, as illustrated in [149] and depicted in Figure 4.1.

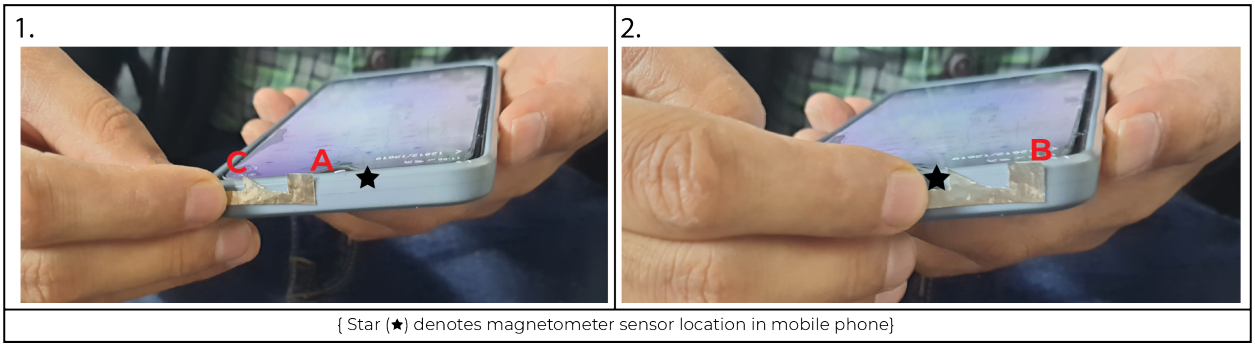

Figure 4.2: Experiment testing procedure

The only prerequisite for MFS is that the metal shield must contain ferromagnetic materials, e.g., iron or nickel [1]. I conducted experiments to investigate the impact of ferromagnetic metal shielding on a magnetic field measuring instrument. Specifically, the objective was to determine how variations in the thickness and geometry of metallic sheets affect the variation in magnetic intensity signals detected by the instrument. Importantly, I did not generate the magnetic field using magnets during these studies. Instead, I utilized the Earth's magnetic field, which is always present and can be easily detected by any magnetometer. This approach eliminated the need to arrange resources such as magnets and the requirement to precisely control the intensity of the magnetic field. It is important to note that the decision not to use a magnet was not due to limitations, but rather to emphasize the versatility of the MFS approach for input sensing.

I used different types of materials, specifically magnetic shields, to explore the questions mentioned earlier. These materials included various metal sheets of different shapes and thicknesses, as shown in Figure 4.3 (first row). To measure and observe the effects of these different metal plates, I used a smartphone [2] as a measuring instrument. I chose smartphones because they are widely available, and almost all smartphones nowadays have a magnetometer sensor that can measure magnetic fields. While any demagnetised material having maximum ferromagnetic content could have been used for testing, I chose to use coated nickel metal sheets with a nickel content of more than 80%. These sheets were se-

[1] https://www.kjmagnetics.com/blog.asp?p=magnetic-shielding-materials
[2] https://www.oppo.com/en/smartphones/series-a/a5s/

lected due to their widespread availability both online [3], and offline. To create metal sheets with different thicknesses, I stacked and taped together five sheets of similar thickness but varying lengths, as shown in Figure 4.3 (marked with 4). Each sheet used in the experiment had the overall dimensions of 30 mm (length) × 10 mm (width) × 0.15 mm (thickness of one sheet). I evaluated the method of shielding the magnetic field (also called as MFS) for input sensing by conducting tests near commonly encountered electromagnetic devices, such as a workstation, laptop, and air purifier (Dyson), all of which were turned on (akin to the reference [155]). Testing in the presence of electromagnetic devices allowed us to observe how the sensor signal varied when magnetic shields (metal plates) were present or absent. During the testing, I held the smartphone in my hand, as shown in Figure 4.2, so that I could conduct the experiment close to the electromagnetic devices (within 30 cm of each).

In each case, I placed the metal sheet on top of a mobile phone and slid it across the surface. While sliding, one end of the metal sheet was securely pressed through a finger against the top edge of the mobile phone (position C in Figure 4.2). To monitor and record any changes in magnetometer signals, I used the Phyphox App [4], which is freely available on both the Android Play Store and iOS store. The app's default sample rate, set at 50 Hz, was used to record sensor data. In addition, the app includes a timer function that allows for setting the experiment duration. Before starting each experiment, I set the timer and then pressed the start button of the app. This procedure was consistently followed for all tests conducted with each metal plate (a total of 4). The experiment was limited to a duration of 20 seconds. During the first five seconds, I collected only raw sensor data without a metal plate present. After that, for the remaining 15 seconds, I slid the metal sheet across the entire surface of the mobile phone, starting just before the designated magnetometer sensor point (position A in Figure 4.2), continuing until the metal sheet reached the opposite end of the mobile phone (position B in Figure 4.2), and then retracing back to position A, as shown in the figure.

[3] https://maccmodels.co.uk/shop/0-015-nickel-silver-sheet-12-x-6/
[4] https://phyphox.org/

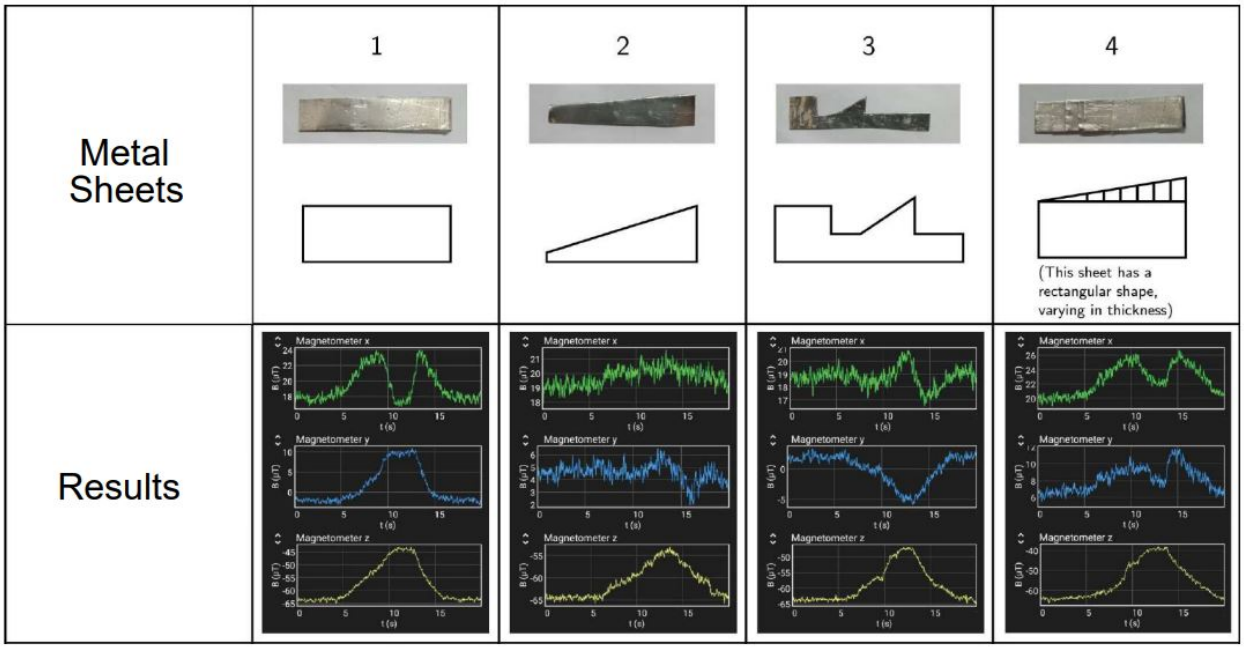

Figure 4.3: First row depicts types of metal shields, and second row demonstrate the obtained experiment results (raw, i.e., unfiltered signals sensor data).

4.3.1 **Findings**

In this study, I thoroughly examined the method of shielding the magnetic field as a technique for input sensing. The results of our investigation are presented in Figure 4.3 with meticulous detail. The obtained findings were extremely significant: the magnetometer signals showed fluctuations whenever a metal sheet, used as a shield, was placed near the sensor. However, the analysis went beyond this observations, revealing a more complex relationship between these variations and two important factors: the thickness and variability in shape of the metal sheet. This discovery is summarized in the fourth column of Figure 4.3 in terms of thickness variability and in the first, second, and third columns in relation to shape. The findings illustrate the fluctuations in magnetometer signals across all four distinct metal plates. It was also observed that in the absence of any shielding (i.e., metal plate) placed on top of the sensor, the magnetometer signals remained stable within the timeframe of 0 to 5 seconds. However, upon the introduction of metal sheets, a noticeable alteration in the magnetometer signals occurred within the period of 5 to 20 seconds.

This suggests that modifying the thickness or shape of the metal sheet directly impacts the magnetometer signal, albeit in different ways. An advantageous aspect of this discovery is that specialized tools are unnecessary for cutting these metal sheets into various shapes due to their thinness. Ordinary scissors, commonly found in labs, homes, and other spaces, are sufficient for the task. Furthermore, even in the presence of electromagnetic devices, signal variation in each of the four scenarios remained resilient, highlighting the effectiveness of the MFS approach for input sensing. The potential applications of this discovery are limitless, opening up possibilities for the design and development of customized interactive interfaces and also in the rapid prototyping process of interactive controls for creators and beyond.

Given the well-documented benefits of tangible interaction, as explained by Ishi et al. [83], and building on previous research such as [97, 156], which introduced an interactive desktop smartphone case with tangible controls, I have adopted this established framework. Based on the experimental results, we have designed specific tangible inputs enclosed in a casing as described in Section III-B to examine and validate the effectiveness of MFS as a real-time input method. The ultimate aim consisted of two primary objectives.

First, the investigation aimed to determine if the change in sensor signal caused by a metal shield, when used for any type of input (e.g., binary or analog), could be easily detected using a simple programming approach. Regarding binary input, the focus was on determining if the magnetometer sensor signal, along any axis, consistently shows a significant deviation from its baseline whenever a metal shield approaches the sensor.

Conversely, when examining the behavior of an analog type associated with a metal shield, the objective was to identify consistent and distinctive patterns and variations in the magnetometer sensor signal across any axis when the shield is moved close to the sensor in one direction. For example, moving the metal shield in one direction might increase in sensor signal response, while movement in the opposite direction could lead to a decrease in signal strength. Specifically focusing on analog aspects, I aimed to investigate whether

the magnitude of these variations at each position, relative to the baseline, can be discerned and effectively used to detect the shift in the metal shield from its initial position using a straightforward logical approach. Second, I aimed to investigate if it is also feasible to classify distinct metal shields when brought near the magnetometer sensor.

4.3.2 Design of Inputs Based on Magnetic Field Shielding

I built three different types of fundamental tangibles as inputs, taking inspiration from [97] and [156], and embedded them in a smartphone table-stand case, which includes a slider, a rotary, and a push-button in order to technically evaluate both questions, as mentioned before. Each of these tangibles is associated with a distinct kind of metal plate (i.e., shield). In this section, I provided and displayed in digital form the actual construction process of all three distinct tangible modalities and their integration process within the case, one by one, below. This demonstration also illustrates how MFS approach (basically ferromagnetic material) can be utilized to design and develop various types of tangible controls, providing an additional avenue for low-threshold prototyping of such controls. Furthermore, because such metal shields are very thin and have sharp corners, sliding them, in the same way, every time accurately on the mobile top boundary through hand, basically fingers, may cause additional discomfort, as I discovered and experienced in the pilot testing, to any participant during technical evaluations (Sections IV-A to IV-C) and the data collection process (Section IV-D). Consequently, further reasons for leveraging a tangible approach were as follows, in addition to showing how metal shields can be utilized to prototype physical (i.e., tangible) controls of any type (binary or analog) as a low-threshold alternative for early-stage prototyping. First, to ensure consistency in the metal sliding over the smartphone's top boundary while investigating MFS as an input method; second, to minimize the potential of human error in the data-gathering process of metal shields, which could stem from the user's irregular movements of the metal shield; and third, to guarantee user safety from the sharp edges of the metal shield.

- Push button (Figure 4.4, parts 1 and 3): This design features a push button suitable for integration into any side of a case. The design incorporates a groove along the case edge to accommodate a thin metal sheet (0.15 mm), with one end floating and the other attached to a physical push object. The physical push object resides within a small enclosure depicted in Figure 4.4, part 3, sky-blue color, and is equipped with a spring to constrain its movement within a specific area. The push button functions as follows: when the physical push button is depressed, the metal plate will obstruct the sensor, thus activating it (ON), and upon release, the spring-induced recoil force will restore the metal plate to its original position, thus deactivating the sensor (OFF). The advantage which it can provide is that button can be employed to handle various actions in an application, e.g., like answering a call while wearing gloves or shooting in a game to prevent screen occlusion. This can be accomplished by easily programming the system (device) to identify signals associated with a variety of button presses, including single, double, and long presses (one such example is presented in Section 4.4.3). Each form of press will be associated with a specific action, thereby guaranteeing a user-friendly and seamless interface.

- Slider (linear translation manipulation) (Figure 4.4, part 1): The slider design necessitated the use of a thin, rectangular object (blue color) produced through 3D printing. As depicted in Figure 4.4, part 1, this object serves as an attachment point for both a slider widget and a metal plate (connected to the object endpoint). As the slider widget moves forward and backward, the shape of the metal plate linked to the object also adjusts accordingly. This movement causes the magnetometer sensor readings to vary, as a new portion of the metal shield covers the sensor, effectively transforming this tangible into an analog input device. It can be employed to translate items linearly, such as adjusting the position of a rocket in a game or controlling brightness while reading or watching a movie without obstructing the smartphone touchscreen.

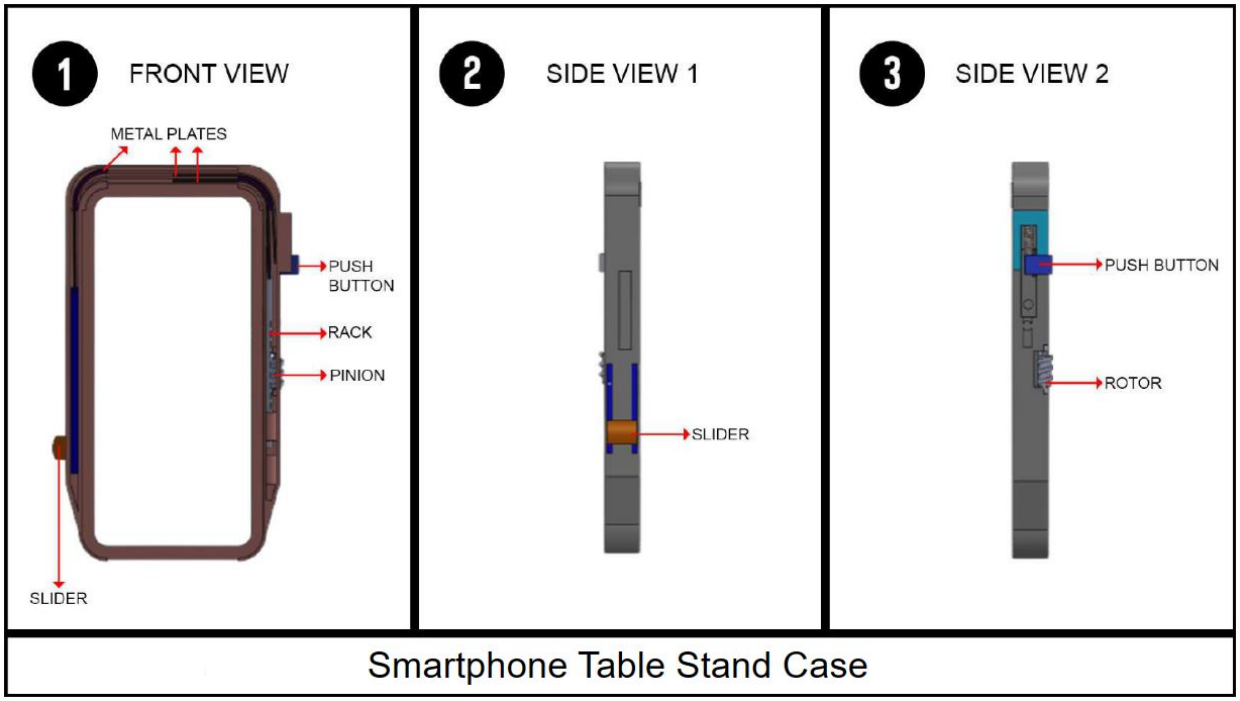

Figure 4.4: Design of tangible inputs based on magnetic field shielding.

- Rotary (rotation manipulation) (Figure 4.4, parts 1 and 3): The rotary mechanism, similar to reference [5], utilizes a rack and pinion system of the helical type. The metal plate is affixed to the tip of the rack. When the pinion rotates clockwise or counterclockwise, the rack experiences linear motion. This movement of the rack, whether forward or backward initially, corresponds to the motion of the triangular-shaped metal plate linked to it. As a result, a variable portion of the metal shield, connected to the rack, moves in front of the sensor, leading to adjustments in the magnetometer sensor readings. This effectively converts it into an analog-type input widget.

For the push button, I used a metal strip that was 0.15 mm thick, as shown in Figure 4.5 (M1). The metal strips with the same thickness, which were used for the slider and rotary controls (analog in nature), are depicted in Figure 4.5 (M2 and M3). Figure 4.4 (part 1) demonstrates how different input types can be easily prototyped using the MFS method. Additionally, Figure 4.4 (part 1) shows the initial position of the metal plates when no

[5]https://www.youtube.com/watch?v=U4wsiaOAnRQ

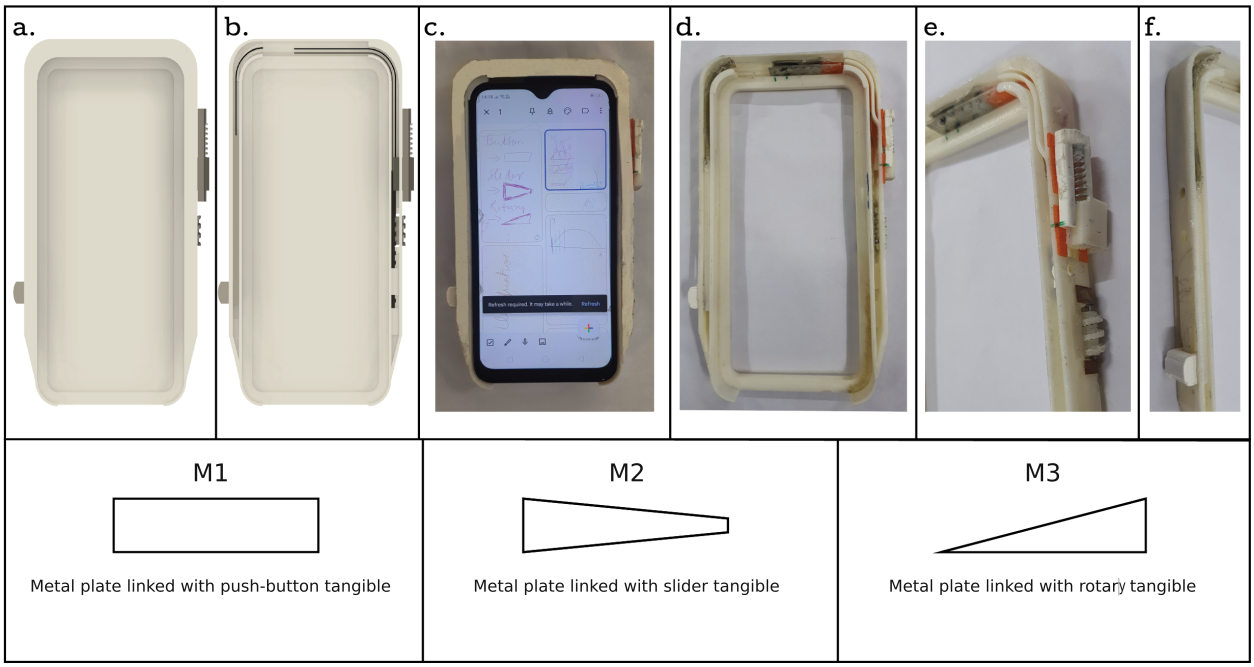

Figure 4.5: The designed passive widget case with integrated button, slider, and rotating widgets is shown in the first row. Images are displayed (in first row) from various angles, as well as by placing the smart device within the case. Metal plate linked with each type of tangible control are shown in the second row.

physical controls are being manipulated. Figures 4.5 (a and b) provide a 3D visualization of how the three different physical controls are assembled and integrated within the table-stand case, while Figures 4.5 (c and d) present actual images of the smartphone table-stand case prototype. Apart from the metal plates, all components of the smartphone table-stand case were produced using 3D printing. However, it is worth noting that this technique does not exclude the use of alternative low-cost technologies, such as laser cutting, for creating the smartphone table-stand case prototype. Furthermore, a physical control can be placed on any side of the smartphone cover, as there are no limitations on using any size of metal plates inside the case depending on the position of the magnetometer sensor (which can be located anywhere on the top edge of a smartphone). The overall measurements of the designed smartphone table-stand case (including all three physical controls) are 165 mm (length) $\times$ 90 mm (width) $\times$ 15 mm (thickness), and it weighs 45 grams.

4.4 Technical Evaluation

To comprehensively assess the effectiveness and strength of the methodology, I set three main objectives for the technical evaluation. First, I aimed to evaluate the consistency and reliability of variations in magnetometer sensor data across all axes when exposed to binary and analog interactions with artificially created physical controls. These controls consisted of metal shields housed within a table-stand case. Second, I aimed to utilize previous research findings to manipulate virtual objects in real-time, to confirm that the observed changes in sensor signals during interactions with metal shields, as reported in prior studies, can be detected through basic programming logic. Additionally, I sought to determine the capability of differentiating between three types of physical interactions—button, rotary, and sliders—created using three different types of metals, and measured using the magnetometer in mobile phone devices. For the evaluations, I used the prototype tangible interface shown in Figure 4.5c, as it meets the required criteria. It includes metal shields in both binary (push-button) and analog (slider and rotary) formats, as well as various types of metal shields within the case. Additionally, it provides safety against thin metal sheets and offers other advantages described in Section III-B, ensuring a smooth and precise data collection process. All assessments were conducted under controlled conditions, taking into account factors such as the influence of electromagnetic devices (similar to Section III-A) and smartphone orientations when attached to a table-stand case.

The combination of the smartphone with the case was securely positioned or held, resembling the stability of conventional table-stands, e.g., [6] [7]. This setup ensured consistency and relevance in the evaluations, aligning with previous research efforts, e.g., [97]. In daily routines also, smartphones often remain stationary during various interactions, whether held in hand or placed on a surface. Users engage in tasks such as reading, messaging, sketching, watching videos, analyzing documents, browsing, taking photographs, and participating

[6] https://rb.gy/iw68n
[7] https://rb.gy/emjhp

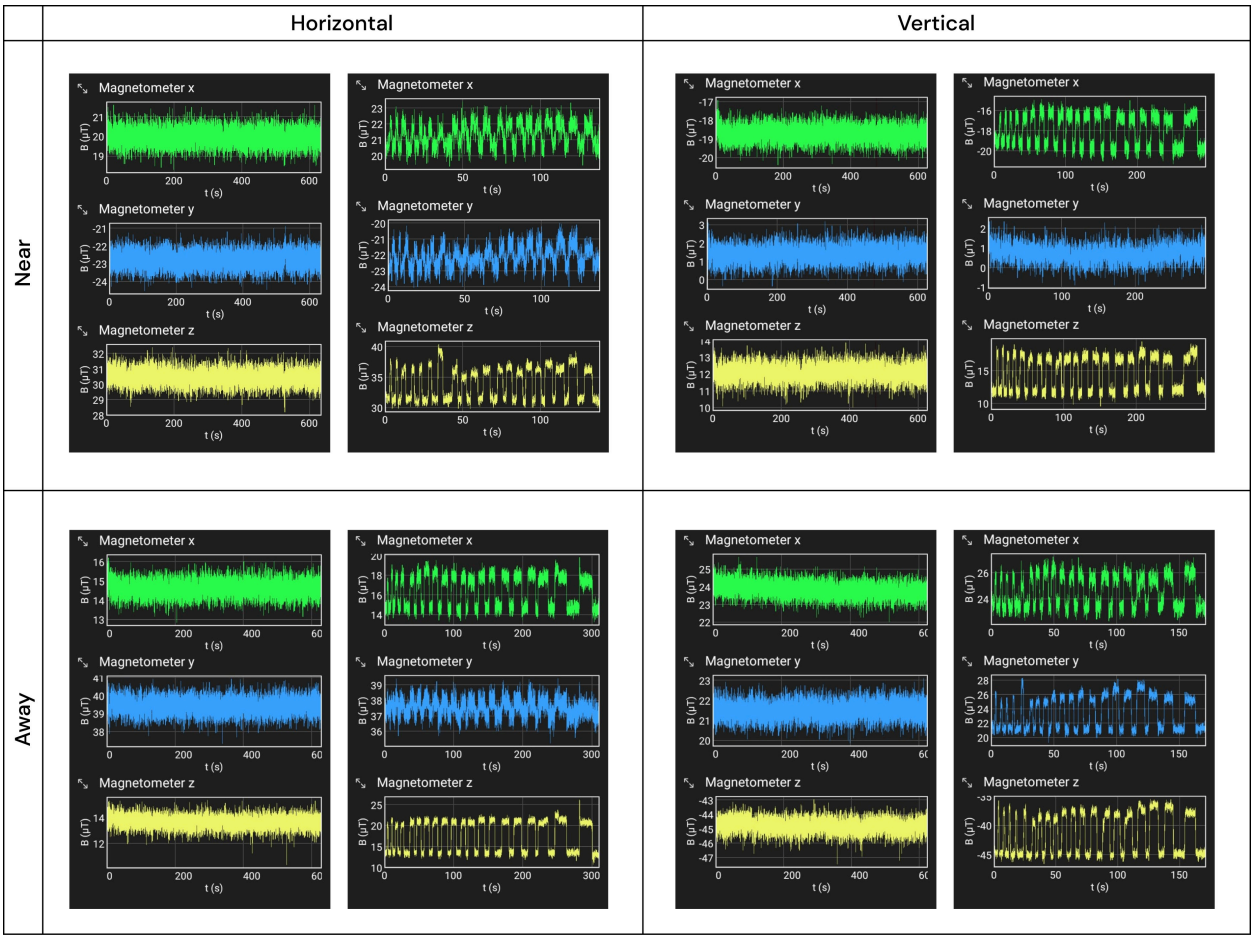

Figure 4.6: The plot illustrates the observed signal variation (always on the right) alongside the baseline data (always on the left) for 20 binary interactions across various conditions and smartphone orientations.

in video conferences (e.g., Meet calls) [157, 158]. Research by Eardley et al. [158, 159] indicates that users adopt stable configurations or resting positions while using their smartphones. These postures typically fall into one of three standard classes: standing, lying down, or sitting at a table with arms resting.

4.4.1 Variations in Magnetometer Sensor Data for Binary Type Interaction

Experiment Objective

The purpose of this experiment is to ascertain whether magnetometer sensor data consistently fluctuate in response to the utilization of a metal shield for binary input.

Experimental Setup and Conditions

The experiment involved a single user conducting tests within a laboratory setting, utilizing a smartphone11 connected to a table stand, as depicted in Figure 4.5. The same application employed in Section III-A was utilized, recording data at a rate of 50 Hz. Two distinct conditions were tested: proximity to electromagnetic devices (< 10 cm), including a workstation, laptop, and air purifier, all operational; and distancing from electromagnetic devices (> 250 cm). Data collection occurred in two primary orientations for each condition: vertical (portrait) and horizontal (landscape) placement of the phone on the table. This setup facilitated the examination of sensor signal variations concerning electromagnetic devices and phone orientations. For binary interaction with a metal shield, the push button of a tangible case connected to the metal shield was utilized.

Experimental Procedure

In each condition, "Near" and "Away," and for each of the two phone orientations, the experiment began with the collection of 10-minute baseline data from the magnetometer sensor (across all three axes), while the phone (with attached case) remained untouched. The baseline data was recorded when no metal plates were near the sensor. Subsequently, the researcher interacted with the binary tangible (connected to the metal shield) 20 times. This process was repeated for the other orientation and condition, with another 10-minute baseline data collection preceding 20 interactions with the push button. To ensure distinct sensor data for each interaction, the researcher maintained temporal gaps between each full interaction and held the push button for a brief period before release to capture any new sensor data. I documented the start and stop times for each interaction. By recording data across all three sensor axes, I aimed to identify consistent behavior irrespective of conditions or orientations. Subsequently, I applied a standard noise removal process from magnetometer data by applying a moving average smoothing with a 20-sample window. The findings, derived from this analysis, are presented in the subsequent section.

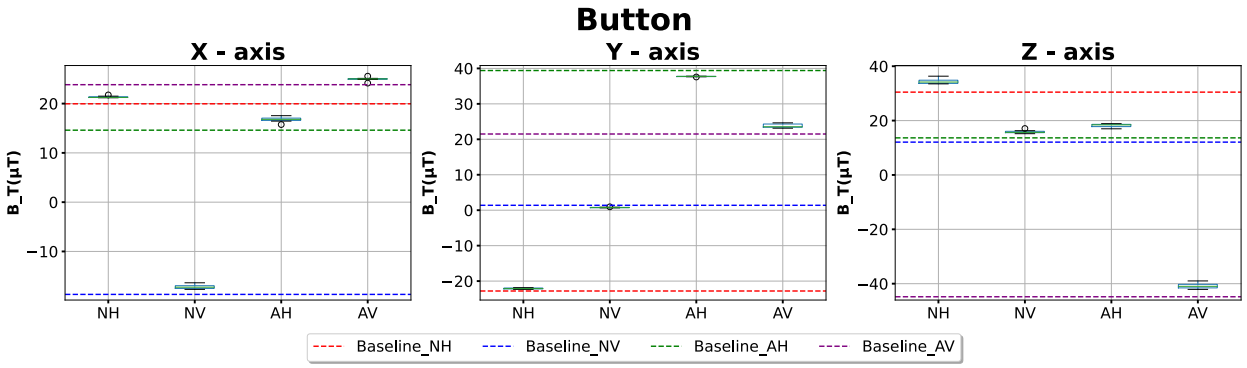

Figure 4.7: The plots illustrate the deviation of each magnetometer sensor axis from its baseline during binary interactions. The abbreviations "H" and "V" denote horizontal and vertical phone orientations, respectively, while "N" (near) and "A" (away) indicate proximity to and distance from electromagnetic equipment, respectively. For example, the "NH" condition represents the phone attached to the case placed horizontally near electromagnetic equipment. Negative and positive values is because a magnetometer detects both field strength and direction.

Table 4.1: t-Test Results for Magnetometer Sensor Axes

	X	**Y**	**Z**
NH	$t_{19} = 4.309,\ p < 0.05$	$t_{19} = 3.97,\ p < 0.05$	$t_{19} = 10.20,\ p < 0.05$
NV	$t_{19} = 8.417,\ p < 0.05$	$t_{19} = -2.3,\ p < 0.05$	$t_{19} = 16.26,\ p < 0.05$
AH	$t_{19} = 10.8,\ p < 0.05$	$t_{19} = -2.16,\ p < 0.05$	$t_{19} = 16.63,\ p < 0.05$
AV	$t_{19} = 7.07,\ p < 0.05$	$t_{19} = 4.77,\ p < 0.05$	$t_{19} = 8.54,\ p < 0.05$

Findings

Figure 4.6 illustrates the observed signal variation (always on the right) alongside the baseline data (always on the left) for 20 binary interactions across various conditions and smartphone orientations. Further, the plots given in figure 4.7 depict the deviation of each magnetometer sensor axis from its baseline during binary interactions, in all four scenarios of interactions. We first tested the normality of data samples collected under various conditions and orientations using the Shapiro–Wilk test. All 20 binary events within each sensor axis exhibited a normal distribution ($p > 0.05$). Following this, we performed one-sample one-tailed t-tests across all four scenarios, considering two conditions each in two orientations, to ascertain if the variations of the binary interactions significantly exceeded the baseline data. This analy-

sis was performed for all three axes of magnetometer data. The t-tests unveiled statistically significant disparities across all four conditions within each sensor axis. The statistical results for all scenarios are summarized in Table 4.1. The results depicted in Figure 4.7 demonstrate that, regardless of the smartphone's placement or orientation, one of its sensor axes consistently responded to the presence of a nearby metal plate, triggered by pressing a push button. In essence, the analysis demonstrated that the data from all three axes were consistently and significantly greater than the baseline across all four scenarios, providing robust evidence of the impact of the binary interactions.

4.4.2 Variations in Magnetometer Data for Analog Interaction with Metal Shield

Experiment Objective

The purpose of this experiment is to confirm the consistency and detectability of variations in magnetometer signals corresponding to the movement of a metal shield across its range of motion.

Experimental Setup and Conditions

The data collection setup and experimental conditions were analogous to those detailed earlier in Section IV-A2.

Experimental Procedure

In each condition, a user placed the phone (attached to the case) in one of the orientations and interacted with analog-type tangible controls (rotary and slider). The user was instructed to collect baseline data for the first 3 minutes without interacting with any tangible controls. After this period, two iterations of interaction were performed with each tangible control linked to a metal shield. Each iteration involved moving the tangible control from its neutral position (C0) to a marked intermediate or end position and then back to the neutral position before moving it to the next position (see figure 4.8). This ensured accurate recording of

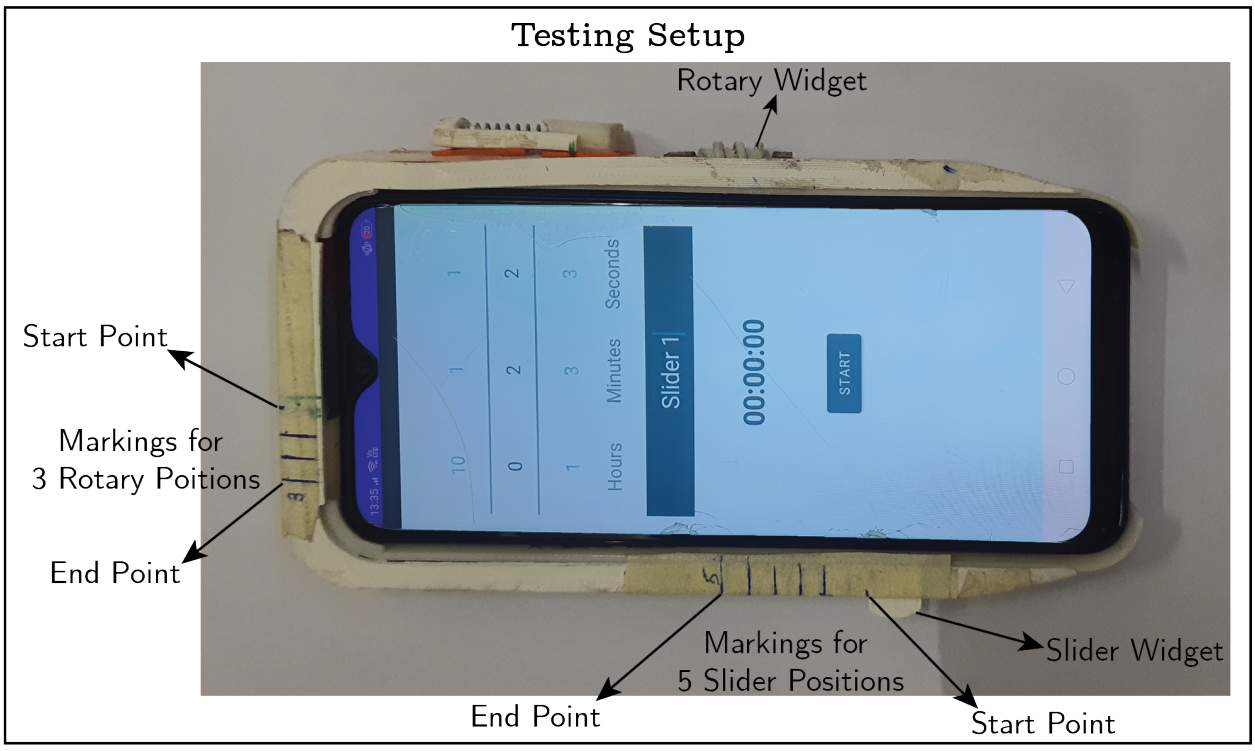

Figure 4.8: Testing Setup

magnetometer signals associated with each position. The testing setup is shown in Figure 4.8, which depicts 5 positions for slider tangible between its zero and full movement and 3 positions for rotary tangible. The advantage of these marked positions is that they will allow the user to easily move the metal shield variably on the smartphone top boundary every time through an analog control near the sensor between its zero to the entire movement.

During each iteration, the user engaged naturally, maintaining a temporal gap before returning the control to its initial position (C0) and when shifting it to another position. This allowed recording of sensor data variations for each position and visualizing signals associated with position changes for analysis. The user performed two back-to-back iterations for each type of analog control in each orientation and condition. After collecting data twice for each position in each condition and orientation, it was stored before repeating the step. This process enabled the collection of signals for both phone orientations and conditions for both types of metal shields linked to analog tangible controls, a slider, and a rotary. After collecting all data related to both metal shields in the abovementioned conditions, I

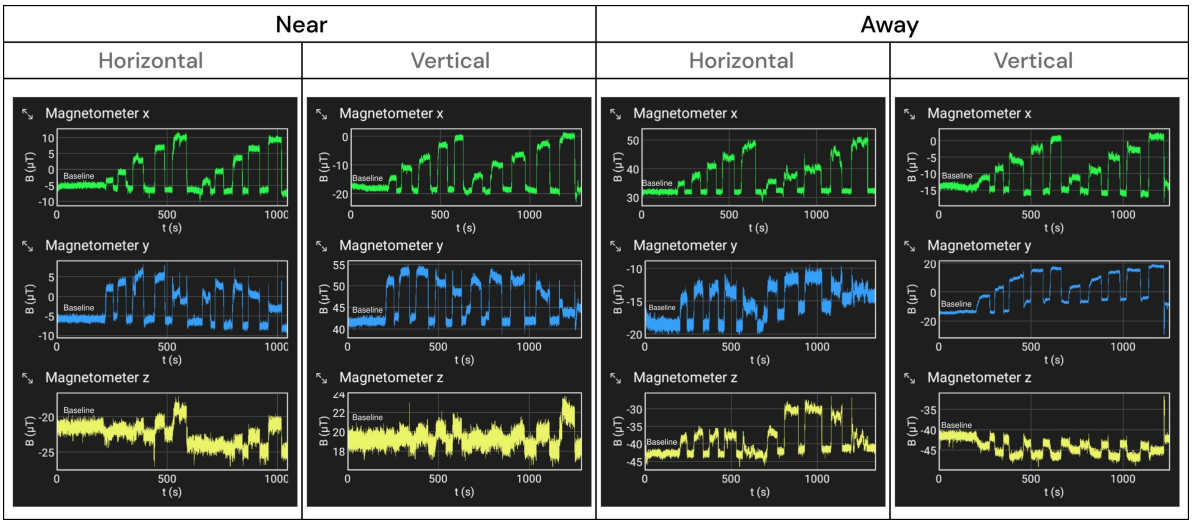

Figure 4.9: Initial baseline data (starting approx 3 minutes) for each sensor axis, with respect to each condition and orientation, is displayed with the obtained unfiltered input signals for slider tangible control movements. Five distinct patterns, corresponding to 5 distinct slider positions C1- C5, can be observed on x-axis after 3 minutes baseline data (i.e., till 200 seconds) irrespective of any condition and orientation of the phone, while on other sensor axes (y and z) at the same time, i.e., when sensor x-axis demonstrate pattern related to a particular position, some variation can be observed with respect to their respective baseline data.

first performed the smoothing process using 20 samples of window size, then performed the analysis and presented the findings in the following section.

In total, I collected 40 sensor signal data points for the slider-type widget (2 times sensor signal data per position x 5 positions x 2 orientations x 2 conditions). For the rotary-type widget, 24 sensor signal data points (2 times sensor signal data per position x 3 positions x 2 orientations x 2 conditions) were recorded. In other words, I collected 8 sample data per position (2 times sensor signal data per position x 2 orientations x 2 conditions) per sensor axis. The objective is to analyze how the sample data for each position deviates from the baseline and other positions within each sensor axis. To achieve this, I used baseline-adjusted data for analysis, which involved adjusting each axis sample data according to Equation 4.1.

$$\text{Adjusted\_values\_sensoraxis} = \text{Realvalue} - \text{Basevalue} \tag{4.1}$$

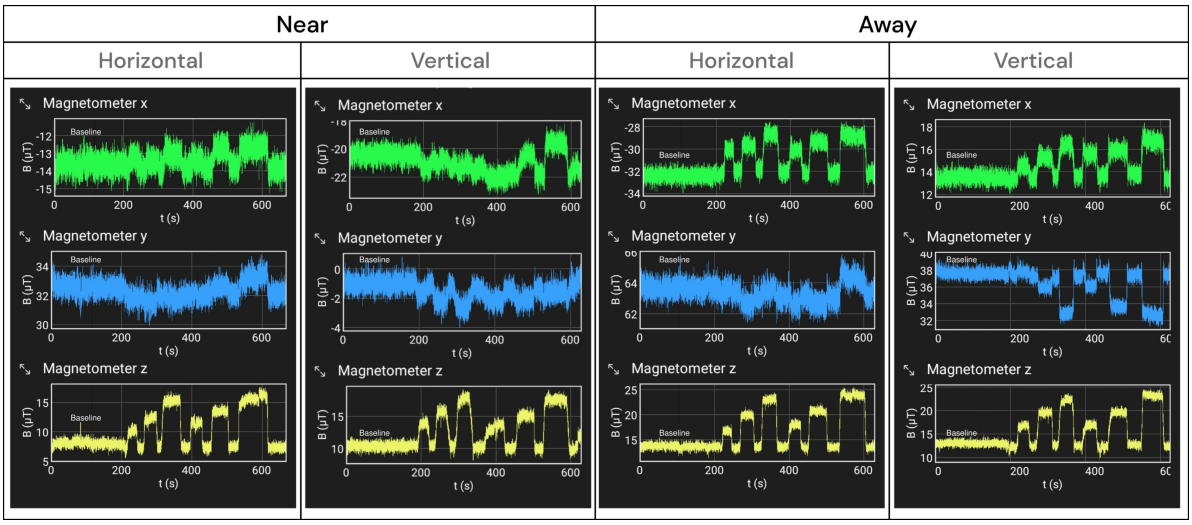

Figure 4.10: Initial baseline data (starting approx 3 minutes) for each sensor axis, with respect to each condition and orientation, is displayed alongside the obtained unfiltered input signals for rotary tangible control movements. Three distinct patterns, corresponding to 3 distinct rotary positions C1- C3, can be observed on z-axis after 3 minutes baseline data (i.e., till 200 seconds) irrespective of any condition and orientation of the phone, while on other sensor axes (x and y) at the same time, i.e., when sensor z-axis demonstrate pattern related to a particular position, some variation can be observed with respect to their respective baseline data.

Findings

As shown in Figures 4.9 and 4.10, I observed that the magnetometer sensor axes, X, Y, and Z, exhibited variations in their measured magnetic field data during analog-type interactions, i.e., while collecting data for each position, with each metal shield through an analog control, regardless of the conditions, near or far, and orientations of the smartphone, whether portrait or landscape. To gain a deeper understanding of the data and determine which sensor axis contains the most significant and reliable information, I conducted a numerical analysis of the collected data samples for each position relative to each sensor axis for both types of analog interactions, a slider and a rotary.

First, I evaluated the normality of the data samples for each position, C1 to C5 for slider and C1 to C3 for rotary, concerning each sensor axis using the Shapiro–Wilk test. The results of the Shapiro–Wilk test indicated ($p > 0.05$) that the data samples for each position

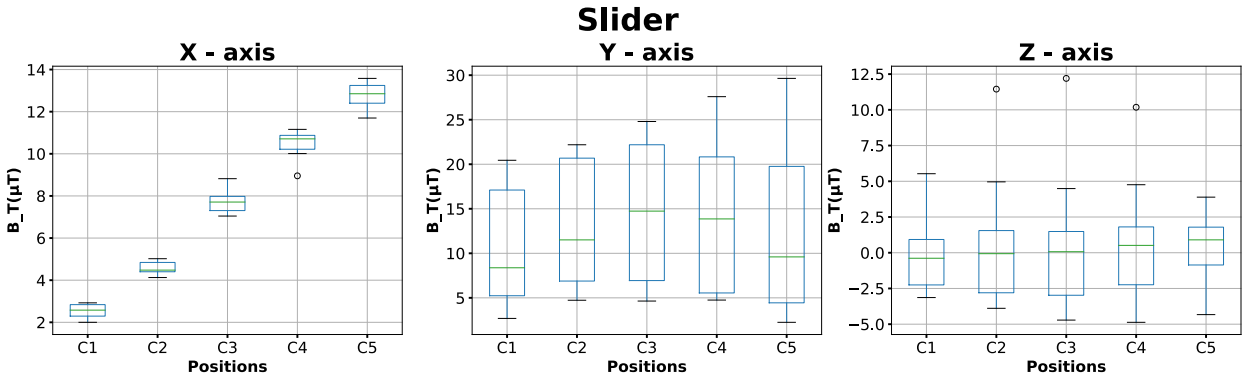

Figure 4.11: Each plot depicts, with respect to each sensor axis, the variations in sensor signal obtained from their respective baseline in relation to each slider tangible position (C1-C5).

with respect to each of the three axes (X, Y, and Z) were normally distributed for both types of analog interaction (slider and rotary). Based on these findings, we proceeded to conduct further analysis of the data associated with slider and rotary-type tangible interactions.

For the slider (figure 4.11), after confirming the normality of the data samples related to each position (C1 to C5) with respect to each sensor axis using the Shapiro-Wilk test, I conducted a one-way ANOVA test to compare the means of the data samples across positions with respect to each sensor axis to which data samples are associated. The ANOVA results revealed a statistically significant difference among the means of the data samples across positions with respect to the sensor X axis ($F(4, 35) = 522.75$, $p < .0001$). However, the test reported no statistically significant difference among the means of the data samples across positions with respect to the sensor Y ($F(4, 35) = 0.314$, $p > .05$) and Z ($F(4, 35) = 0.0581$, $p > .05$) axis. Hence, we performed post hoc analysis using Tukey's Honestly Significant Difference (HSD) test only on the sensor X-axis data samples to investigate further if any specific differences exist between the data samples of each position. The results of the Tukey HSD test confirmed ($p < 0.05$) that significant differences between the data samples of each position exist. These findings suggest that the data samples from different positions exhibit distinct characteristics with respect to sensor X axis. However, the data samples from different positions exhibit similar characteristics with respect to the

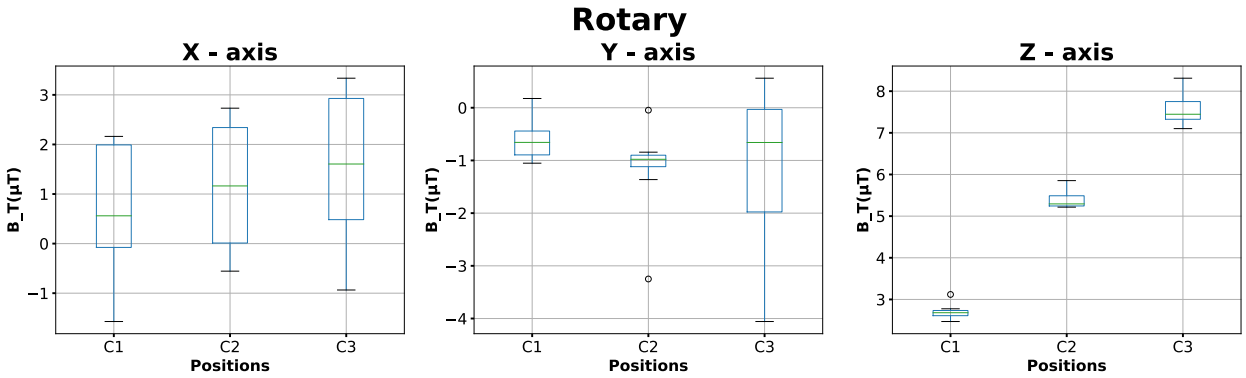

Figure 4.12: Each plot depicts, with respect to each sensor axis, the variations in sensor signal obtained from their respective baseline in relation to each rotary tangible position (C1- C3).

sensor Y and Z axes.

When analyzing the rotary tangible data (figure 4.12), I found that the ANOVA results revealed a statistically significant difference among the means of the data samples across positions with respect to the sensor Z axis ($F(2, 21) = 462.93$, $p < .0001$). However, the test reported no statistically significant difference among the means of the data samples across positions with respect to the sensor X ($F(2, 21) = 0.8422$, $p > .05$) and Y ($F(2, 21) = 0.67573$, $p > .05$) axes. Hence, I performed post hoc analysis using Tukey's Honestly Significant Difference (HSD) test only on the sensor Z-axis data samples. The results of the Tukey HSD test ($p < 0.05$) confirmed that there are significant differences between the data samples of each position. These findings suggest that the data samples from different positions exhibit distinct characteristics with respect to sensor Z. However, the data samples from different positions exhibit similar characteristics with respect to the sensor X and Y axes.

The statistical findings from Figures 4.11 & 4.12, supported by qualitative evidence from Figures 4.9 & 4.10, indicate that sensor X-axis data corresponds directly to the slider's position, while sensor Z-axis data corresponds directly to the rotary mechanism's position. These findings are highly valuable for early-stage prototypers, as they demonstrate that signal changes are easily noticeable and consistent on at least one axis of the sensor. This

approachable technique thus also shows that, during the early phases of ideation, creators may rapidly prototype low-fidelity analog inputs using metal shields alone.

4.4.3 Utilizing Signal Variations from Tangible Inputs for Interactive Applications

Experimental Objective

The objective of this experiment was to demonstrate the practical significance of the preceding section's findings, namely, the real use of a metal shield for digital interaction in both binary and analog forms using straightforward programming logic. I utilized the same tangible case (refer to Fig. 4.5 c) because it involves the utilization of metal shields in both binary and analog forms.

Experimental Setup and Procedure

To validate this concept, I made a program using MIT App Inventor [8]. This choice was motivated by several factors. Firstly, MIT App Inventor is renowned for its user-friendly interface, catering to a wide range of users, from students embarking on their learning journey to seasoned researchers engaged in prototyping applications. Second, the MIT tool provides seamless integration with smartphone sensors, enabling the development of interactive applications based on sensor data inputs.

Two applications were designed to demonstrate the potential utility of MFS approach as another low-threshold alternative for early-stage prototyping. The first application aimed to validate if a virtual object within the App could be controlled in an analog manner. In this scenario, a rocket character was introduced in the App, and its positioning in space could be controlled linearly (i.e., up and down) through interaction with an analog control. Out of the two available analog controls, the slider was randomly chosen for use.

Based on the previous findings concerning the slider-type control, the x-axis data of the magnetometer sensor was used in MIT App Inventor for this analog application. Using the

[8]https://appinventor.mit.edu/

findings from the previous section, which showed that the slider corresponded to a maximum sensor signal change of approximately 12 μT from the baseline, I developed the logic for the slider control. In this logic, I mapped the movement of the rocket character from its starting position to full movement based on the change in magnetometer sensor X-axis values ranging from 0 to 12 μT.

The second application aimed to validate if the App could easily detect signal changes as binary events associated with any single-event actions. In this case, a static ball (Meteor) was placed in the virtual space. The ball would start moving within the virtual environment whenever the physical push button on the smartphone table-stand case was pressed. The overall application and MIT App Inventor-based designed code is shown in Figure 4.13 A and B. While implementing the binary logic in the MIT App as per the findings of the previous section related to binary input where I found the maximum shift of approximately 6 μT in magnetometer sensor z axis, I used the threshold of 3 μT (although any other value could also be used). Therefore, whenever the sensor signal on the magnetometer Z-axis exceeded 3 μT, the Meteor would start moving in space; otherwise, it would remain in its initial position.

I know that changing the position affects the Earth's magnetic field readings. Hence, I also examined how well the method can handle changes in the orientation and position of the table (or phone) stand case. Since, real-world users might place or hold the case in various ways, I (basically a researcher) conducted tests in two situations: holding the case and placing it on a table. When adjusting the case's position, I recorded the initial magnetometer sensor values and incorporated this data into the mobile application. However, fluctuations in Earth's magnetic field readings resulting from changes in position or orientation are unlikely to pose significant challenges for facilitating tangible interaction in real-world scenarios. In real-time settings, it is feasible to seamlessly integrate magnetometer data with gyroscope information to capture alterations in orientation. Additionally, accelerometer data can effectively manage shifts in position. During real-time operation, magnetometer readings linked to changes in orientation or position can be readily disregarded. Once the object's position stabilizes, the

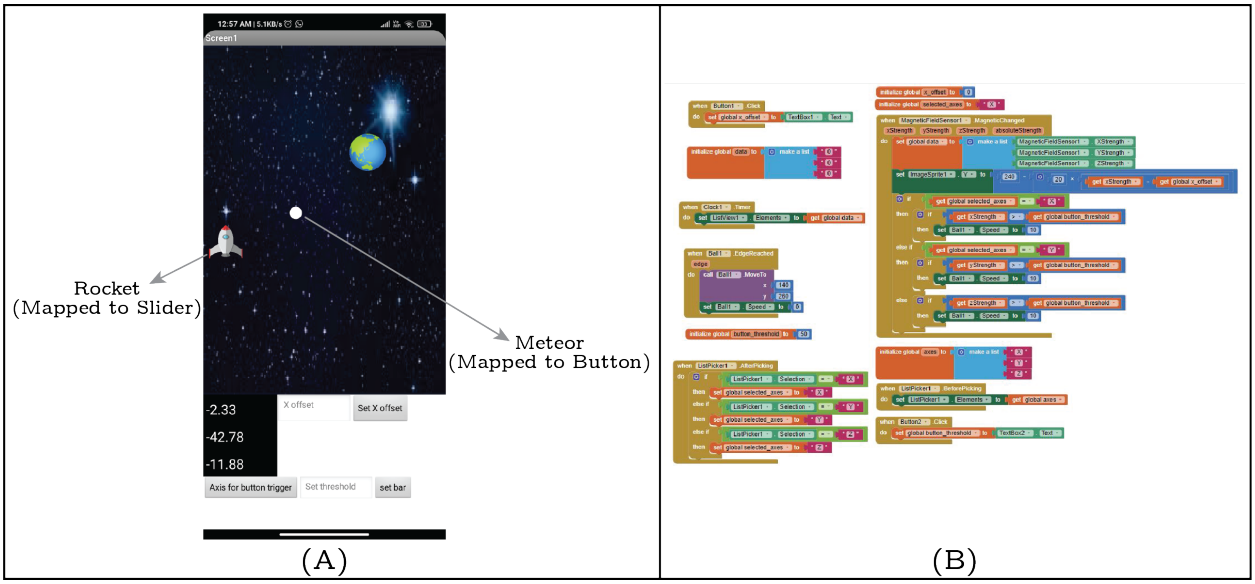

Figure 4.13: Application is shown on left hand side (A). MIT App inventor code is shown on right hand side (B).

current magnetometer readings can be conveniently established as the new baseline value, a solution also proposed in previous works [160, 161]. Additionally, for the analog case, utilizing the previous stored information related to widget position and current changes in signal value from baseline, the new shift/widget position can be easily identified. In conclusion, in this experiment, I aimed to explore and simultaneously also demonstrate the potential of utilizing signal variations from tangible inputs for interactive applications without using any advanced algorithms (i.e., from a quick prototyping perspective).

Findings

During real-time testing of the designed App (Figure 4.13), I observed that virtual characters could be effortlessly manipulated using the corresponding tangible controls. When the push button was pressed, the ball initiated movement in the virtual space. Similarly, when the slider was moved in a forward or backward direction, the associated virtual object, in this case, a rocket, mirrored this movement. Additionally, I observed that interaction with the tangible input to control the virtual character in the App was consistently effective, regardless of whether the case was held in hand or placed on the table. Moreover, the results from

all three experiments highlight a crucial insight for prototyping: Earth's magnetic field can serve as a viable resource for constructing tangible interactions. This resource proved to be functional and valuable across a range of common resting configurations, irrespective of user location (indoor or outdoor), as highlighted in previous references [157, 158]. Hence, this discovery holds substantial importance from a prototyping perspective, offering a versatile, freely accessible, and omnipresent resource for designing interactive systems.

4.4.4 **Classifying Tangible Controls with Machine Learning**

In the previous three assessments, I showed how the variations can be used in magnetometer sensor readings for input interaction, both in binary and analog formats. However, the experiments also revealed that each metal shield produces a unique pattern in magnetometer sensor readings. This led us to realize that these differences in signals, which come from the different shapes of the metal shields, could be used as input for a digital system. This could be accomplished by linking each pattern to a specific digital interaction. In particular, in this experiment, I aimed to explore distinct crucial aspects of the MFS method as an input sensing by addressing the following inquiries:

- Is it possible to accurately differentiate between various tangible controls?
- How do basic machine learning techniques accurately classify tangible control types?
- How well does the model function in a user-independent setting?

Before conducting the classification test for tangible interaction types, I performed a statistical test to determine and confirm the significance of signal variations between different interactions. I positioned the phone on the table and collected 30 sample data for each tangible control. Additionally, I gathered sensor baseline data for 15 minutes. The sample data were separated using start and stop times, with each interaction lasting until 30 points were collected. Each tangible control was fully interacted with by a single user to gather all 30 samples.

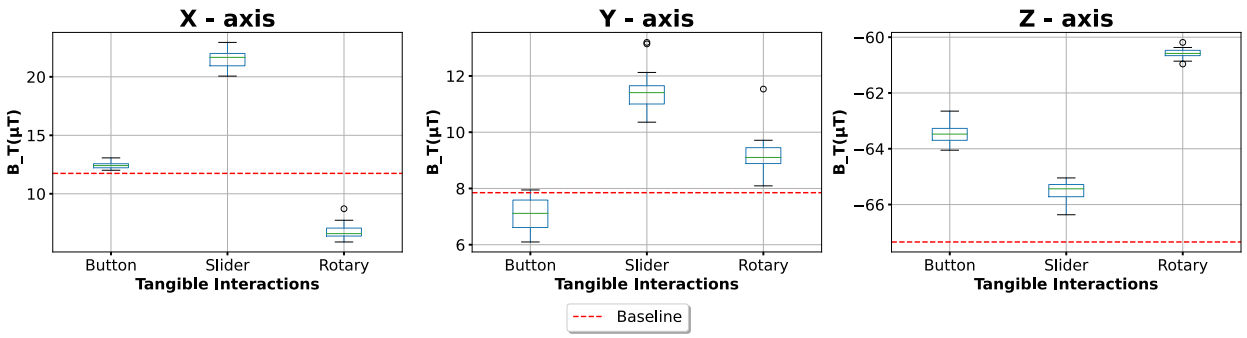

Figure 4.14: Each plot depicts, with respect to each sensor axis, the variations in sensor signal obtained from the baseline in relation to each type of tangible interaction performed.

Figure 4.14 depicts the baseline and tangibles interaction magnetometer signals obtained for each axis. After confirming the normality of the data samples across all tangible interactions, including baseline, with respect to each sensor axis using the Shapiro-Wilk test ($p > 0.05$), a one-way ANOVA test was conducted to compare the means of the data samples across tangible interaction, including baseline. The ANOVA results indicated a statistically significant difference among the means of the data samples across all tangible interactions, including baseline, with respect to each sensor axis, i.e., X ($F(3, 116) = 669.02739$, $p < .0001$), Y ($F(3, 116) = 67.25106$, $p < .0001$), and Z ($F(3, 116) = 623.07099$, $p < .0001$). Subsequently, post hoc analysis using Tukey's Honestly Significant Difference (HSD) test was performed, revealing that significant differences exist ($p < .05$) between the data samples across all tangible interactions, including baseline, with respect to each sensor axis. In other words, these findings suggest that the data samples from distinct metal shields exhibit distinct characteristics with respect to each sensor axis. These initial tests' results aided my comprehension by illustrating that tangible interaction (i.e., tangibles linked with distinct ferromagnetic metal sheets) can also be classified. This encouraged us to do a comprehensive analysis, which is described in the following subsections.

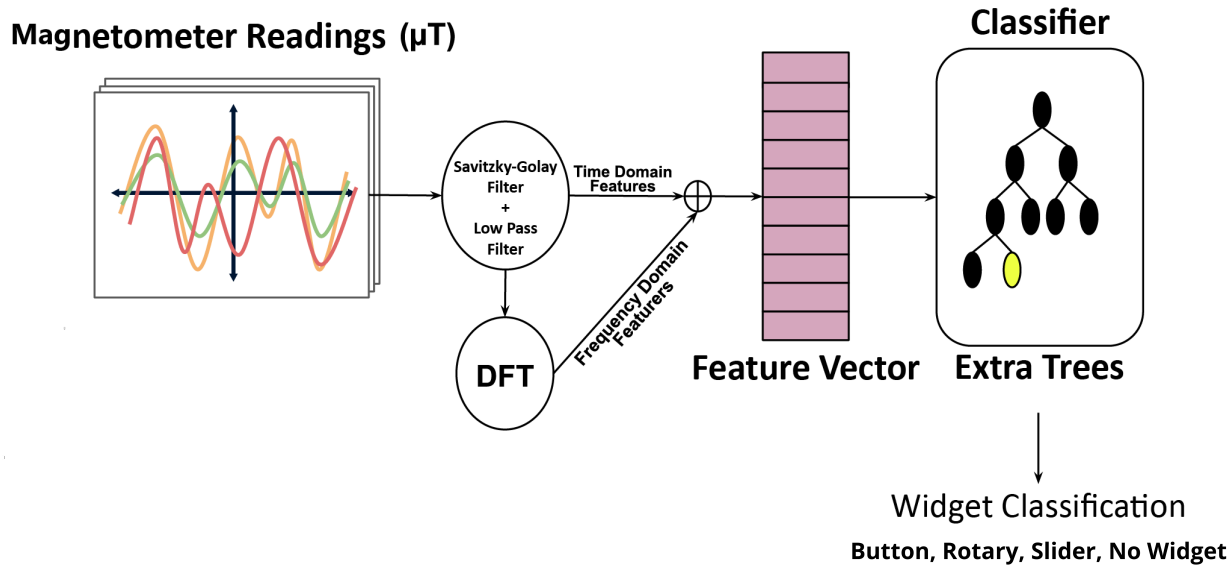

Figure 4.15: Classification pipeline overview

Overall Pipeline / System Design

The software of my system primarily consists of a recognition algorithm, which is further divided into the following components: continuous extraction, processing of one-second windows from the magnetometer data stream, and a classifier to identify the type of interacting tangible controls, as shown in Figure 4.15.

- **Preprocessing -** Initially, a sliding window procedure with a duration of 1 second, chosen experimentally as mentioned before, with a step size of 500 milliseconds was executed on the incoming sensor signals. The magnetometer signals were baseline-adjusted and filtered using Savitzky- Golay and Butterworth filters to remove low-frequency and high-frequency noise.

- **Features extraction and selection -** Temporal and frequency domain features were extracted from denoised signals. Time domain features comprised mean, standard deviation, median absolute deviation, maximum and minimum values, signal magnitude area, and energy. Frequency domain features were obtained via discrete fourier transform, including mean frequency, skewness, kurtosis, and band energy. The feature set

Table 4.2: Top 10 selected features names and descriptions

Feature name	Feature description
max_x	Maximum value of X-axis signal
sma_x	Signal magnitude area of X-axis signal
mean_x	Mean value of X-axis signal
energy_x	Sum of the squares divided by the number of values of X-axis of signal
min_x	Minimum value of X-axis of signal
bandenergy_x	Energy of a frequency interval of the DFT of each window of X-axis signal
meanfreq_x	Weighted average of the frequency components to obtain a mean frequency of X-axis signal
std_z	Standard deviation of Z-axis signal
meanfreq_z	Weighted average of the frequency components to obtain a mean frequency of Z-axis signal
std_x	Standard deviation of the X-axis of signal

comprised 7-time domain and 4 frequency domain features, resulting in a 33-feature vector (11 features per axis X 3 axes) for 3D magnetometer data. Minimum Redundancy Maximum Relevance (mRMR) [162] algorithm was used for the feature selection to optimize inference time during deployment. I identified the top 10 most significant features and, similar to [99], used them for further classification analysis. Only the X and Z axis features were deemed significant. The features identified are listed in Table 4.2.

- **Classification -** The algorithm should be capable of classifying distinct metal shield types (basically tangible widgets). The designed algorithm employs the ExtraTrees classifier for the classification stage, which was chosen after comparing its recognition accuracy (using a 10-fold cross-validation method on the collected data) with the top 5 best-performing classification models using the PyCaret library [9]. The performance of all the top 5 best-performing classification models is presented in Figure 4.16 A.

[9]https://pycaret.org/

Evaluation Process

During the evaluation, I used the Oppo smartphone [10] and the smartphone table-stand case prototype shown in Fig. 4.8, which included binary (a push button) and analog (a slider and a rotary) widgets.

- **Participants:** Ten right-handed participants (average age: 26.4, three female, SD: 9.6) were recruited to participate in this study. All of them participated voluntarily after informed consent. The experiments adhered to the ethical guidelines set by Internal Review Board (IRB).

- **Setup:** The research took place in the same room as the previous study. Participants were seated in a chair and asked to engage with physical controls, which were integrated into a table-stand case. They interacted with a smartphone, which was connected to this prototype table-stand case, in two different scenarios: one where the smartphone was resting on the table, and the other when it was held in their hand. The setup for this study involved the use of an Android smartphone, and a smartphone table-stand case prototype, as illustrated in Figure 4.8. Data collection was facilitated by an Android application (Phyphox) that included a timer function.The selection of this particular case prototype was based on its inclusion of distinct types of metal plates, i.e., shields, and because of its advantages as mentioned before, which it will provide during the data collection process. Particularly in minimizing the potential for human error in the data-gathering process of metal shields, which could stem from the user's irregular movements of the metal shield.

- **Design and Procedure:** Each participant was initially asked to sit in front of the study setup, which was placed on a desk. The setup consisted of a mobile phone and a smartphone table-stand case. Before the formal session commenced, one of the researchers provided each participant with a training session to help them become

[10] https://www.oppo.com/en/smartphones/series-a/a5s/specs/

acquainted with how to use and interact with all the physical controls. Following this training, the participants were instructed to perform five consecutive, complete cycles of using all three physical controls, namely, slider, rotary, and binary, on the prototype smartphone table-stand case. They could choose any of the available scenarios for this practice. The primary goal of this brief practical session was to ensure that the participants were comfortable with how these physical controls worked. After this initial familiarization, the participants were guided to engage in 20 complete cycles of interaction with each of the physical controls. To perform 20 cycles with a metal shield linked with a slider and rotary controls, this involved performing both upward and downward movements of these tangible controls. While 20 cycles related to a metal shield associated with push button involved a full press and release action of push button. These interactions took place in both the "hand" and "table" scenarios.

Participants had the freedom to interact with various tangible controls (i.e., input devices) and complete a total of 20 interactions in any order they preferred. I didn't regulate how they held the combination of the phone and its table-stand case. Instead, we simply asked them to adopt a comfortable and stable posture while using these tangible controls. I collected data from these tangible controls using Phyphox android application. To make sense of this data, participants were instructed to enter the name of the tangible control they interacted with, such as "slider," into the Android app after each interaction. This step helped us identify the type of signals recorded during these interactions. To help with data segmentation, participants were guided to start their interaction with the tangible control at the 5-second mark indicated by the app. When they finished, they were required to press the stop button on a timer. After every 20 interactions, participants were given a 5-minute break. In total, I collected and analyzed data from 1200 interactions, involving 10 participants, three types of metal shields each linked with one kind of widget, two scenarios (handheld and on a table), and 20 repetitions. The entire study, including all the outlined procedures, took

approximately 40 minutes for each participant to complete.

- **Dataset and Annotation:** Upon completion of the study, two researchers meticulously reviewed the collected data, specifically focusing on the tangible control signals. Their objective was to determine the initiation and termination points of each participant's interaction with the widgets. In terms of interaction duration, the shortest recorded duration was 0.47 seconds, related to the button tangible input and on the other hand, the longest duration observed was 980 milliseconds. These observations indicate that participants may require varying amounts of time to complete a push-button interaction. To standardize the data segmentation, it was decided to use 1-second segments. These segments were extracted from the complete signal cycles of the slider and rotary tangible controls, starting from their respective initiation points and ending at their termination points. To facilitate data organization and preparation for analysis, a data-gathering app was utilized during the experiment. This app allowed participants to label the clipped segments with the name of the tangible control they were interacting with. Ultimately, I collected an average of 382 labeled segments per participant, totaling 3820 segments for 10 participants. In addition, I incorporated time-shifted windows (50% overlap) of these labeled segments for augmenting our dataset, resulting in a total of 5748 labeled segments.

Evaluation Findings

We used learning-based predictive analysis on the acquired data to support the exploration of the research questions. This section outlines the analysis techniques employed and presents the findings from several testing scenarios.

- **Tangible Controls Classification-** The objective of this evaluation was to evaluate the effectiveness of the classification model in distinguishing between various types of tangible controls that a user interacts with. To assess the performance of the chosen

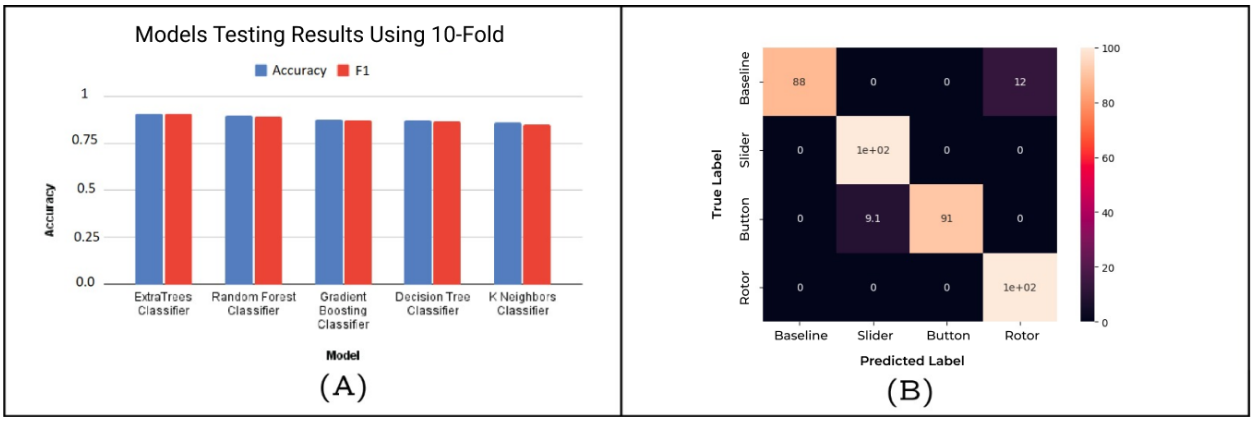

Figure 4.16: A.) Recognition accuracy (and F1) under various prediction methods, B) Confusion matrix for the best model (ExtraTrees classifier) on the best fold. Each values in matrix are in percentage.

ExtraTrees classifier, a 10-fold cross-validation method was employed. The data were divided into training and testing sets at the user level, with nine users' data (5173 samples) allocated for training and one user's data (575 samples) for testing. The confusion matrix for the classifier is presented in Figure 4.16(B). The obtained weighted F1 score was 0.94, and the classification accuracy was 94.3%. I also performed the Mann-Whitney U Test on our 10-fold cross-validation accuracy. I found that the obtained accuracy is significantly higher than the accuracy in classification by chance ($U = 11$, $Z = 3.74185$, $p < 0.05$). In essence, this represent that the selected model performed significantly better than classification by chance (25% probability for four-class classification), thereby indicative of a highly accurate tangible inputs classification system. Furthermore, this discovery also validates that the distinct metal shield, having different geometries, provides distinct signal patterns that can be utilized as an input to the digital system.

- **Universality-** Universality measures whether a current model applies to a wide range of users. The obtained accuracy results also demonstrated the robustness of the classification model, ExtraTrees Classifier, against other factors such as the speed with which users interacted with tangibles. This is due to the fact that the data I gathered

and on which the model is tested also includes hidden information about each user's rate of widget interaction.

4.5 Example Applications of Magnetic Field Shielding

Previously, I showed technically that the sensor produces noticeable changes anytime ferromagnetic material is introduced (i.e., slide) close to the magnetometer, whether in an analog fashion (section 4.2) or a binary fashion (section 4.1). Additionally, I verified that, with the help of a straightforward programming technique (section 4.3), it is possible to use the signal variation (i.e., obtained findings of section 4.1 and 4.2) produced by the ferromagnetic material in magnetometer signals to prototype any kind of functional tangible control, whether it be in binary or analog form. In addition to demonstrating the efficacy of the ferromagnetic material (known as the magnetic shielding approach) in prototyping the input interaction in any form, i.e., binary or analog type within the tangible user interface domain, now in this section, I demonstrate its applicability (i.e., towards generating inputs in any form like binary or analog) with common daily use objects as well. The advantage which our explored finding provides beyond low-threshold prototyping of tangible control is that it can be applied to extend the use of such daily use objects for giving digital input of any type (i.e., binary or analog) beyond their primary use without instrumenting them. To demonstrate that with such objects that involve ferromagnetic material content users can utilize it to give input in any form (i.e., binary or analog), I arranged two widely used objects in our daily lives. The first object is the Stylus-type ballpoint pen, a versatile writing tool that also functions as a stylus for precise interaction with touchscreens. The second category encompasses regular rings, in which materials like iron, nickel, or cobalt are commonly utilized. People wear these rings as jewelry for their fashion and occasions or for their personal interests. Particularly, I was interested in demonstrating how ferromagnetic material-related objects could also be used to conduct an analog and binary sort of interaction with digital device when they were introduced, i.e., slide, in a manner akin to the way the metal sheet moved

near to the sensor. By binary interaction, I mean that when such objects are brought near the sensor for a second or so, they cause a significant change in the sensor signal. And by analog interaction, I mean that when these objects are slid near the sensor in a variable manner, akin to a metal sheet sliding on the top edge of a smartphone within a case, a distinct pattern of signal changes emerges.

Furthermore, I presented another application of my prototyped tangible case from a VR perspective, which features distinct, tangible controls such as a slider and a rotary knob (i.e., in a miniature form). I demonstrated, in contrast to VR controllers (typically capturing buttoned input only [64]), how this passive tangible case could also serve as a proxy for a precision hand-held tool's miniature control by users, offering a valuable and low-cost way for experiencing realism when manipulating a miniature control of virtual precision hand-held tools such as vernier calipers and micrometers.

4.5.1 **Stylus-type ballpoint pen**

Today, pens with integrated stylus features have become commonplace, resembling ballpoint pens but also incorporating a conductive foam rubber at their rear end. This allows users to transition between writing notes and controlling touchscreens seamlessly. However, beyond touchscreen control, such pens often lack additional functionalities, such as the ability to adjust light intensity without direct touchscreen interaction.

Some pens, as illustrated in Figure 4.17 (A or B) and represented in [11] [12] [13], already incorporate ferromagnetic type material. Additionally, for pens lacking such material [14], introducing ferromagnetic-type metal plates (e.g., nickel, iron, cobalt) onto or within the pen can enhance its capabilities without requiring electronic components. With such a pen in hand, users can effortlessly adjust screen brightness while reading or drawing by sliding the pen along the top edge of the smartphone. Furthermore, rapidly sliding up and down (or

[11] https://rb.gy/tffx9
[12] https://rb.gy/f129x
[13] https://rb.gy/enbf3
[14] https://rb.gy/s8oyt

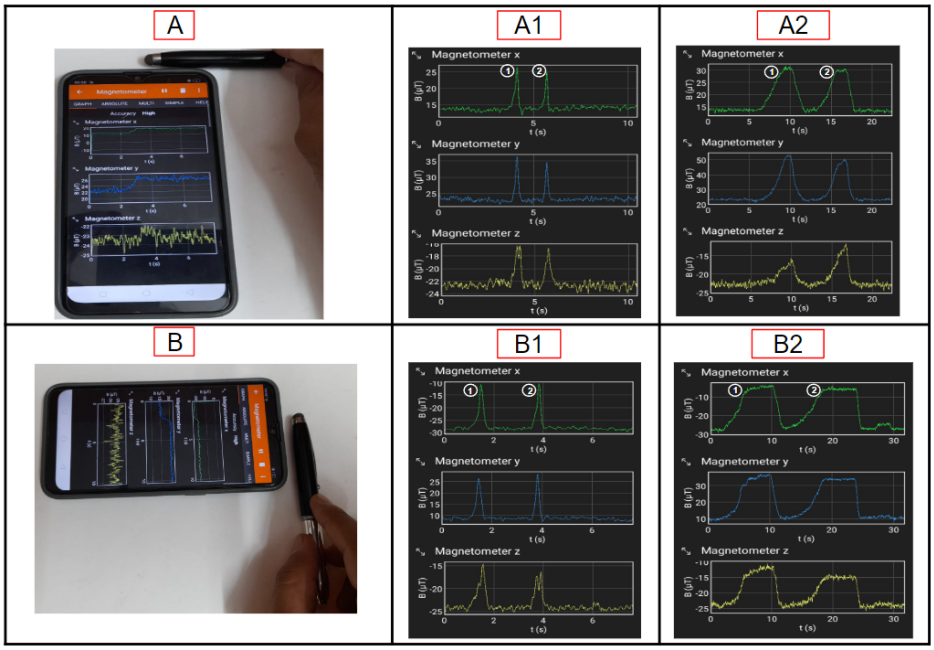

Figure 4.17: Regarding the Stylus-type ballpoint pen, A1 and B1 represent single-tap signal responses (magnetometer x-axis), while A2 and B2 represent responses to sliding gestures (magnetometer x-axis). A and B figures depict different orientation of the smartphone in which interaction occurred.

touching on the top boundary) the same pen within a short duration, say, within a second, can be recognized as a binary input by the mobile device. This capability can be harnessed, for instance, to swiftly capture snapshots of the displayed content on touchscreen while reading or conducting an analysis, eliminating the need to exert effort on pressing multiple smartphone buttons simultaneously or executing additional gestures on the touchscreen.

Overall such additional features are particularly advantageous, as previous traditional methods are associated with two significant issues: one they create occlusion issues and second disturb (i.e., disrupt) focus when reading, drawing, analyzing or intensely focused on some digital content.

In Figure 4.17 (A & B), I depict a stylus-type ballpoint pen equipped with stylus functionality at one end and containing a magnetic shield inside it (i.e., surface is of ferromagnetic material type). Without changing or adding anything on the pen surface, I conducted two evaluations: one involved swiftly touching the pen on the top boundary, and the other was

a slower back-and-forth sliding motion of a pen. These evaluations were performed in two smartphone orientations. The results (as shown in Figure - 4.17 (A1, A2, B1, B2) and in the video) displayed substantial signal variations between the two pen interactions due to the presence of the metallic shield within the pen. Moreover, both orientations exhibited similar signal patterns (significantly on magnetometer x-axis) for each type of pen interaction on the top boundary. This affirms the potential of the stylus-type ballpoint pen to facilitate additional types of interactions, as previously mentioned.

4.5.2 Unlocking Digital Interactions with Fashionable Rings

In the realm of fashion and personal preference, people often wear rings on their fingers, ranging from one to several. Materials like nickel, iron, and cobalt are frequently employed in crafting unique and stylish rings [163–165], catering to a wide array of fashion tastes and individual interests [15] [16] [17]. However, beyond their ornamental value, these rings do not typically serve any digital interaction purpose.

My approach can introduce a novel dimension of digital interaction, enabling such rings to be utilized for input without any alteration to the user or the ring itself. To demonstrate and confirm it, I conducted assessments by wearing an iron ring first on the thumb and then on the index finger. These assessments included three types of interaction using a ring: first, a tap at the middle of the top boundary; second, a swift double-tap; and third, a sliding motion along the top boundary. To check its robustness, I conducted the evaluation in two orientations of the smartphone (shown in Figure - 4.18 A & B) near the electromagnetic devices. While interacting with a handheld smartphone in all three ways and both orientations, I recorded (using the App) corresponding signal variations for analysis.

The results (as shown in Figure - 4.18 (A1, B1) and in the shared video) indicate distinctive signal patterns for each of the three interactions. Moreover, both orientations exhibited

[15] https://rb.gy/ycmfi
[16] https://t.ly/sIXwR
[17] http://abi0l9.lnkiy.in/0tb2J

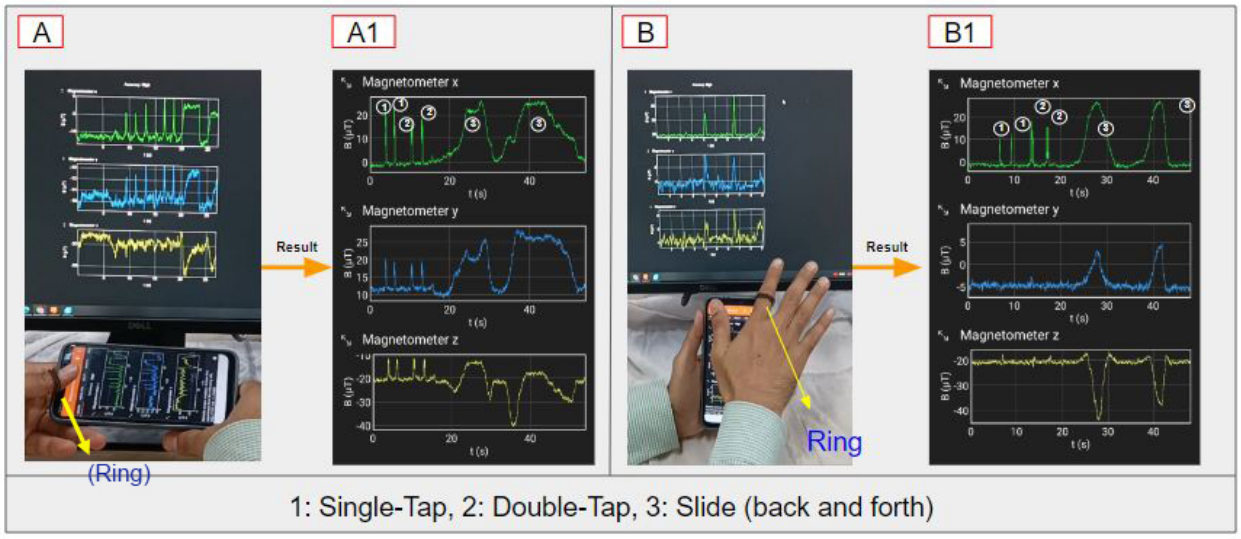

Figure 4.18: Regular ring-based interaction depicted in A and B, representing ring interaction using different fingers and orientations, while A1 and B1 represent the corresponding signal responses (magnetometer x-axis) for various interactions occurred.

similar signal changes on the magnetometer x-axis for each of the three types of interaction (tap, double tap, and slide). These findings underscore the potential for using these commonly worn rings for digital interaction, enhancing their practical utility beyond mere adornment. For instance, a user taking a photograph can employ their fashionable ring for a single-tap input to capture a photo without adjusting their grip on the phone, and execute a swift double-tap to switch camera modes. Another scenario involves a user reclining in bed while watching a movie. A double-tap allows for fast-forwarding, while a single-tap starts or pauses the movie without direct screen contact, streamlining content engagement. Additionally, in situations where a user's hand is wet from activities like cleaning, the ring-based single and double-tap input can be used to answer a call and activate the speaker, preventing potential damage to the smartphone screen.

4.5.3 **Experience of a Miniature Control Manipulation in VR**

The concept of interaction with a virtual object or its feature in VR suggests that physical and cognitive interaction with virtual information, such as through tangible interfaces, en-

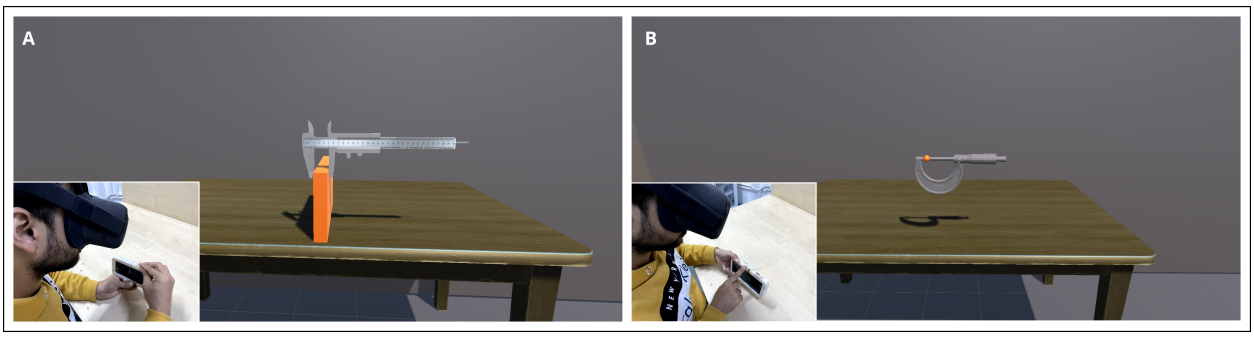

Figure 4.19

hances people's comprehension of the information being manipulated. Studies [72, 94, 122]) have already shown that tangible interfaces promote natural interaction, are faster and more intuitive to use, and benefit human spatial memory. In the same vein, I discover the potential to interact with a miniature control of virtual engineering tools through the physical controls of a designed case, providing a realistic experience while manipulating them in virtual reality. Examples of engineering tools associated with miniature manipulation include vernier calipers and retractable knives, which have linear translation motion of their embedded miniature control, and micrometers and spherometers, which have rotary motion along a single axis of their embedded miniature control. One can easily interact, experience, and receive training on the use (i.e., manipulating and handling aspects) of a miniature control of numerous hand-held engineering instruments by using the case miniature controls as proxies in VR. Figure 4.19 (A and B) illustrates the use of embedded distinct types of miniature control, such as rotary and slider within a case, to genuinely experience the manipulation aspects of a virtual miniature control of hand-held tools in VR.

4.6 Discussion, Implications, and Limitations

This study confirms the effectiveness of the MFS approach, utilizing ferromagnetic materials, as an innovative input sensing technique. Through systematic exploration of various metal shields, I consistently observed significant signal changes, demonstrating MFS's potential for use as an input technique with digital devices to create diverse types of inputs, whether

binary or analog. This highlights MFS's reliability in prototyping tangible interactions with digital systems, expanding possibilities for input design in HCI.

Beyond experimental validation, obtained findings hold practical implications for researchers/ designers/practitioners in HCI and product development. First, the research demonstrates the potential of ferromagnetic materials as input mechanisms for smart devices, opening up avenues for exploration across diverse domains such as interactive artifacts and installations. Second, the findings also hold significant implications for industries producing metallic-type wearable/handheld items. By incorporating ferromagnetic materials into the body of objects such as metallic pens (e.g., metal body pen [18]) or fashionable rings (e.g., stylish iron ring [19]), these items can be transformed into functional input devices, eliminating the need for electronics or magnets, which demand extra space and can increase the product's cost. Third, the simplicity and accessibility of the MFS technique facilitate rapid prototyping, enabling the creation of functional tangible controls during the ideation phase without the need for advanced algorithms. Fourth, to the best of the knowledge, this is the first work demonstrating the use of Earth's magnetic field for prototyping tangible inputs. It will encourage future researchers to use this free, ubiquitous resource instead of magnets such as neodymium because prior studies have revealed that continous exposure to magnets' magnetic fields might have negative health effects [146, 148].

Moving forward, several limitations must be addressed for expanding the implementations in diverse real-world settings. Future research should explore the generalizability of the MFS approach across diverse applications, considering different mobile devices, the impact of a strong magnetic field zone due to permanent magnets, and environmental factors such as variations in temperature and humidity. Additionally, long-term usability and durability assessments are needed to evaluate the reliability and sustainability of MFS technology in real-world contexts. The proposed MFS approach poses no health risks, as it leverages the Earth's magnetic field rather than magnets, which remains well below the recommended

[18]https://rb.gy/tffx9
[19]https://www.etsy.com/in-en/listing/1647015374/

overall magnetic field strength of 0.1-0.5 μT [166]. Moreover, it's essential to clarify that the current design proposal does not address the possibility of simultaneous use of physical controls within the presented prototyped tangible case. As previously mentioned, our primary objective was to showcase how metal shields could serve as a versatile means to prototype various types of physical controls, whether binary or analog, particularly for early-stage prototyping. Furthermore, it's worth noting that even in existing mobile phone devices, not all interaction inputs can be utilized simultaneously. For instance, while adjusting the volume using the volume up/down button, users may find it impossible to turn off the device using the power button simultaneously. Hence, as long as it is possible to effectively differentiate between different signals, as demonstrated in Section IV, the simultaneous operation of interactions may not pose a significant challenge. However, I acknowledge the potential benefits of enabling simultaneous interactions, and this aspect could be explored in future design iterations.

4.7 Conclusions and Future Work

In this study, I introduced a new method for input sensing by utilizing MFS, a concept commonly used in electronics for protective purposes. The research revealed that different shapes of metal shields produce unique patterns in magnetometer sensor signals. These findings served as the basis for creating prototypes of various tangible inputs. During the technical investigations, I successfully validated the signal variations associated with each specific tangible input, highlighting the significance of different metal shields. Additionally, I demonstrated the analog behavior of tangible controls of the analog type. Finally, based on data collected from a sample of 10 participants, I have effectively confirmed the significant classification of distinct metal plates, primarily in the form of tangible widgets. This highlights the potential of metal shields as a unique input method for creating digital interactive systems, such as smart security locks or board games. In summary, the findings not only enhance the input-sensing toolkit available to HCI practitioners but also offer opportunities for

researchers, industries, and practitioners to investigate new interaction artifacts/installations surrounding smart gadgets, turning their products into input devices, and from the perspective of early-stage prototyping. One promising direction in future work is improving signal processing and machine learning methods to enhance the precision and reliability of input sensing through MFS. Moreover, integrating MFS with other input sensing modalities, such as capacitive or ultrasonic sensing, has the potential to unlock new possibilities for hybrid input methods.

CHAPTER 5
THESIS CONCLUSIONS AND FUTURE RESEARCH DIRECTIONS

5.0.1 Overall Conclusion

The findings from a literature survey in the domain of haptic feedback and input device prototyping for VR highlight a significant gap in the evolution of accessible haptic feedback and input device prototyping methods when compared to other technological advancements. This gap underscores the urgent need for a paradigm shift towards designing technologies that are inclusive and usable by diverse user groups, including those in resource-constrained settings. The implications of this thesis extend beyond academic discourse, providing a foundational vision for developing methods that simplify the prototyping of haptic feedback and input devices while minimizing barriers to entry. Through projects like HaptiDrag, Non-Smart Object Interactions, and Precise Manipulation in VR, this thesis encourages future research by suggesting that adopting similar thesis objectives to tackle prototyping barriers in other areas of haptic feedback and input methods could open doors to more accessible and scalable innovations, thereby expanding the reach and impact of these technologies.

Ultimately, this thesis asserts that prioritizing accessibility in the design and prototyping of haptic feedback and input devices is not just necessary but essential for fostering broader innovation and inclusivity. Empowering individuals from diverse backgrounds to engage with these technologies—whether for prototyping or new research—can drive advancements in digital interaction, leading to richer, more equitable, and universally beneficial experiences. By bridging this gap, we can ensure that the evolution of haptic feedback and input device technologies contributes to a more inclusive digital landscape.

5.0.2 Future Research Directions

Building on the insights gained from this research, several avenues for future work are identified:

- **Enhanced User Studies with Diverse Demographics:** Future research should conduct extensive user studies across varied demographics to validate the generalizability of the developed methods. This includes examining different age groups, cultural backgrounds, and varying levels of technological familiarity to ensure the solutions meet diverse user needs.

- **Integration with Emerging Technologies:** Investigating the integration of haptic and physical interaction methods with emerging technologies such as augmented reality (AR), mixed reality (MR), and the Internet of Things (IoT) can enhance immersive experiences. This exploration may lead to new applications and use cases that were previously unexplored.

- **Scalability and Cost-Effectiveness in Large-Scale Deployments:** Future work should focus on optimizing the scalability and cost-effectiveness of these methods for large-scale deployments. This includes refining manufacturing processes, reducing production costs, and ensuring ease of implementation across various settings, from educational institutions to healthcare facilities.

- **Advancements in Material Science and Engineering:** Exploring new materials in science and engineering can facilitate the development of more sophisticated and durable haptic feedback mechanisms. Research into innovative materials can provide more nuanced haptic sensations while maintaining affordability and ease of production.

- **Longitudinal Studies on User Engagement and Satisfaction:** Conducting longitudinal studies to assess the long-term impact of these haptic technologies on user engagement, satisfaction, and overall experience will provide valuable insights into their

effectiveness and areas for improvement. These studies can help refine the methods to better meet user needs over time.

- **Cross-Disciplinary Collaborations:** Encouraging cross-disciplinary collaborations between researchers in fields such as computer science, psychology, design, and engineering can foster innovative solutions that address the multifaceted challenges of haptic feedback and input device design. Such collaborations can lead to the development of more holistic and user-centered approaches.

By pursuing these future research directions, the field of haptic technologies and physical interactions can continue to evolve, ensuring that solutions remain at the forefront of innovation and inclusivity. This will ultimately contribute to a future where enriched digital experiences are accessible to all, regardless of their resource settings.

Appendices

APPENDIX A

A.1 Publications

1. **A. Mishra,** P. Kumar, J. Shukla, and A. Parnami, ***"HaptiDrag: A Device with the Ability to Generate Varying Levels of Drag (Friction) Effects on Real Surfaces,"*** Proceedings of the ACM on Interactive, Mobile, Wearable and Ubiquitous Technologies, vol. 6, no. 3, pp. 1–26, September 11-15, Atlanta, USA and Cambridge, UK, 2022.

2. **A. Mishra,** H. V. Singh, A. Parnami, and J. Shukla, ***"MobiTangibles: Enabling Virtual Hand-Held Tools' Miniature Control Interaction Experiences in VR,"*** IEEE Transactions on Visualization and Computer Graphics, Accepted, 2024.

3. **A. Mishra,** M.N. Siddiqui, A. Parnami, and J. Shukla, ***"Exploring Magnetic Field Shielding as an Input Sensing Technique"*** IEEE Transactions on Instrumentation & Measurement, 2024 [**Under Review**]

A.2 Other Publication

1. Arora, J., Mathur, K., Goel, M., Kumar, P., **Mishra, A.**, & Parnami, A. (2019). ***"Design and evaluation of dio construction toolkit for co-making shared constructions,"*** Proceedings of the ACM on Interactive, Mobile, Wearable and Ubiquitous Technologies, , 3(4), 1-25.

REFERENCES

[1] J. M. Hillis, M. O. Ernst, M. S. Banks, and M. S. Landy, "Combining sensory information: Mandatory fusion within, but not between, senses", *Science*, vol. 298, no. 5598, pp. 1627–1630, 2002.

[2] M. Slater, "Place illusion and plausibility can lead to realistic behaviour in immersive virtual environments", *Philosophical Transactions of the Royal Society B: Biological Sciences*, vol. 364, no. 1535, pp. 3549–3557, 2009.

[3] M. Meehan, B. Insko, M. Whitton, and F. P. Brooks Jr, "Physiological measures of presence in stressful virtual environments", *Acm transactions on graphics (tog)*, vol. 21, no. 3, pp. 645–652, 2002.

[4] E.-L. Sallnäs, K. Rassmus-Gröhn, and C. Sjöström, "Supporting presence in collaborative environments by haptic force feedback", *ACM Transactions on Computer-Human Interaction (TOCHI)*, vol. 7, no. 4, pp. 461–476, 2000.

[5] R. Viciana-Abad, A. R. Lecuona, and M. Poyade, "The influence of passive haptic feedback and difference interaction metaphors on presence and task performance", *Presence*, vol. 19, no. 3, pp. 197–212, 2010.

[6] G. Robles-De-La-Torre, "The importance of the sense of touch in virtual and real environments", *Ieee Multimedia*, vol. 13, no. 3, pp. 24–30, 2006.

[7] J. K. Salisbury and M. A. Srinivasan, "Phantom-based haptic interaction with virtual objects", *IEEE Computer Graphics and Applications*, vol. 17, no. 5, pp. 6–10, 1997.

[8] G. Nikolakis, D. Tzovaras, S. Moustakidis, and M. G. Strintzis, "Cybergrasp and phantom integration: Enhanced haptic access for visually impaired users", in *9th Conference Speech and Computer*, 2004.

[9] M. K. Saleem, C. Yilmaz, and C. Basdogan, "Tactile perception of virtual edges and gratings displayed by friction modulation via ultrasonic actuation", *IEEE Transactions on Haptics*, vol. 13, no. 2, pp. 368–379, 2019.

[10] The Verge, *Meta's haptic glove prototype article*, `https://www.theverge.com/2021/11/16/22782860/meta-facebook-reality-labs-soft-robotics-haptic-glove-prototype`, 2021.

[11] N. Li *et al.*, "Haplinkage: Prototyping haptic proxies for virtual hand tools using linkage mechanism", in *Proceedings of the 33rd Annual ACM Symposium on User Interface Software and Technology*, 2020, pp. 1261–1274.

[12] T. Verge, *Oculus touch review - the verge*, 2016.

[13] HTC, *Htc newsroom - march 2015*, `https://www.htc.com/us/newsroom/2015-03-01-3/`, Accessed: 2024-10-02, 2015.

[14] J. Arora, A. Saini, N. Mehra, V. Jain, S. Shrey, and A. Parnami, "Virtualbricks: Exploring a scalable, modular toolkit for enabling physical manipulation in vr", in *Proceedings of the 2019 CHI Conference on Human Factors in Computing Systems*, 2019, pp. 1–12.

[15] C. Honnet *et al.*, "Democratizing intelligent soft wearables", 2024.

[16] K. Watanabe, R. Yamamura, and Y. Kakehi, "Foamin: A deformable sensor for multimodal inputs based on conductive foam with a single wire", in *Extended Abstracts of the 2021 CHI Conference on Human Factors in Computing Systems*, 2021, pp. 1–4.

[17] V. Levesque *et al.*, "Enhancing physicality in touch interaction with programmable friction", in *Proceedings of the SIGCHI conference on human factors in computing systems*, 2011, pp. 2481–2490.

[18] J. Mullenbach, C. Shultz, J. E. Colgate, and A. M. Piper, "Exploring affective communication through variable-friction surface haptics", in *Proceedings of the SIGCHI Conference on Human Factors in Computing Systems*, 2014, pp. 3963–3972.

[19] D. Horodniczy and J. R. Cooperstock, "Free the hands! enhanced target selection via a variable-friction shoe", in *Proceedings of the 2017 CHI Conference on Human Factors in Computing Systems*, 2017, pp. 255–259.

[20] O. Bau, I. Poupyrev, A. Israr, and C. Harrison, "Teslatouch: Electrovibration for touch surfaces", in *Proceedings of the 23nd annual ACM symposium on User interface software and technology*, 2010, pp. 283–292.

[21] M. Weiss, C. Remy, and J. Borchers, "Rendering physical effects in tabletop controls", in *Proceedings of the SIGCHI Conference on Human Factors in Computing Systems*, 2011, pp. 3009–3012.

[22] M. A. Price and F. C. Sup IV, "A handheld haptic robot for large-format touchscreens", *IEEE/ASME Transactions on Mechatronics*, vol. 23, no. 5, pp. 2347–2357, 2018.

[23] G. Millet, M. Otis, D. Horodniczy, and J. R. Cooperstock, "Design of variable-friction devices for shoe-floor contact", *Mechatronics*, vol. 46, pp. 115–125, 2017.

[24] T. Watanabe and S. Fukui, "A method for controlling tactile sensation of surface roughness using ultrasonic vibration", in *Proceedings of 1995 IEEE International Conference on Robotics and Automation*, IEEE, vol. 1, 1995, pp. 1134–1139.

[25] G. J. Monkman, "An analysis of astrictive prehension", *The International Journal of Robotics Research*, vol. 16, no. 1, pp. 1–10, 1997.

[26] H. Prahlad, R. Pelrine, S. Stanford, J. Marlow, and R. Kornbluh, "Electroadhesive robots—wall climbing robots enabled by a novel, robust, and electrically controllable adhesion technology", in *2008 IEEE international conference on robotics and automation*, IEEE, 2008, pp. 3028–3033.

[27] P. Verma, "Flying user interface", in *Proceedings of the 29th Annual Symposium on User Interface Software and Technology*, 2016, pp. 203–204.

[28] P. Verma, "Stick user interface", in *The Adjunct Publication of the 32nd Annual ACM Symposium on User Interface Software and Technology*, 2019, pp. 60–62.

[29] R. Hinchet, V. Vechev, H. Shea, and O. Hilliges, "Dextres: Wearable haptic feedback for grasping in vr via a thin form-factor electrostatic brake", in *Proceedings of the 31st Annual ACM Symposium on User Interface Software and Technology*, 2018, pp. 901–912.

[30] V. Lévesque, L. Oram, K. MacLean, J. E. Colgate, and M. A. Peshkin, "Restoring physicality to touch interaction with programmable friction", in *2011 IEEE International Conference on Consumer Electronics (ICCE)*, IEEE, 2011, pp. 61–62.

[31] O. Bau and I. Poupyrev, "Revel: Tactile feedback technology for augmented reality", *ACM Transactions on Graphics (TOG)*, vol. 31, no. 4, pp. 1–11, 2012.

[32] K. Amano and A. Yamamoto, "An interaction on a flat panel display using a planar 1-dof electrostatic actuator", in *Proceedings of the ACM International Conference on Interactive Tabletops and Surfaces*, 2011, pp. 258–259.

[33] A. Yamamoto, S. Tsuruta, and T. Higuchi, "Planar 3-dof paper sheet manipulation using electrostatic induction", in *2010 IEEE International Symposium on Industrial Electronics*, IEEE, 2010, pp. 493–498.

[34] T. Nakamura and A. Yamamoto, "A multi-user surface visuo-haptic display using electrostatic friction modulation and capacitive-type position sensing", *IEEE Transactions on Haptics*, vol. 9, no. 3, pp. 311–322, 2016.

[35] J. Huang, Y. Zhou, L. Dong, Z. Zhou, and X. Zeng, "Enhancing insulating performances of presspaper by introduction of nanofibrillated cellulose", *Energies*, vol. 10, no. 5, p. 681, 2017.

[36] J. Guo, T. Bamber, M. Chamberlain, L. Justham, and M. Jackson, "Optimization and experimental verification of coplanar interdigital electroadhesives", *Journal of Physics D: Applied Physics*, vol. 49, no. 41, p. 415 304, 2016.

[37] J. Webster, *22. Webster, J. G. (ed.), Medical instrumentation: application and design, Fourth edition, John Wiley Sons, Hoboken, NJ, 2010.* Jan. 2010.

[38] M. Kono, T. Takahashi, H. Nakamura, T. Miyaki, and J. Rekimoto, "Design guideline for developing safe systems that apply electricity to the human body", *ACM Transactions on Computer-Human Interaction (TOCHI)*, vol. 25, no. 3, pp. 1–36, 2018.

[39] D. Spelmezan, D. R. Sahoo, and S. Subramanian, "Sparkle: Hover feedback with touchable electric arcs", in *Proceedings of the 2017 CHI Conference on Human Factors in Computing Systems*, 2017, pp. 3705–3717.

[40] *WHO housing and health guidelines*. Geneva, Switzerland: World Health Organization, 2018, ISBN: 9789241550376.

[41] T. S. EM Sterling A. Arundel, *Criteria for human exposure to humidity in occupied buildings*.

[42] Y. Li, M. K. Ediriweera, F. S. Emms, and A. Lohrasby, "Development of precision dc high-voltage dividers", *IEEE Transactions on Instrumentation and Measurement*, vol. 60, no. 7, pp. 2211–2216, 2011.

[43] A. Küchler, *High Voltage Engineering: Fundamentals-Technology-Applications*. Springer, 2017, pp. 413–414.

[44] T. N. Cornsweet, "The staircase-method in psychophysics", *The American journal of psychology*, vol. 75, no. 3, pp. 485–491, 1962.

[45] S. H. Yoon *et al.*, "Hapsense: A soft haptic i/o device with uninterrupted dual functionalities of force sensing and vibrotactile actuation", in *Proceedings of the 32nd Annual ACM Symposium on User Interface Software and Technology*, 2019, pp. 949–961.

[46] S. Yoshida, Y. Sun, and H. Kuzuoka, "Pocopo: Handheld pin-based shape display for haptic rendering in virtual reality", in *Proceedings of the 2020 CHI Conference on Human Factors in Computing Systems*, 2020, pp. 1–13.

[47] J. Gong *et al.*, "Jetto: Using lateral force feedback for smartwatch interactions", in *Proceedings of the 2018 CHI Conference on Human Factors in Computing Systems*, 2018, pp. 1–14.

[48] H. Ebbinghaus, "Memory: A contribution to experimental psychology", *Annals of neurosciences*, vol. 20, no. 4, p. 155, 2013.

[49] C. D. Shultz, M. A. Peshkin, and J. E. Colgate, "Surface haptics via electroadhesion: Expanding electrovibration with johnsen and rahbek", in *2015 ieee world haptics conference (whc)*, IEEE, 2015, pp. 57–62.

[50] F. G. Hamza-Lup and W. H. Baird, "Feel the static and kinetic friction", in *International Conference on Human Haptic Sensing and Touch Enabled Computer Applications*, Springer, 2012, pp. 181–192.

[51] D. I. Grow, L. N. Verner, and A. M. Okamura, "Educational haptics.", in *AAAI Spring Symposium: Semantic Scientific Knowledge Integration*, 2007, pp. 53–58.

[52] J. E. Stone, J. Gullingsrud, and K. Schulten, "A system for interactive molecular dynamics simulation", in *Proceedings of the 2001 symposium on Interactive 3D graphics*, 2001, pp. 191–194.

[53] P. L. Dickrell, "Building skills in engineering: Hand and power tool workshops for confidence and retention", in *2018 ASEE Annual Conference & Exposition*, 2018.

[54] F. Osiurak and A. Badets, "Tool use and affordance: Manipulation-based versus reasoning-based approaches.", *Psychological review*, vol. 123, no. 5, p. 534, 2016.

[55] A. Ricca, A. Chellali, and S. Otrnane, "The influence of hand visualization in tool-based motor-skills training, a longitudinal study", in *2021 IEEE Virtual Reality and 3D User Interfaces (VR)*, IEEE, 2021, pp. 103–112.

[56] *Precise carving*, `https://www.youtube.com/shorts/9ceqt9cW4Hk`.

[57] *Jewelry polishing*, `https://www.youtube.com/watch?v=Yl11bBLNfng`.

[58] *Precision movable syringes*, `https://www.fishersci.com/us/en/browse/90150618/medical-syringes`.

[59] *Precise syringe dropping*, `https://www.pond5.com/stock-footage/item/84239468-syringe-dropping-blue-liquid-substance`.

[60] *Precise desoldering smd components*, `https://www.youtube.com/shorts/TRfinTJjZmY`.

[61] *Precise soldering/desoldering*, `https://www.youtube.com/watch?v=0yaE_RQC0D0`.

[62] K. Hinckley, R. Pausch, J. C. Goble, and N. F. Kassell, "Passive real-world interface props for neurosurgical visualization", in *Proceedings of the SIGCHI conference on Human factors in computing systems*, 1994, pp. 452–458.

[63] R. B. Loftin *et al.*, "Virtual environments in training: Nasa's hubble space telescope mission", in *Interservice/industry training systems & education conference*, 1994, pp. 1–10.

[64] C. Fang, Y. Zhang, M. Dworman, and C. Harrison, "Wireality: Enabling complex tangible geometries in virtual reality with worn multi-string haptics", in *Proceedings of the 2020 CHI Conference on Human Factors in Computing Systems*, 2020, pp. 1–10.

[65] B. Smus and C. Riederer, "Magnetic input for mobile virtual reality", in *Proceedings of the 2015 ACM International Symposium on Wearable Computers*, 2015, pp. 43–44.

[66] *Htc vive*, `https://www.vive.com/sea/`.

[67] *Meta quest*, `https://www.meta.com/quest/products/quest-2/`.

[68] M. Feick, C. Biyikli, K. Gani, A. Wittig, A. Tang, and A. Krüger, "Voxelhap: A toolkit for constructing proxies providing tactile and kinesthetic haptic feedback in virtual reality", in *Proceedings of the 36th Annual ACM Symposium on User Interface Software and Technology*, 2023, pp. 1–13.

[69] F. Nascimbeni and S. Vosloo, "Digital literacy for children: Exploring definitions and frameworks", *Scoping Paper*, vol. 1, 2019.

[70] B. Keeley and C. Little, *The State of the Worlds Children 2017: Children in a Digital World.* ERIC, 2017.

[71] S. Heo, C. Chung, G. Lee, and D. Wigdor, "Thor's hammer: An ungrounded force feedback device utilizing propeller-induced propulsive force", in *Proceedings of the 2018 CHI Conference on Human Factors in Computing Systems*, 2018, pp. 1–11.

[72] M. Feick, S. Bateman, A. Tang, A. Miede, and N. Marquardt, "Tangi: Tangible proxies for embodied object exploration and manipulation in virtual reality", in *2020 IEEE international symposium on mixed and augmented reality (ISMAR)*, IEEE, 2020, pp. 195–206.

[73] J. Lee, M. Sinclair, M. Gonzalez-Franco, E. Ofek, and C. Holz, "Torc: A virtual reality controller for in-hand high-dexterity finger interaction", in *Proceedings of the 2019 CHI conference on human factors in computing systems*, 2019, pp. 1–13.

[74] K. Zhu, T. Chen, F. Han, and Y.-S. Wu, "Haptwist: Creating interactive haptic proxies in virtual reality using low-cost twistable artefacts", in *Proceedings of the 2019 CHI Conference on Human Factors in Computing Systems*, 2019, pp. 1–13.

[75] R. Kovacs *et al.*, "Haptic pivot: On-demand handhelds in vr", in *Proceedings of the 33rd Annual ACM Symposium on User Interface Software and Technology*, 2020, pp. 1046–1059.

[76] E. Strasnick, C. Holz, E. Ofek, M. Sinclair, and H. Benko, "Haptic links: Bimanual haptics for virtual reality using variable stiffness actuation", in *Proceedings of the 2018 CHI Conference on Human Factors in Computing Systems*, 2018, pp. 1–12.

[77] B. Ens *et al.*, "Revisiting collaboration through mixed reality: The evolution of groupware", *International Journal of Human-Computer Studies*, vol. 131, pp. 81–98, 2019.

[78] R. Arisandi, Y. Takami, M. Otsuki, A. Kimura, F. Shibata, and H. Tamura, "Enjoying virtual handcrafting with tooldevice", in *Adjunct proceedings of the 25th annual ACM symposium on User interface software and technology*, 2012, pp. 17–18.

[79] T. Kashiwagi, K. Sumi, S. Fels, Q. Zhou, and F. Wu, "Crystal palace: Merging virtual objects and physical hand-held tools", in *2019 IEEE Conference on Virtual Reality and 3D User Interfaces (VR)*, IEEE, 2019, pp. 1411–1412.

[80] P. L. Strandholt, O. A. Dogaru, N. C. Nilsson, R. Nordahl, and S. Serafin, "Knock on wood: Combining redirected touching and physical props for tool-based interaction in virtual reality", in *Proceedings of the 2020 CHI Conference on Human Factors in Computing Systems*, 2020, pp. 1–13.

[81] J. Yang, H. Horii, A. Thayer, and R. Ballagas, "Vr grabbers: Ungrounded haptic retargeting for precision grabbing tools", in *Proceedings of the 31st Annual ACM Symposium on User Interface Software and Technology*, 2018, pp. 889–899.

[82] B. Spittle, M. Frutos-Pascual, C. Creed, and I. Williams, "A review of interaction techniques for immersive environments", *IEEE Transactions on Visualization and Computer Graphics*, 2022.

[83] H. Ishii and B. Ullmer, "Tangible bits: Towards seamless interfaces between people, bits and atoms", in *Proceedings of the ACM SIGCHI Conference on Human factors in computing systems*, 1997, pp. 234–241.

[84] P. Dourish, *Where the action is: the foundations of embodied interaction*. MIT press, 2001.

[85] A. Manches and C. O'malley, "Tangibles for learning: A representational analysis of physical manipulation", *Personal and Ubiquitous Computing*, vol. 16, pp. 405–419, 2012.

[86] S. Henderson and S. Feiner, "Opportunistic tangible user interfaces for augmented reality", *IEEE Transactions on Visualization and Computer Graphics*, vol. 16, no. 1, pp. 4–16, 2009.

[87] P.-A. Cabaret, T. Howard, G. Gicquel, C. Pacchierotti, M. Babel, and M. Marchal, "Does multi-actuator vibrotactile feedback within tangible objects enrich vr manipulation?", *IEEE Transactions on Visualization and Computer Graphics*, 2023.

[88] A. Cockburn and B. McKenzie, "Evaluating the effectiveness of spatial memory in 2d and 3d physical and virtual environments", in *Proceedings of the SIGCHI conference on Human factors in computing systems*, 2002, pp. 203–210.

[89] B. Ens *et al.*, "Uplift: A tangible and immersive tabletop system for casual collaborative visual analytics", *IEEE Transactions on Visualization and Computer Graphics*, vol. 27, no. 2, pp. 1193–1203, 2020.

[90] A. L. Simeone, E. Velloso, and H. Gellersen, "Substitutional reality: Using the physical environment to design virtual reality experiences", in *Proceedings of the 33rd Annual ACM Conference on Human Factors in Computing Systems*, 2015, pp. 3307–3316.

[91] L. Besançon, P. Issartel, M. Ammi, and T. Isenberg, "Mouse, tactile, and tangible input for 3d manipulation", in *Proceedings of the 2017 CHI conference on human factors in computing systems*, 2017, pp. 4727–4740.

[92] L. Besançon, P. Issartel, M. Ammi, and T. Isenberg, "Hybrid tactile/tangible interaction for 3d data exploration", *IEEE transactions on visualization and computer graphics*, vol. 23, no. 1, pp. 881–890, 2016.

[93] M. White, J. Gain, U. Vimont, and D. Lochner, "The case for haptic props: Shape, weight and vibro-tactile feedback", in *Proceedings of the 12th ACM SIGGRAPH Conference on Motion, Interaction and Games*, 2019, pp. 1–10.

[94] T. Muender, A. V. Reinschluessel, S. Drewes, D. Wenig, T. Döring, and R. Malaka, "Does it feel real? using tangibles with different fidelities to build and explore scenes in virtual reality", in *Proceedings of the 2019 CHI Conference on Human Factors in Computing Systems*, 2019, pp. 1–12.

[95] E. Strasnick, J. Yang, K. Tanner, A. Olwal, and S. Follmer, "Shiftio: Reconfigurable tactile elements for dynamic affordances and mobile interaction", in *Proceedings of the 2017 CHI Conference on Human Factors in Computing Systems*, 2017, pp. 5075–5086.

[96] S. Greenberg and C. Fitchett, "Phidgets: Easy development of physical interfaces through physical widgets", in *Proceedings of the 14th annual ACM symposium on User interface software and technology*, 2001, pp. 209–218.

[97] S. Hwang, M. Ahn, and K.-y. Wohn, "Maggetz: Customizable passive tangible controllers on and around conventional mobile devices", in *Proceedings of the 26th annual ACM symposium on User interface software and technology*, 2013, pp. 411–416.

[98] C. Xiao, K. Bayer, C. Zheng, and S. K. Nayar, "Vidgets: Modular mechanical widgets for mobile devices", *ACM Transactions on Graphics (TOG)*, vol. 38, no. 4, pp. 1–12, 2019.

[99] G. Laput, E. Brockmeyer, S. E. Hudson, and C. Harrison, "Acoustruments: Passive, acoustically-driven, interactive controls for handheld devices", in *Proceedings of the 33rd Annual ACM Conference on Human Factors in Computing Systems*, 2015, pp. 2161–2170.

[100] C. Zheng and E. Y.-L. Do, "Mechamagnets: Tactile mechanisms with embedded magnets", in *Proceedings of the Twelfth International Conference on Tangible, Embedded, and Embodied Interaction*, 2018, pp. 57–64.

[101] T. Abe and D. Sakamoto, "Magnetrack: Magnetic field separation method for continuous and simultaneous 1-dof tracking of two-magnets", in *Proceedings of the 23rd International Conference on Mobile Human-Computer Interaction*, 2021, pp. 1–11.

[102] F. Matulic, A. Ganeshan, H. Fujiwara, and D. Vogel, "Phonetroller: Visual representations of fingers for precise touch input with mobile phones in vr", in *Proceedings of the 2021 CHI Conference on Human Factors in Computing Systems*, 2021, pp. 1–13.

[103] N. G. Lipari and C. W. Borst, "Handymenu: Integrating menu selection into a multifunction smartphone-based vr controller", in *2015 IEEE Symposium on 3D User Interfaces (3DUI)*, IEEE, 2015, pp. 129–132.

[104] C. B. Wilkes, D. Tilden, and D. A. Bowman, "3d user interfaces using tracked multitouch mobile devices", 2012.

[105] M. Kari and C. Holz, "Handycast: Phone-based bimanual input for virtual reality in mobile and space-constrained settings via pose-and-touch transfer", in *Proceedings of the 2023 CHI Conference on Human Factors in Computing Systems*, 2023, pp. 1–15.

[106] C. Harrison and S. E. Hudson, "Abracadabra: Wireless, high-precision, and unpowered finger input for very small mobile devices", in *Proceedings of the 22nd annual ACM symposium on User interface software and technology*, 2009, pp. 121–124.

[107] D. Ashbrook, P. Baudisch, and S. White, "Nenya: Subtle and eyes-free mobile input with a magnetically-tracked finger ring", in *Proceedings of the SIGCHI Conference on Human Factors in Computing Systems*, 2011, pp. 2043–2046.

[108] H. Ketabdar, K. A. Yüksel, and M. Roshandel, "Magitact: Interaction with mobile devices based on compass (magnetic) sensor", in *Proceedings of the 15th international conference on Intelligent user interfaces*, 2010, pp. 413–414.

[109] H. Ketabdar, M. Roshandel, and K. A. Yüksel, "Magiwrite: Towards touchless digit entry using 3d space around mobile devices", in *Proceedings of the 12th international conference on Human computer interaction with mobile devices and services*, 2010, pp. 443–446.

[110] F. Salemi Parizi, E. Whitmire, and S. N. Patel, "Auraring: Precise electromagnetic finger tracking", *GetMobile: Mobile Computing and Communications*, vol. 25, no. 3, pp. 34–37, 2022.

[111] K. Lyons, "2d input for virtual reality enclosures with magnetic field sensing", in *Proceedings of the 2016 ACM International Symposium on Wearable Computers*, 2016, pp. 176–183.

[112] R.-H. Liang, K.-Y. Cheng, C.-H. Su, C.-T. Weng, B.-Y. Chen, and D.-N. Yang, "Gausssense: Attachable stylus sensing using magnetic sensor grid", in *Proceedings of the 25th annual ACM symposium on User interface software and technology*, 2012, pp. 319–326.

[113] T. Tsuchida, K. Fujita, K. Ikematsu, S. Sarcar, K. Takashima, and Y. Kitamura, "Tetraforce: A magnetic-based interface enabling pressure force and shear force input applied to front and back of a smartphone", *Proceedings of the ACM on Human-Computer Interaction*, vol. 6, no. ISS, pp. 185–206, 2022.

[114] A. Chulliat *et al.*, "The us/uk world magnetic model for 2015-2020", 2015.

[115] T. Feix, J. Romero, H.-B. Schmiedmayer, A. M. Dollar, and D. Kragic, "The grasp taxonomy of human grasp types", *IEEE Transactions on human-machine systems*, vol. 46, no. 1, pp. 66–77, 2015.

[116] Z. Wang, R. T. Stone, and J. Y.-M. Kim, "Hand tool evaluation: A review of existing hand tool evaluation and selection studies", *International Journal of Human Factors and Ergonomics*, vol. 10, no. 1, pp. 15–40, 2023.

[117] F. T. Farago and M. A. Curtis, *Handbook of dimensional measurement*. Industrial Press Inc., 1994.

[118] *Oppo a5s*, `https://www.oppo.com/en/smartphones/series-a/a5s/`.

[119] *Ultimaker*, https://ultimaker.com/3d-printers/s-series/ultimaker-s5/.

[120] *Phyphox*, https://phyphox.org/g.

[121] L. Barnard, J. S. Yi, J. A. Jacko, and A. Sears, "An empirical comparison of use-in-motion evaluation scenarios for mobile computing devices", *International Journal of Human-Computer Studies*, vol. 62, no. 4, pp. 487–520, 2005.

[122] A. Hettiarachchi and D. Wigdor, "Annexing reality: Enabling opportunistic use of everyday objects as tangible proxies in augmented reality", in *Proceedings of the 2016 CHI Conference on Human Factors in Computing Systems*, 2016, pp. 1957–1967.

[123] *Unity3d*, https://unity.com/.

[124] *Matlab mobile app*, https://www.mathworks.com/help/matlabmobile/ug/install-matlab-mobile-on-your-device.html.

[125] *Matlab to unity game engine*, https://www.mathworks.com/help/ros/ug/set-up-and-connect-to-unity-game-engine.html.

[126] L. Zhang, W. He, H. Bai, Q. Zou, S. Wang, and M. Billinghurst, "A hybrid 2d–3d tangible interface combining a smartphone and controller for virtual reality", *Virtual Reality*, vol. 27, no. 2, pp. 1273–1291, 2023.

[127] H. Bai, L. Zhang, J. Yang, and M. Billinghurst, "Bringing full-featured mobile phone interaction into virtual reality", *Computers & Graphics*, vol. 97, pp. 42–53, 2021.

[128] B. Bossavit, A. Marzo, O. Ardaiz, L. D. De Cerio, and A. Pina, "Design choices and their implications for 3d mid-air manipulation techniques", *Presence: Teleoperators and Virtual Environments*, vol. 23, no. 4, pp. 377–392, 2014.

[129] L. Sun *et al.*, "Shrinkykit: 3d printing shrinkable adaptations for everyday objects", in *Extended Abstracts of the 2020 CHI Conference on Human Factors in Computing Systems*, 2020, pp. 1–7.

[130] Y. Ye, S. Wan, S. Li, and X. He, "Mechanical wind sensor based on additive manufacturing technology", *IEEE Transactions on Instrumentation and Measurement*, vol. 71, pp. 1–8, 2022.

[131] N. J. Goddard, H. J. Dixon, N. Toole, and R. Gupta, "3-d printed instrumentation for point-of-use leaky waveguide biochemical sensor", *IEEE Transactions on Instrumentation and Measurement*, vol. 69, no. 9, pp. 6390–6398, 2020.

[132] B. Han, X. Liu, C. C. Yen, and C. Zheng, "Maskcircuit: 3d circuits with acrylic sheets and laser cutting", in *Extended Abstracts of the 2023 CHI Conference on Human Factors in Computing Systems*, 2023, pp. 1–7.

[133] N. Pourjafarian, M. Koelle, F. Mjaku, P. Strohmeier, and J. Steimle, "Print-a-sketch: A handheld printer for physical sketching of circuits and sensors on everyday surfaces", in *Proceedings of the 2022 CHI Conference on Human Factors in Computing Systems*, 2022, pp. 1–17.

[134] F. Hong, C. Myant, and D. E. Boyle, "Thermoformed circuit boards: Fabrication of highly conductive freeform 3d printed circuit boards with heat bending", in *Proceedings of the 2021 CHI Conference on Human Factors in Computing Systems*, 2021, pp. 1–10.

[135] E. Edmonds, "Shaping form s17", in *Proceedings of the 2017 CHI Conference Extended Abstracts on Human Factors in Computing Systems*, 2017, pp. 1431–1432.

[136] J. Yamaoka and Y. Kakehi, "Protomold: An interactive vacuum forming system for rapid prototyping", in *Proceedings of the 2017 CHI Conference on Human Factors in Computing Systems*, 2017, pp. 2106–2115.

[137] Y. Iravantchi, M. Goel, and C. Harrison, "Beamband: Hand gesture sensing with ultrasonic beamforming", in *Proceedings of the 2019 CHI Conference on Human Factors in Computing Systems*, 2019, pp. 1–10.

[138] Y. Liu, Y. Fan, Z. Wu, J. Yao, and Z. Long, "Ultrasound-based 3-d gesture recognition: Signal optimization, trajectory, and feature classification", *IEEE Transactions on Instrumentation and Measurement*, vol. 72, pp. 1–12, 2023.

[139] Y. Iravantchi, Y. Zhang, E. Bernitsas, M. Goel, and C. Harrison, "Interferi: Gesture sensing using on-body acoustic interferometry", in *Proceedings of the 2019 CHI Conference on Human Factors in Computing Systems*, 2019, pp. 1–13.

[140] Y. Zhang, G. Laput, and C. Harrison, "Electrick: Low-cost touch sensing using electric field tomography", in *Proceedings of the 2017 CHI Conference on Human Factors in Computing Systems*, 2017, pp. 1–14.

[141] Y. Zhang and C. Harrison, "Pulp nonfiction: Low-cost touch tracking for paper", in *Proceedings of the 2018 CHI Conference on Human Factors in Computing Systems*, 2018, pp. 1–11.

[142] Y. Zhang, R. Xiao, and C. Harrison, "Advancing hand gesture recognition with high resolution electrical impedance tomography", in *Proceedings of the 29th Annual Symposium on User Interface Software and Technology*, 2016, pp. 843–850.

[143] S. A. Iacolina, A. Soro, and R. Scateni, "Improving ftir based multi-touch sensors with ir shadow tracking", in *Proceedings of the 3rd ACM SIGCHI symposium on Engineering interactive computing systems*, 2011, pp. 241–246.

[144] H. Matsui, T. Hashizume, and K. Yatani, "Al-light: An alcohol-sensing smart ice cube", *Proceedings of the ACM on interactive, mobile, wearable and ubiquitous technologies*, vol. 2, no. 3, pp. 1–20, 2018.

[145] M. Alshawabkeh *et al.*, "Highly stretchable additively manufactured capacitive proximity and tactile sensors for soft robotic systems", *IEEE Transactions on Instrumentation and Measurement*, vol. 72, pp. 1–10, 2023.

[146] S. Geetha, K. Satheesh Kumar, C. R. Rao, M Vijayan, and D. Trivedi, "Emi shielding: Methods and materials—a review", *Journal of applied polymer science*, vol. 112, no. 4, pp. 2073–2086, 2009.

[147] W. Wang and Z. Jiang, "Magnetic shielding design for magneto-electronic devices protection", *IEEE Transactions on Magnetics*, vol. 44, no. 11, pp. 4175–4178, 2008.

[148] L. Wang, W. Wang, H. Dai, and S. Liu, "Magsound: Magnetic field assisted wireless earphone tracking", *Proceedings of the ACM on Interactive, Mobile, Wearable and Ubiquitous Technologies*, vol. 7, no. 1, pp. 1–32, 2023.

[149] R.-H. Liang, H.-C. Kuo, L. Chan, D.-N. Yang, and B.-Y. Chen, "Gaussstones: Shielded magnetic tangibles for multi-token interactions on portable displays", in *Proceedings of the 27th annual ACM symposium on User interface software and technology*, 2014, pp. 365–372.

[150] A. Sears and J. A. Jacko, "Input technologies and techniques ken hinckley", in *The Human-Computer Interaction Handbook*, CRC Press, 2002, pp. 183–200.

[151] R. G. Jackson, *Novel sensors and sensing*. CRC Press, 2019.

[152] O. Hilliges, "Input recognition", *Computational Interaction*, pp. 65–94, 2018.

[153] T. Schlegl, M. Neumayer, S. Mühlbacher-Karrer, and H. Zangl, "A pretouch sensing system for a robot grasper using magnetic and capacitive sensors", *IEEE Transactions on Instrumentation and Measurement*, vol. 62, no. 5, pp. 1299–1307, 2013.

[154] X. Zhou, X. Li, S. Li, G.-W. An, and T. Cheng, "Magnetic field sensing based on spr optical fiber sensor interacting with magnetic fluid", *IEEE Transactions on Instrumentation and Measurement*, vol. 68, no. 1, pp. 234–239, 2018.

[155] F. S. Parizi, E. Whitmire, and S. Patel, "Auraring: Precise electromagnetic finger tracking", *Proceedings of the ACM on Interactive, Mobile, Wearable and Ubiquitous Technologies*, vol. 3, no. 4, pp. 1–28, 2019.

[156] A. Visschedijk, H. Kim, C. Tejada, and D. Ashbrook, "Clipwidgets: 3d-printed modular tangible ui extensions for smartphones", in *Sixteenth International Conference on Tangible, Embedded, and Embodied Interaction*, 2022, pp. 1–11.

[157] K. Lukoff, C. Yu, J. Kientz, and A. Hiniker, "What makes smartphone use meaningful or meaningless?", *Proceedings of the ACM on Interactive, Mobile, Wearable and Ubiquitous Technologies*, vol. 2, no. 1, pp. 1–26, 2018.

[158] R. Eardley, A. Roudaut, S. Gill, and S. J. Thompson, "Investigating how smartphone movement is affected by body posture", in *Proceedings of the 2018 CHI Conference on Human Factors in Computing Systems*, 2018, pp. 1–8.

[159] R. Eardley, S. Gill, A. Roudaut, S. Thompson, and J. Hare, "Investigating how the hand interacts with different mobile phones", in *Proceedings of the 18th International Conference on Human-Computer Interaction with Mobile Devices and Services Adjunct*, 2016, pp. 698–705.

[160] J. Chan and S. Gollakota, "Data storage and interaction using magnetized fabric", in *Proceedings of the 30th Annual ACM Symposium on User Interface Software and Technology*, 2017, pp. 655–663.

[161] G. Zhao, Y. Yan, and Z. Yang, "Low-cost and non-visual labels using magnetic printing", *Proceedings of the ACM on Human-Computer Interaction*, vol. 7, no. EICS, pp. 1–18, 2023.

[162] C. Ding and H. Peng, "Minimum redundancy feature selection from microarray gene expression data", *Journal of bioinformatics and computational biology*, vol. 3, no. 02, pp. 185–205, 2005.

[163] A. F. Rose and A. Cirino, *Jewelry making and design*. BoD–Books on Demand, 2023.

[164] A. Julander, J. Kettelarij, and C. Lidén, "Cobalt", *Kanerva's Occupational Dermatology*, pp. 661–669, 2020.

[165] S. D. Guler, M. Gannon, and K. Sicchio, *Crafting wearables: Blending technology with fashion*. Apress, 2016.

[166] I. C. on Non-Ionizing Radiation Protection *et al.*, "Guidelines on limits of exposure to static magnetic fields", *Health Physics*, vol. 96, no. 4, pp. 504–514, 2009.